ALTISSIMO CONSULTING

ROAD SURFACE NOISE

Analysis of Low-Noise Asphaltic Mix Surfaces

Client: Waka Kotahi / NZ Transport Agency
Date: 13 February 2023
Ref: 22-105-R01-B

Prepared for (the Client)
Waka Kotahi / NZ Transport Agency

Prepared by the Consultant)
Altissimo Consulting Ltd

Project	Road Surface Noise
Report	Analysis of Low-Noise Asphaltic Mix Surfaces
Reference	22-105-R01-B

Prepared by

George Bell

Consultant

Reviewed by

Robin Wareing
Principal Acoustics Engineer

Version history:

Version	Date	Comment
A	10/1/2023	Preliminary report for client review
B	13/2/2023	Updated following client comments

Report disclaimer and limitations:

This report has been prepared in accordance with the usual care and thoroughness of the consulting profession for the use of the Client. It is based on generally accepted practices and standards at the time it was prepared. No other warranty, expressed or implied, is made as to the professional advice included in this report.

This report should be read in full. No responsibility is accepted for use of any part of this report in any other context or for any other purpose or by third parties. This report does not purport to give legal advice. Legal advice can only be given by qualified legal practitioners.

Abstract

This investigation aimed to collate, analyse, and interpret existing data to further develop knowledge in low-noise asphaltic mix road surfaces. Three projects (Christchurch Northern Corridor, Christchurch Southern Motorway – Stage 2, and Sawyers to Groynes) were considered. The trial sites were comprised of a range of asphaltic mixtures and construction parameters. The correlations between the close proximity sound level ($L_{CPX,}$) and mean profile depth (MPD), thickness, and void fraction were explored for a range of surface types. Thickness and MPD variation accounted for up to 79% of the variability in noise for the porous surfaces in the evaluated projects.

For porous surfaces, thickness had a negative non-linear correlation with the overall L_{CPX}. The L_{CPX} had an average proportionality with thickness of 1.5 to 1.7 dB per /10 mm of thickness. Void fraction influenced the effects of thickness and MPD. Low void fractions (<10%), essentially negated any thickness effects, and exacerbated MPD impacts. The high-strength (12 to 16%) porous asphalt on CNC demonstrated the best performance for comparable thicknesses.

For non-porous surfaces, noise was strongly influenced by surface texture. Low frequencies were positively correlated with MPD. High frequencies were negatively correlated with MPD.

Ageing effects were analysed in a 1 year 8-month range (starting 1 year 3 months after initial surfacing). It was observed that low frequencies (<1,000 Hz) typically decreased with time, which was potentially due to reducing surface texture. High frequencies (>1,250 Hz) typically increased with time, which was potentially due to reducing void fraction by the accumulation of debris.

At the time of writing, the quietest surface was a 50 mm thick EPA7 with a void fraction of 20 to 25%. Limited improvements may be achieved through reducing MPD and a further increase in thickness. It is recommended that void fraction is explored in a future study to understand the underlying interactions with noise and any potential improvements.

Contents

Abstract iii
Contents iv
Glossary vi
1. Introduction 1
1.1 Background 1
1.2 Mechanisms 2
1.3 Scope 2
1.4 Report Structure 2
2 Methodology 3
2.1 Projects and Trial Sections 3
2.2 Data 3
2.3 Processing 4
2.3.1 CNC 4
2.3.2 CSM2 4
2.3.3 S2G 5
2.4 Plotting and Analysis 5
2.4.1 Noise, MPD, and Thickness 5
2.4.2 QA Documentation 7
2.4.3 Ageing 8
3 Results and Discussion 9
3.1 CNC Trial Sites 9
3.1.1 Overall Results 9
3.1.2 Bulk Thickness 11
3.1.3 Measured Void Fraction 11
3.1.4 Detailed Observations 12
3.2 CSM2 18
3.2.1 Overall Results 18
3.2.2 Detailed Observations 19
3.3 S2G 21
3.3.1 Overall Results 21
3.3.2 Detailed Observations 21
3.3.3 Ageing 22
3.4 Overall Thickness 22
3.5 Overall MPD 23
4 Future Investigations 25

5 Conclusions 26
6 References 27
7 Appendix A - Detailed Results 28
7.1 Christchurch Northern Corridor (CNC) 28
7.1.1 SMA7 28
7.1.2 PA7 LV 36
7.1.3 PA7 HS 43
7.1.4 PA7 50
7.1.5 PA10 57
7.1.6 EPA7-50 mm 64
7.1.7 PA7 and PA10 71
7.1.8 PA7-30 mm and EPA7-50 mm 78
7.2 Road Science Hawkeye vs. WDM HSD for CSM2 85
7.3 Christchurch Southern Motorway – Stage 2 (CSM2) 86
7.4 Sawyers to Groynes (S2G) 92
8 Appendix B – Project and Trial Section Locations 98
9 Appendix C – Lane Numbering 99

Glossary

CNC	Christchurch Northern Corridor
CPX	Close proximity
CSM2	Christchurch Southern Motorway stage 2
EPA	Epoxy-modified porous asphalt
Lane 1	Closest lane to the centre of the road (see Figure 92).
Lane 2	Second-closest lane to the centre of the road (see Figure 92).
L_{CPX}	Close proximity sound pressure level. All measurements were conducted using the P1 tyre at a nominal speed of 80 km/h (L_{CPX} = $L_{CPX,P1,80}$)
MIT	Magnetic imaging tomography. Method used for measuring asphalt thickness.
MPD	Mean profile depth
NB	Northbound
NDM	Nuclear densometer
PA	Porous asphalt
PA7 HS	Porous asphalt high strength
PA7 LV	Porous asphalt low voids
S2G	Sawyers to Groynes
SB	Southbound
SLP	Stationary laser profilometer
SMA	Stone mastic asphalt
t	Asphalt surface thickness
WBB	Western Belfast Bypass
WDM HSD	WDM is the provider for the High-Speed Data survey.

1. Introduction

Waka Kotahi have been conducting targeted investigations to develop knowledge in the area of low-noise surfaces for New Zealand's state highway network (Wareing, Bull, Chiles, & Jackett, 2021) (Jackett, 2021). Two primary noise measurement techniques have been used, (1) a close-proximity (CPX) tyre/road noise trailer, and (2) vehicle pass-by measurements at the wayside. Numerous trial sections of road surfaces have been constructed, with close monitoring of key parameters.

The three projects with trial sections considered in this report are Christchurch Northern Corridor (CNC), Christchurch Southern Motorway – Stage 2 (CSM2), and Sawyers to Groynes (S2G). Trials have included sections with a range of thicknesses, void fractions, chip sizes, and binder compositions.

1.1 Background

The bulk porous asphalt thickness effect has previously been estimated based on the 2018 Western Belfast Bypass (WBB) thickness trial (Bull, Wareing, Chiles, & Jackett, 2021). The WBB thickness trial included three sections of EPA7 with target thicknesses of 30 mm, 40 mm, and 50 mm. Core samples indicated that the as-built thickness deviated from the nominal by up to 15 mm.

The 2018 WBB project (Bull J. , 2019) was used to investigate the changes of multiple parameters, but the absence of local as-built thickness limited the depth of the study. Since 2018, existing methods of reliably measuring surface thickness were identified and used successfully on sections of the CSM2 and CNC roading projects.

The 2017 trial on S2G (Wareing, Bull, Chiles, & Jackett, 2021) showed that the high voids section (25 to 30%) had higher tyre/road noise than the standard voids section (20 to 25%). This led to a focus on standard voids mixes in the small chip size and thickness trials that followed in late-2017 and 2018.

The hypothesis was that while porosity is beneficial in low-noise surfaces, an increase in air voids causes an increase in surface macrotexture that has a detrimental effect on noise. The CNC low voids trial sections were constructed to test this hypothesis and determine the air voids content of the suite of 30 mm asphalt surfaces that offers the lowest noise. Noise is only one factor in road surface performance, other engineering requirements may influence the final specification.

The other finding from the high voids trial was that the stone size played a key role in the tyre/road noise with the EPA10 trial section being significantly quieter than the EPA14 trial section. The small chip trials in late-2017 and 2018 (Wareing, Bull, Chiles, & Jackett, 2021) that followed did not have adjacent contemporaneous control sections and the stone size effect was not able to be quantified. For this reason, a PA10 section was included in the CNC trial to allow direct comparison with the PA7 surface.

The surface of the road changes with time due to environmental and loading factors. The surface texture changes due to stone erosion and realignment. For porous surfaces, the void fraction may be reduced by the collection of debris. To date, there has only been limited analysis of ageing of asphalt surfaces in New Zealand (Jackett, 2021).

1.2 Mechanisms

There are multiple noise generation mechanisms for a rolling tyre, (1) tread impact on the surface, (2) the compression and displacement of air at the front edge of the tyre-surface interface, and (3) aero-acoustic noise from the translation and rotation of the tyre. The transmission to the roadside of sound is via several pathways, including (1) direct emission from sources, (2) amplification in the leading and trailing air wedges at the tyre-road interface ("horn effect"), (3) excitation of the tyre, and (4) reflections on the road and other surfaces (Peeters & Kuijpers, 2008) (Hamet, 2004).

The tyre noise is affected by multiple properties of the surface, including surface macrotexture, thickness, and air void fraction. The surface macrotexture is the shape of the top level of the surface and is presently characterised by the mean profile depth (MPD). The thickness of the surface is from the top level of the surface to the top of the next layer (generally a chipseal layer). The air void fraction is the as-built percentage of air voids in the surface, there are nominal ranges for each surface type.

1.3 Scope

The overall objective of the present work was to determine the critical parameters of low-noise road surfaces . The sensitivity of key specification parameters on tyre noise is quantified. These include the effects of surface thickness, surface macro texture, and void fraction. In addition to the overall level, the frequency distributions are evaluated. The effect of ageing on noise is investigated and quantified. The analysis primarily focused on identifying correlations between a range of short (4 to 20 m segments) within trial sites (several hundred meters) and longer (several km) lengths of projects. Options for future investigations are identified.

1.4 Report Structure

The Methodology section contains a description of projects and surfaces, data sources, and a brief overview of the processing steps. The method is only intended as an overview, and not for purposes of reproducing the analysis. The same analysis was conducted for each surface type, a description of the contents and underlying inputs into each table and figure is included.

The Results and Discussion section presents the overall and detailed findings from each project and trial section. Only key tables and figures are included within the body of the report. All figures and tables are included in the Appendix. The combined effects are then presented and discussed.

2 Methodology

This section contains a descriptive overview of the methodology used for the analysis. No descriptions of the measurement methodologies are included in this report. CPX measurement details can be found in (Wareing, Canterbury Road Surface Noise 2022 Measurement Summary, 2022).

2.1 Projects and Trial Sections

Data from three separate projects were used within the analysis. The project and nominal surface parameters for each section are shown in Table 1. Maps of the considered projects and trial sites are shown in Appendix B – Project and Trial Section Locations Figure 91. The analysed sections of CNC and S2G primarily consisted of short trial sections of different surface types. The analysis of CSM2 is of several km of a nominally consistent surface.

TABLE 1. NOMINAL SURFACE PARAMETERS FOR EACH PROJECT AND SECTION.

Project	Name	Length – m*	Stone Size – mm	Thickness – mm	Voids - %
CNC	SMA7	425	7	30	2-6
	PA7 LV	360	7	30	8-10
	PA7 HS	320	7	30	12-16
	PA7	340	7	30	20-25
	PA10	380	10	30	20-25
	EPA7 50 mm	1,100	7	50	20-25
CSM2	EPA7 40 mm	2,740	7	40	20-25
S2G	EPA10	240	10	30	20-25
	EPA10 HV	300	10	30	25-30
	EPA14	260	14	30	20-25

*Lengths are after the sections have been filtered for end-effects in the data.

2.2 Data

Table 2 shows the data sources used for the analysis of each project. Table 3 contains the surfacing and measurement dates for all projects. Data that was available but was not used is not stated as present (e.g., paving shift records for S2G). For all projects, only the left wheel path was included in the analysis.

TABLE 2. DATA SETS USED FOR EACH PROJECT.

Parameter	Data	CNC	CSM2	S2G
Tyre/road noise	Overall and one third octave $L_{CPX:P1,80}$	✓	✓	✓
As-built thickness	Paving shift records (trace sheets)	✓	✓	
	MIT-SCAN thickness measurements	✓		
	Manual survey thickness measurements		✓	
Macrotexture	Stationary laser profilometer	✓		
	Road Science Hawkeye	✓	✓	
	WDM HSD		✓	✓
Air void content	Laboratory reports	✓	✓	

	Nuclear densometer measurements	✓	✓	
Surface properties	CAPTIF surface properties database	✓	✓	✓

TABLE 3. SURFACING AND MEASUREMENT DATES FOR ALL PROJECTS.

Project		CNC	CSM2	S2G
Surfacing		Feb-Mar 2022	Mar-Apr 2021	Mar 2017
CPX		Jun 2022 3 m	Jun 2022 1 y, 3 m	Jul 2018 – Mar 2020 1 y, 4 m to 3 y
MPD	WDM HSD	-	Jan 2022 10 m	Jan 2018 – Jan 2022 10 m to 4 y, 10 m
	Road Science	Apr 2022 1 m	Apr 2021 1 m	-

2.3 Processing

The pre-analysis processing and merging of data is described below for each project. This is not intended for full reproducibility of the analysis. All processing scripts have been provided to Waka Kotahi.

2.3.1 CNC

The start and end points for each trial section were adjusted based on a subjective review of the longitudinal variation in L_{CPX} and MPD.

The CPX segment length was reduced from 20 m to 4 m. The intra-segment variation between 4 m and 20 m is shown in Figure 8. The local MIT-SCAN thickness was merged into the encapsulating 4 m CPX segment. The thickness measurements a randomly distributed within their respective CPX segments.

The Road Science Hawkeye MPD data was linked to the CPX segments by using the mean of the internal 4 m of data and the external 10 m in both directions.

2.3.2 CSM2

Both lanes have a thickness tapering effect of approximately 100 m at either end before abutting to the adjacent SMA sections. The tapered sections were excluded from the analysis.

All data was merged into 20 m segments. Where there were multiple measurements within one segment (e.g., MPD and thickness), an unweighted average was applied.

The Road Science Hawkeye Survey and HSD texture data were both available. An initial comparison was made for the Southbound lane in Figure 72 and Figure 73. This initial review showed differences in longitudinal and average values, but the scope of the present investigation did not allow time for further analysis. The WDM HSD data was used for all analysis for CSM2 as the measurement date was within five months of the CPX testing (compared to 1 year, 2 months for the Road Science Hawkeye).

2.3.3 S2G

The CPX data was reviewed in 20 m segments. The HSD MPD data was merged into the CPX data by numerically averaging the 10 m HSD segments.

For the non-transient analysis, the HSD and CPX data from the beginning of 2019 were used.

For the ageing analysis, all available HSD MPD data was used; this spanned from Jan 2018 to Jan 2022. Only CPX data from Sep 2018 to Mar 2020 was used. The CPX data was limited to data where the physical trailer configuration was known to be the same and common enclosure corrections ("02") were used. Differences outside of the timespan were not analysed. It is not recommended that historical absolute L_{CPX} levels from S2G are used for comparisons with more recent measurements.

2.4 Plotting and Analysis

Common analyses were conducted across multiple sites. This section provides a brief description of each type of analysis and corresponding table or figure. Note that all analyses have not been conducted for every included project and trial section.

2.4.1 Noise, MPD, and Thickness

For the analysis of noise, MPD, and thickness a common series of figures and tables were produced for each surface type. A description of each table and figure is contained in Table 4.

TABLE 4. DESCRIPTION OF TABLES AND FIGURES GENERATED FOR EACH TRIAL SITE.

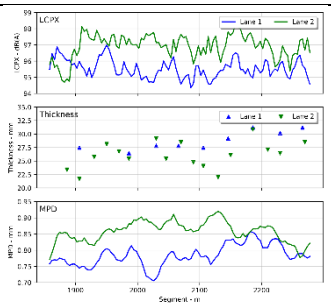 Example: Figure 9	**Longitudinal** Displays the longitudinal measurements of L_{CPX}, thickness, and MPD for each lane. L_{CPX} and MPD are shown as line charts as the data is effectively continuous. Thickness measurements are discrete and therefore displayed as points where data is available.
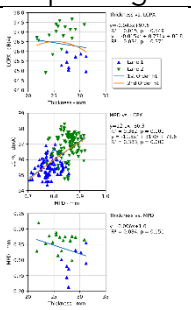 Example: Figure 10	**Independent Correlations** Displays the three independent combinations of L_{CPX}, thickness, and MPD. The first and second order polynomial fits are included with their associated R^2 and p-values. The points are displayed by lane. The best-fit approximations include both lanes. MPD vs. thickness is included to check for any correlation that would invalidate the multi-variable regression.
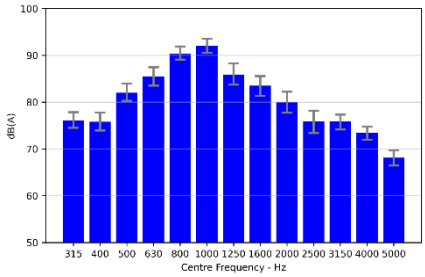 Example: Figure 11	**One-Third Octave Bands** Shows the average one-third octave band distribution for the entire section. The additional bars show the 10th to 90th percentile longitudinal range.
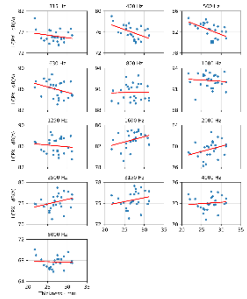 Example: Figure 12	**One-Third Octave Bands versus Thickness** Displays scatter plots of the one-third octave band sound level versus thickness for each segment. A linear model of best fit is included in each plot, irrespective of statistical significance.
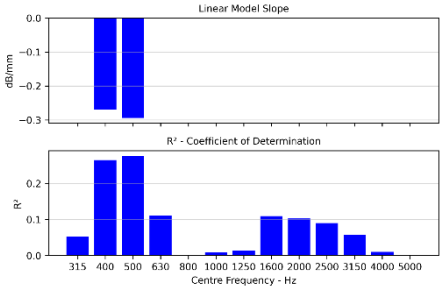 Example: Figure 14	**One-Third Octave Bands versus Thickness Correlations** The top sub-plot shows the slope in dB/mm of the linear best fit line for each frequency band. The bottom chart shows the R^2 value. Slopes are only displayed where the R^2 value is greater than 0.25.

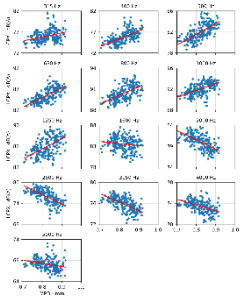

Exammple: Figure 13

One-Third Octave Bands versus MPD
Displays scatter plots of the one-third octave band sound level versus MPD for each segment. A linear model of best fit is included in each plot, irrespective of statistical significance.

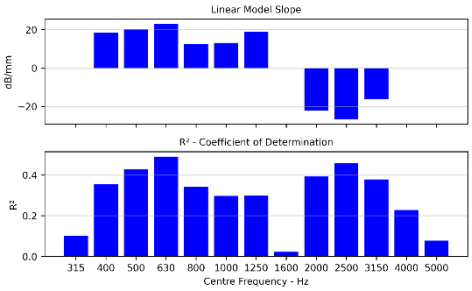

Example: Figure 15

One-Third Octave Bands versus MPD Correlations
The top sub-plot shows the slopes in dB/mm of the linear best fit line for each frequency band. The bottom chart shows the R^2 value. Slopes are only displayed where the R^2 value is greater than 0.25.

Overall multi-variable analysis
Example: Table 12

Overall Multi-Variable Regression
A multi-variable regression was conducted using the L_{CPX}, MPD, and thickness for each segment. The table contains the R^2, adjusted R^2, linear slope for each variable, and p-value for each linear model. Only linear models were considered.

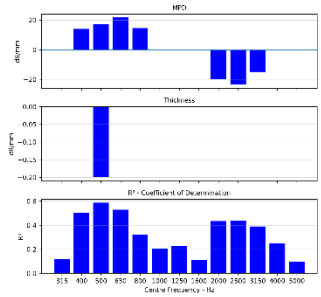

Example: Figure 16

One-Third Octave Band Multi-Variable Regression
Displays a summary of the multi-variable regression between each one-third octave band level, MPD, and thickness, within each segment. The first and second plots show the linear best-fit slopes for MPD and thickness, respectively. The bottom plot shows the R^2 value for the model. Slopes are only shown where the R^2 value is greater than 0.25 and the p-value is greater than 0.025.

2.4.2 QA Documentation

The bulk thickness and void fraction were reviewed using the provided QA documentation.

For each paving shift, a truck-by-truck record is captured that includes overall mass, area paved, and paver location (calculated by distance from the start of the shift). The average thickness was calculated by dividing the total area paved by the total mass and average density. The average density was the mean of those extracted from the laboratory testing for batches within the shift. The average bulk thickness for a section was compared to the average of the local measurements (MIT Scan or direct survey).

The local thickness was calculated at a truck-level for CSM2; however, it was found that the location and timing data offered no alignment with the actual thickness, therefore no further analysis was done with this resolution. It is recommended that trace-sheet data is not used to estimate local thickness.

The NDM void fraction measurements were compared to the laboratory measurements. The distribution of NDM measurements was reviewed alongside the average laboratory measurement void fraction for each trial section on CNC.

2.4.3 Ageing

The figures and analysis methodologies conducted to review ageing effects are described in Table 5. Ageing effects were only considered for the Sawyers to Groynes project.

TABLE 5. DESCRIPTION OF FIGURES GENERATED FOR AGEING ANALYSIS.

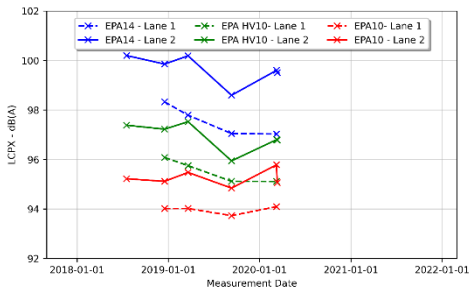

Example: Figure 85

Overall L_{CPX} versus Time

Shows the overall average L_{CPX} for each surface type and lane. Each marker point represents a set of measurement runs. The time axis was aligned with the available MPD data.

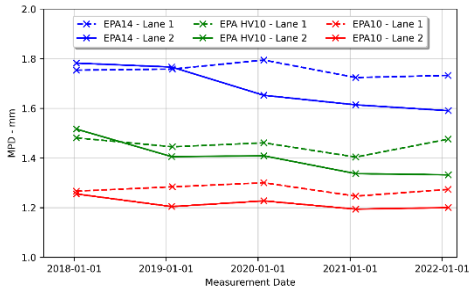

Example: Figure 86

Average MPD versus Time

Shows the average MPD for each surface type and lane. Each marker point represents a measurement.

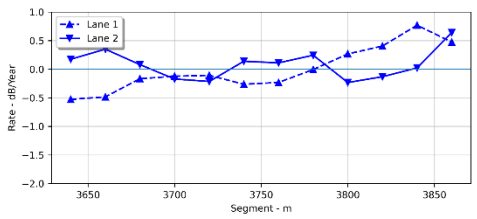

Example: Figure 87

Longitudinal L_{CPX} Rate of Change

For each CPX segment, a linear best fit was applied between L_{CPX} and time. The resulting slope is plotted for each segment and lane. Each marker is the start point of the segment.

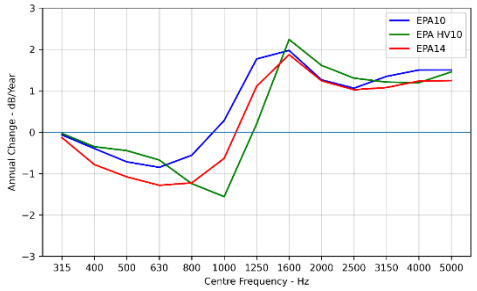

Example: Figure 90

Rate of Change by One-Third Octave Band

A linear best-fit model was applied to the average one-third octave band level versus time. The resulting slope is then plotted for each frequency band and surface type.

3 Results and Discussion

The results for each project are first presented and discussed individually followed by a collated summary of the overall effects. The key tables and figures are included within this section and all reference data is in 7 Appendix A - Detailed Results.

3.1 CNC Trial Sites

3.1.1 Overall Results

The mean L_{CPX}, MPD, and thickness for each surface type are shown in Table 6. Boxplots for all measurement points of L_{CPX}, MPD, and thickness for each surface type are shown in Figure 1. The 50 mm EPA 7 was the best performing surface with a mean L_{CPX} of 92.1 dB. Within the suite of nominally 30 mm surfaces, the PA7 HS section demonstrated the lowest level at 93.4 dB.

TABLE 6. MEAN L_{CPX}, MPD, AND THICKNESS FOR EACH SURFACE TYPE ON CNC.

	EPA7 50 mm	PA7 HS	PA7 LV	SMA7	PA7	PA10
L_{CPX} – dB	92.1	93.4	94.7	96.2	96.6	97.1
MPD – mm	0.83	0.74	0.75	0.82	0.93	1.14
Thickness - mm	48.1	33.1	30.1	27.1	32.1	36.4

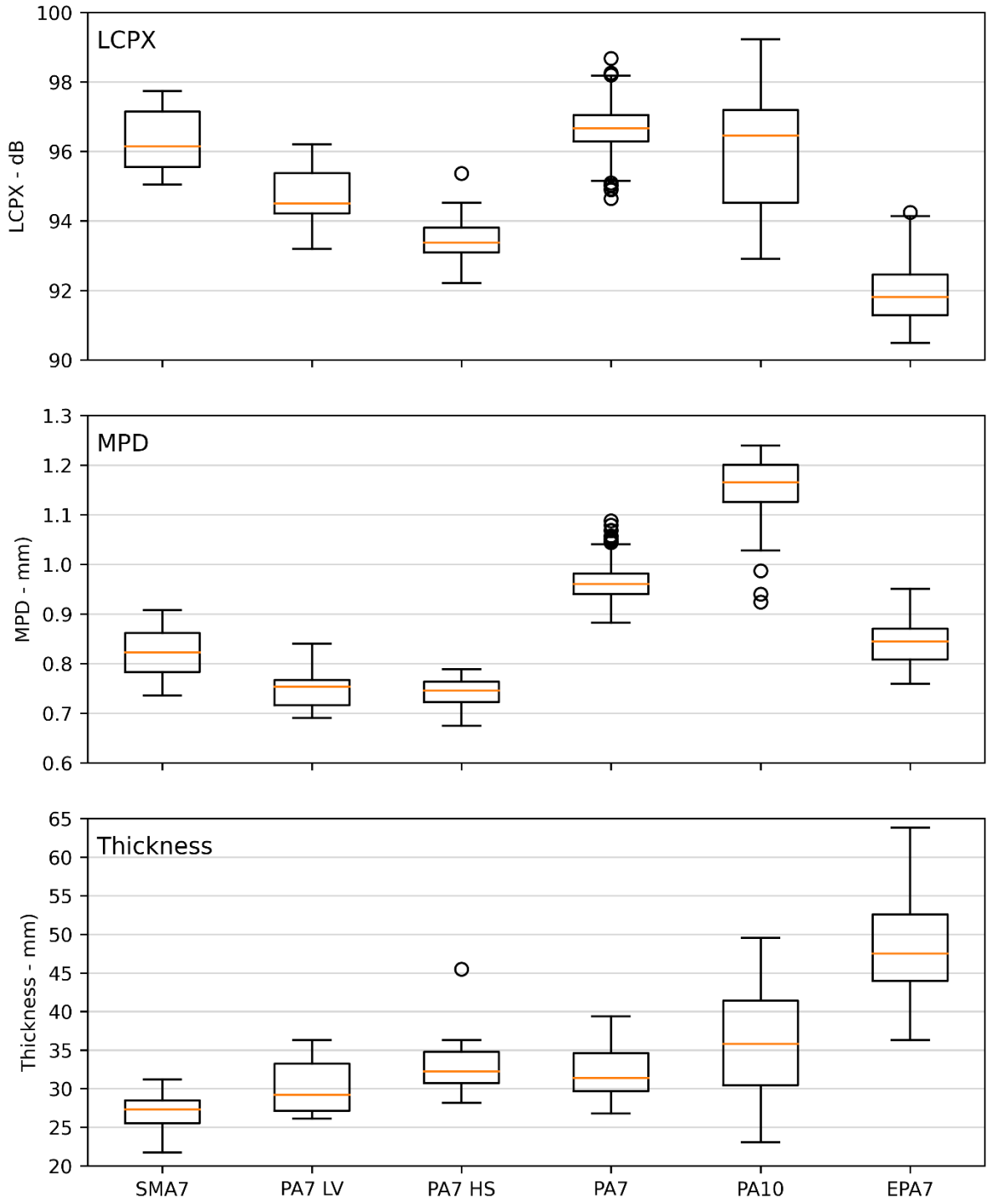

FIGURE 1. BOXPLOTS OF L_{CPX}, MPD, AND THICKNESS FOR ALL SURFACES ON CNC.

3.1.2 Bulk Thickness

Figure 2 contains a comparison between the average bulk thickness calculated from the QA data for each trial section and the average direct thickness measurements. Bulk thickness underpredicted the measured thickness by up to 15% with an average of 6%. Assuming lateral consistency, bulk thickness may be used as a coarse prediction of average thickness.

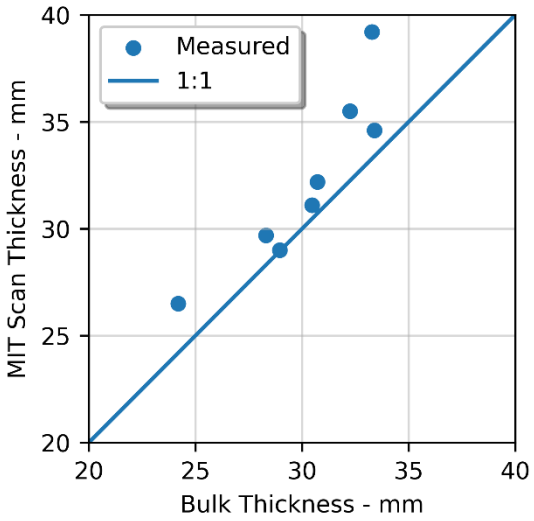

FIGURE 2. BULK VS. MIT SCAN THICKNESS MEASUREMENTS FOR TRIAL SITES ON CNC.

3.1.3 Measured Void Fraction

Figure 3 contains boxplots of the NDM measured void fraction for each trial section with the corresponding average void fraction (red dots) measured during asphalt production (i.e., laboratory testing). At the time of writing, definitive core sample results were not available.

The NDM provided satisfactory results for void fractions above 20% but offered limited or no correspondence for low void fraction surfaces. An in-depth study of in-situ void fraction would be required to understand the absolute accuracy of NDM and laboratory compaction testing.

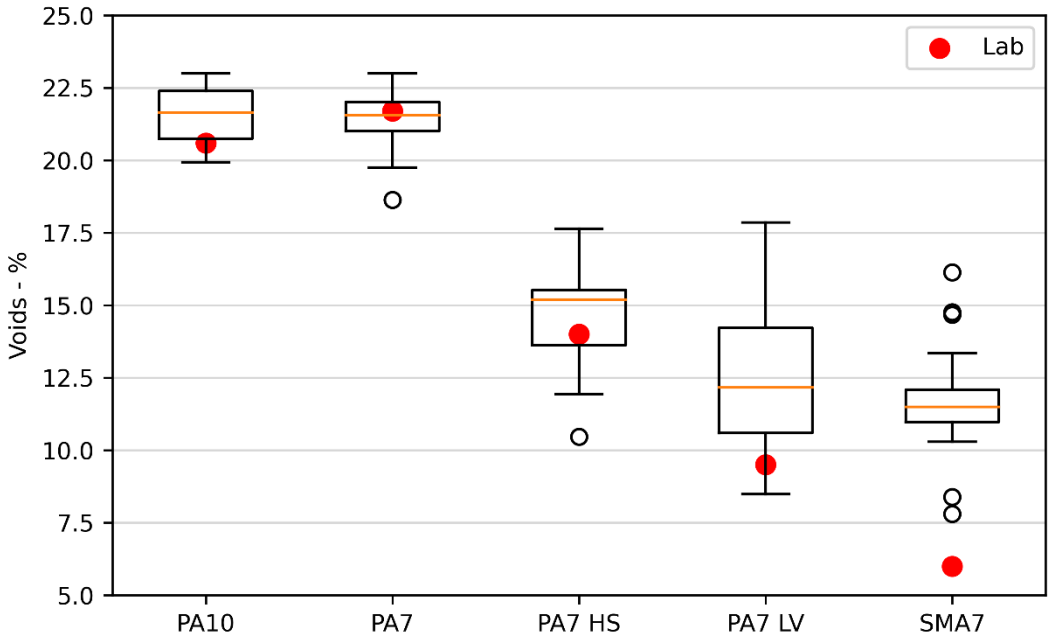

FIGURE 3. VOID FRACTIONS FOR CNC TRIAL SITES USING NDM AND LABORATORY TESTING.

3.1.4 Detailed Observations

The results for each surface type and specific combinations are discussed in this section.

3.1.4.1 SMA7

All results for SMA7 are presented in Table 11 and Table 12, and Figure 9 to Figure 16.

The overall level of 96.2 dB for an SMA surface is relatively low (SMA10 on CSM2 averages 99.7 dB). The mean MPD of 0.82 mm is also relatively low (SMA10 on CSM2 averages 1.1 mm)); this is likely due to the grade 7 stone size. Lane 2 had an overall greater L_{CPX}, which is likely driven by its greater mean MPD.

Table 12 contains the results of the overall multi-variable regression between L_{CPX}, and MPD and thickness. There was no significant correlation between thickness and L_{CPX}. There was a positive linear correlation of 11 dB/mm between L_{CPX} and MPD.

The A-weighted one-third octave band distribution is shown in Figure 11. 800 and 1,000 Hz were the dominant frequency bands. The greatest longitudinal variations occurred in the 315 to 630 Hz and 1,250 to 2,500 Hz bands, which aligns with the MPD correlations. The lowest variations occurred in the 800 and 1,000 Hz bands, which aligns with the low standard deviation of 0.96 dB in the overall L_{CPX} level.

The multi-variable one-third octave band correlations are shown in Figure 16. The L_{CPX} had positive correlations with MPD in the 400 to 800 Hz bands. The L_{CPX} had negative correlations with MPD in the 2,000 to 3,150 Hz bands. The L_{CPX} had a negative correlation with thickness in the 500 Hz band.

The positive correlations with MPD may be due to an increase in the mechanical impact of the tyre tread on the road surface. The negative correlations with MPD may be due to decreasing resistance to air dispersion at the forward tyre-road interface. The negative thickness correlation may be due to a low-void effect, another unknown mechanism, or a data artefact.

3.1.4.2 PA7 LV

All results for PA7 LV are presented in Table 13 and Table 14, and Figure 17 to Figure 24.

The overall level of 94.7 dB is lower than both the SMA7 and PA7 sections. The mean MPD of 0.75 mm is relatively low and is expected to be due to a combination of the low voids and small stone size. The elevated level for lane 2 was likely driven by decreased thickness relative to lane 1. There were large local variations in MPD for both lanes. Waka Kotahi has commissioned a future study to investigate texture and construction data.

No significant overall multi-variable correlations were observed for PA7 LV. There was a very weak independent negative correlation between L_{CPX} and MPD; this may indicate a lower limit for MPD with a low-voids surface (i.e., L_{CPX} may increase below an MPD level).

The A-weighted one-third octave band distribution is shown in Figure 19. 800 and 1,000 Hz were the dominant frequency bands. The greatest longitudinal variation occurred in the 1,600 and 2,500 Hz bands.

The multi-variable one-third octave band correlations are shown in Figure 24. The L_{CPX} had positive correlations with MPD in the 400 to 630 Hz bands. The L_{CPX} had negative correlations with MPD in the 1,250 to 5,000 Hz bands. The L_{CPX} had a negative correlation with thickness in the 500 Hz band. These characteristics are like those of SMA7 and may have the same driving mechanisms for surface texture-driven noise generation and air displacement.

The positive and negative correlations between L_{CPX} and MPD suggests an optimal point may exist for a given void fraction. For the low-voids (8-10%) surface, an MPD of 0.8 mm (measured by the Road Science Hawkeye system) appeared to result in a minimum overall L_{CPX}; this may be due to this representing the point where the noise generated by the impact of the tyre tread and air dispersion are balanced; further analysis is required to understand this effect.

3.1.4.3 *PA7 HS*

All results for PA7 HS are presented in Table 15 and Table 16, and Figure 25 to Figure 32.

The overall level of 93.4 dB was the lowest achieved by the suite of nominally 30 mm surfaces on CNC. The mean MPD of 0.74 mm is relatively low and is expected to be due to a combination of the low voids and small stone size. The effect on other engineering requirements (e.g., skid resistance) must be considered further. There were several local measurements where the L_{CPX} increased by approximately 2 dB, the cause for this could not be deduced from the available data.

The range of both MPD and thickness was small, which limited the ability to draw correlations within this trial section. No significant relationships were observed in the overall or one-third octave band multi-variable regressions.

The A-weighted one-third octave band distribution is shown in Figure 27. 800 and 1,000 Hz were the dominant frequency bands. The greatest longitudinal variation occurred in the 630 Hz band.

Based on correlations from other trial sections, a method to achieve further reductions in the total level may be by reducing the 800 and 1000 Hz bands via increased thickness.

3.1.4.4 PA7

All results for PA7 are presented in Table 17 and Table 18, and Figure 33 to Figure 41.

The PA7 had a high L_{CPX} of 96.6 dB, relative to SMA7 (96.2 dB) and PA10 (97.1 dB). The MPD for the 30 mm PA7 was 0.1 mm greater than that for the 50 mm EPA7, which may have partially caused the elevated level. The sub-section where the lane 2 level is greater than lane 1 was likely caused by increased surface texture.

The A-weighted one-third octave band distribution is shown in Figure 35. 800 and 1,000 Hz were the dominant frequency bands. The greatest longitudinal variations occurred in the 1,250, 1,600, and 2,500 Hz bands.

No correlations were observed between the overall L_{CPX}, and MPD and thickness. The L_{CPX} had positive correlations with MPD in the 315 to 500 Hz bands. The positive correlations with MPD may be due to an increase in the mechanical impact of the tyre tread on the road surface.

3.1.4.5 PA10

All results for PA10 are presented in Table 19 and Table 20, and Figure 42 to Figure 47.

The overall level of 97.1 dB was the highest for all surface types on CNC. The mean MPD of 1.14 mm was the highest for all surfaces and is likely due to the larger stone size. The wide range (6 dB) appeared to be caused by large thickness and MPD variations of 26 mm and 0.3 mm, respectively. Lane 2 had a greater L_{CPX} due to reduced thickness and greater surface texture.

The A-weighted one-third octave band distribution is shown in Figure 42. 630 to 1,000 Hz were the dominant frequency bands. The greatest longitudinal variation occurred in the 1,000 Hz band, with significant variation in the 800, 1,250, and 2,000 Hz bands.

The multi-variable one-third octave band correlations are shown in Figure 47. The L_{CPX} had positive correlations with MPD in the 500 and 800 Hz bands. L_{CPX} had a negative correlation with thickness in the 500 Hz band.

3.1.4.6 EPA7-50 mm

All results for the 50 mm EPA7 are presented in Table 21 and Table 22, and Figure 48 to Figure 55.

The overall level of 92.1 dB was the quietest for all surfaces on CNC. The large overall range (5 dB) was primarily due to thickness variability (35-64 mm). The elevated level for lane 2 was likely due to the thickness reducing to 40 mm. The MPD for lane 1 was 0.1 mm higher than lane 2 for the first 700 m, the values converge beyond this point.

Table 22 contains the results of the overall multi-variable regression between L_{CPX}, and MPD and thickness. There was a negative linear correlation of -0.7 dB/10 mm between L_{CPX} and thickness. There was no significant correlation between MPD and L_{CPX}.

The A-weighted one-third octave band distribution is shown in Figure 50. 800 and 1,000 Hz were the dominant frequency bands, with significant contributions from the 500, 630, and 1,250 Hz bands. The greatest longitudinal variation occurred in the 630, 800, and 1,250 Hz bands.

The multi-variable one-third octave band correlations are shown in Figure 55. There was a weak negative correlation between MPD and thickness, which meant the components cannot be fully decoupled.

3.1.4.7 PA7 and PA10

PA7 only offered a marginally better L_{CPX} of 96.6 dB compared to the 97.1 dB of the PA10 surface; this was explored further by comparing the one-third octave band distributions and then by combining the two surfaces into one data set. All results for PA7 and PA10 can be found in Table 23, and Figure 56 to Figure 63.

The average thickness for the nominally 30 mm PA10 was 36.4 mm, which was 4.3 mm greater than the PA7. The greater average thickness of the PA10 surface may be contributing to the comparable result with PA7.

The A-weighted one-third octave band distributions are shown for both surfaces in Figure 58. PA7 had a lower L_{CPX} in all bands except the 800 to 1,250 Hz bands. The higher level for PA10 in the 315 to 630 Hz bands may be caused by its greater MPD. The lower level for PA10 in the 800 to 1,250 Hz bands was likely due to it having a greater mean thickness.

Table 23 contains the results of the overall multi-variable regression between L_{CPX}, and MPD and thickness. There was no significant correlation between MPD and L_{CPX}. There was a weak negative correlation of -0.9 dB/10 mm between L_{CPX} and thickness.

The multi-variable one-third octave band correlations are shown in Figure 63. The L_{CPX} had positive correlations with MPD in the 315 to 630, 2,000, and 2,500 Hz bands. L_{CPX} had a negative correlation with thickness in the 630 Hz band. This analysis is limited given the two surfaces have grouped MPDs, which would tend to correlate with any difference.

The effect of decreasing stone size was evident in the reduced MPD and subsequent decline in low frequency noise. The benefit of using a small stone size was likely negated by the reduced thickness of PA7 compared to PA10. When the L_{CPX} was adjusted to both surfaces having thicknesses of 30 mm using Equation 1, the levels increase to 97.3 and 99.1 dB for PA7 and PA10, respectively.

3.1.4.8 PA7 30 mm and EPA7 50 mm

The 30 mm PA7 and 50 mm EPA7 were combined to provide an extended range of thickness. The core assumption behind this analysis was that the noise characteristics of a surface are not significantly affected by the addition of epoxy.

All results for this analysis are shown in Table 24, and Figure 64 to Figure 71.

The MPD for sections of the 30 mm PA7 had an elevated MPD, which contributed to the weak negative correlation between MPD, and thickness seen in Figure 65.

The A-weighted one-third octave band distributions for both surfaces are shown in Figure 66. The 50 mm EPA7 had a lower L_{CPX} in all bands except 2,000 Hz. The greatest reductions were in the 800 and 1,000 Hz bands; these were likely due to thickness effects. The levels effectively converged below 500 Hz and above 2,500 Hz.

Table 24 contains the results of the overall multi-variable regression between L_{CPX}, and MPD and thickness. There was a positive linear correlation of 12.4 dB/mm between L_{CPX} and MPD. There was a negative correlation of -1.5 dB/10 mm between L_{CPX} and thickness. These results were limited by the collinearity between MPD and thickness. However, MPD had a 95% confidence interval of ±0.14 mm (15% of the mean), compared to the ±19 mm (45% of the mean) range of thickness, which enabled limited use of the dominant relationship with thickness. The MPD correlation should not be utilised.

The multi-variable one-third octave band correlations are shown in Figure 71. The L_{CPX} had positive correlations with MPD in the 1,000 and 1,250 Hz bands. The L_{CPX} had negative correlations with thickness in the 630, 800, and 1,000 Hz bands. The positive correlations with MPD may have been due to an increase in the noise generated by the tyre tread on the road surface. The negative thickness correlations were likely due to increasing absorption of the surface. These results are also limited by the co-linearity between MPD and thickness.

An independent comparison between L_{CPX} and thickness is shown in Figure 65. The second-order polynomial fit (Equation 1) gives an R^2 value of 0.70. Differentiation shows the rate of change of L_{CPX} with thickness (Equation 2). The frequency effect appeared to be left-shifted with thickness, which aligns with the theory of porous absorbers (Berengier, Hamet,, & Bar, 1990). It also explained the better fit for a second order model, where the dominant 1,000 Hz band becomes less affected by thickness.

$$L_{CPX} = 0.006t^2 - 0.717t + 112.9 \text{ dB} \qquad \textbf{EQUATION 1}$$

$$\frac{dL_{CPX}}{dt} = 0.012t - 0.717 \text{ dB/mm} \qquad \textbf{EQUATION 2}$$

Where t is the surface thickness in mm.

There may be scope to further improve the 50 mm EPA7 surface by reducing the average MPD by 0.1 mm or a small (up to 10 mm) increase in thickness. Other engineering requirements (e.g., skid resistance) must be considered.

3.1.4.9 SMA7, PA7 LV, PA7 HS, PA7

The one-third octave band distributions for SMA7, PA7 LV, PA7 HS, and PA 7 are shown in Figure 4. All surfaces are nominally 30 mm thick and have a stone size of 7 mm.

Lack of improvement of PA7 over SMA was likely due to the elevated surface texture of the PA7 having a higher generation level in the 1000 Hz band. Void fraction may have been the cause of the lower levels in the 1600 to 2500 Hz bands; further analysis is required to isolate and quantify this.

PA7 HS had lower L_{CPX} through the 800 to 1250 Hz bands compared to the PA7; the cause of this difference is unknown. The improvement at lower frequencies was likely driven by decreased MPD for the PA7 HS.

Similar MPD and thickness between PA7 LV and PA7 HS, allowed for an indicative comparison of nominal void fraction. These differed through 800 to 1600 Hz. There was likely a small thickness effect in the 800 and 1000 Hz bands. The residual reduced level of the PA7 HS in the 1250 and 1600 Hz bands may be attributable to void fraction and absorption effects. Further analysis is required to understand the actual effects of void fraction.

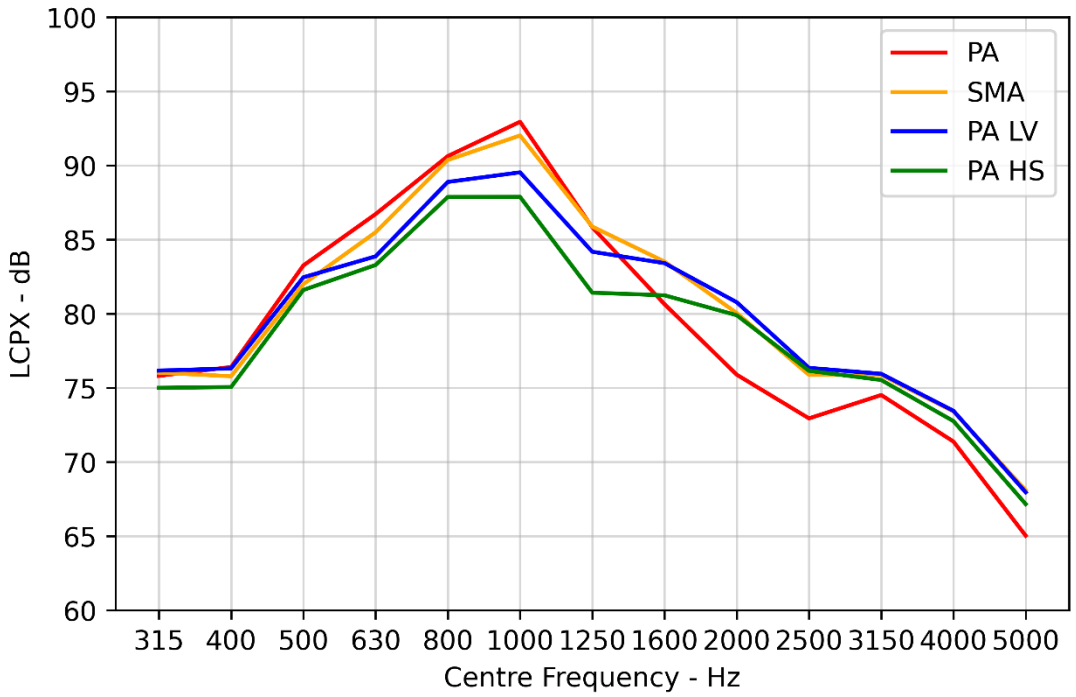

FIGURE 4. ONE-THIRD OCTAVE BAND DISTRIBUTIONS FOR PA, SMA, PA7 LV, AND PA7 HS ON CNC.

3.2 CSM2

3.2.1 Overall Results

The mean L_{CPX}, MPD, and thickness for each lane are shown in Table 7. Longitudinal plots of L_{CPX}, MPD, and thickness are shown in Figure 5. All other results can be found in Table 25, and Figure 74 to Figure 80

TABLE 7. MEAN L_{CPX}, MPD, AND THICKNESS FOR SB AND NB LANES ON CSM2.

	SB	NB	SB & NB*
Surface	EPA7 40 mm	EPA7 40 mm	
Length – m	1,620 m	1,120	2,740
L_{CPX} – dB	93.8	94.2	94.0
L_{CPX} – n	81	56	137
MPD – mm	0.94	0.98	0.97
MPD – n	162	112	274
Thickness - mm	44.4	42.6	43.3
Thickness - n	540	370	910

*Mean is weighted on length.

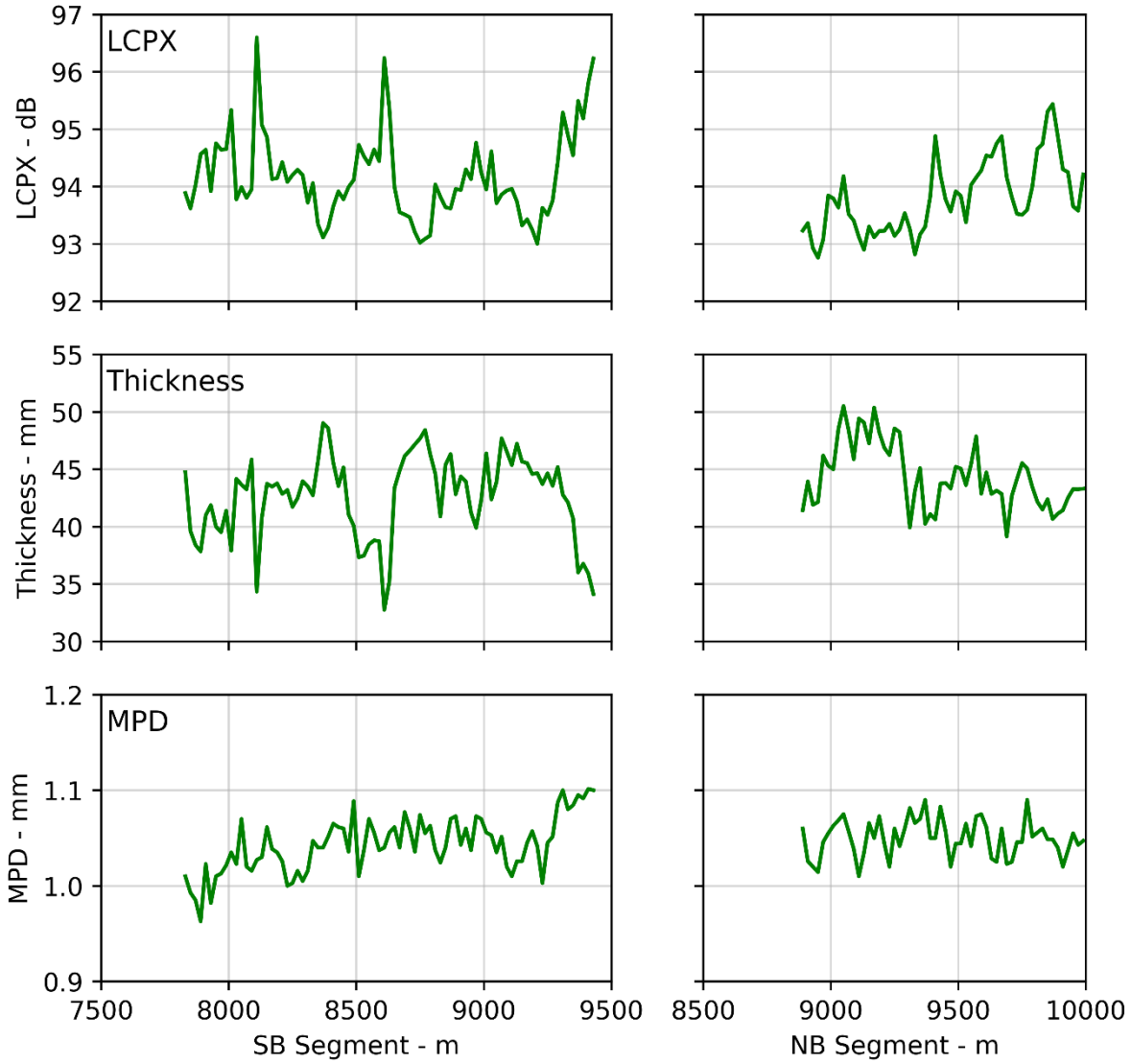

FIGURE 5. EPA7 ON CSM2. LONGITUDINAL PLOTS OF L_{CPX}, THICKNESS, AND MPD.

3.2.2 Detailed Observations

The overall average L_{CPX} of 94.0 dB for both lanes represented a quiet surface. The L_{CPX} varied from 92.8 to 96.6 dB, which can be primarily attributed to variations in thickness and MPD. The greatest range of parameters occurred in the Southbound lane for the analysed sections.

The MPD and thickness were weakly correlated in the Northbound lane, therefore the multi-variable analysis was limited to the Southbound lane. Table 25 contains the results of the overall multi-variable regression between L_{CPX}, and MPD and thickness. The overall regression had an R^2 value of 0.74. There was a positive linear correlation of 4.5 dB/mm between L_{CPX} and MPD. There was a negative linear correlation of -1.7 dB/10 mm between L_{CPX} and thickness.

The A-weighted one-third octave band distribution is shown in Figure 75. The distribution was relatively flat, with the dominant frequency range being 500 to 1,250 Hz. The greatest longitudinal variation occurred in the 500 to 800, 1,250, and 1,600 Hz bands.

The multi-variable one-third octave band correlations are shown in Figure 80. The L_{CPX} had positive correlations with MPD in the 1,250 and 1,600 Hz bands. L_{CPX} had negative correlations with thickness in the 630 to 1,000, 2,000, and 2,500 Hz bands. The L_{CPX} had positive correlations with thickness in the 1,250 and 1,600 Hz bands.

The large range of thickness allowed for further grouping into three bands, 30-35, 37.5-42.5, and 45-50 mm. The A-weighted one-third octave band distributions are shown in Figure 6 for each grouping. There was no thickness effect in the 315 to 500, and 3,150 to 5,000 Hz bands. There appeared to be a left-shift in the absorption frequency with increasing thickness.

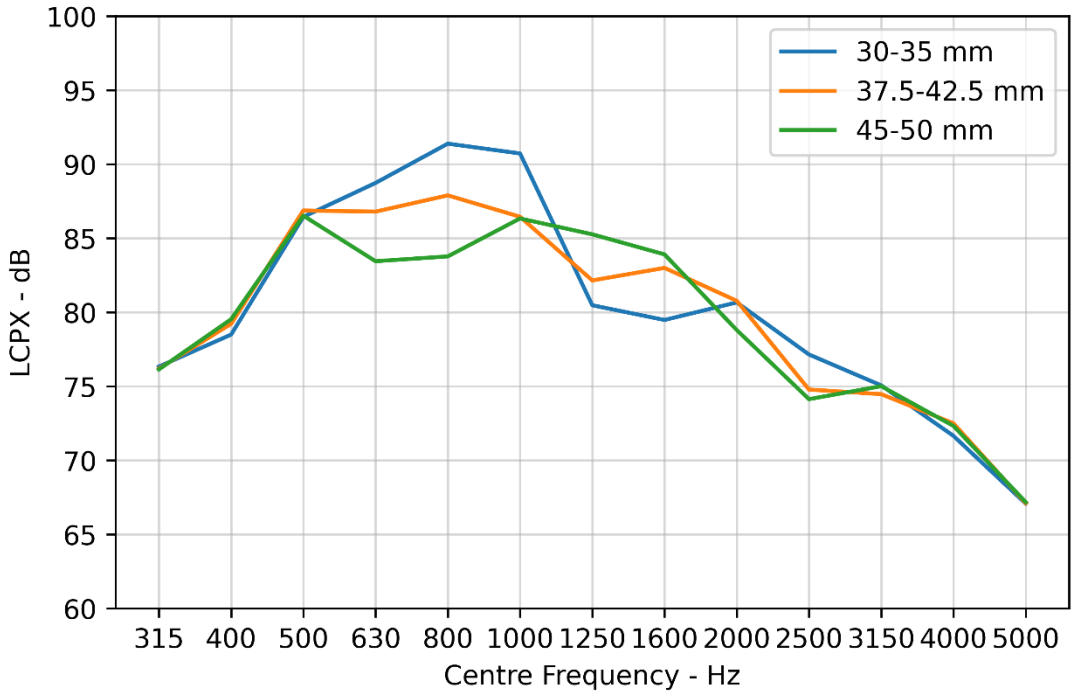

FIGURE 6. EPA7 ON CSM2. ONE-THIRD OCTAVE BAND DISTRIBUTIONS FOR THREE THICKNESS GROUPS.

Independent comparison between L_{CPX} and thickness is shown in Figure 74. The second-order polynomial fit (Equation 3) gives an R^2 value of 0.56. Differentiating the second order fit (Equation 4) showed there was diminishing reductions with increasing thickness. The limit could not be extrapolated from the current data, but may be 50-60 mm. The diminishing return on thickness may be due to moving the absorption frequency outside of the primary noise generation bands.

$$L_{CPX} = 0.008t^2 - 0.806t + 114.4 \text{ dB} \quad \text{EQUATION 3}$$

$$\frac{dL_{CPX}}{dt} = 0.016t - 0.806 \text{ dB/mm} \quad \text{EQUATION 4}$$

Where t is the surface thickness in mm.

3.3 S2G

3.3.1 Overall Results

The mean L_{CPX} and MPD for each surface type are shown in Table 8. Boxplots for all measurement points of L_{CPX} and MPD for each surface type are shown in Figure 7. All other results can be found in Figure 81 to Figure 84.

TABLE 8. MEAN L_{CPX} AND MPD FOR EACH TRIAL SURFACE ON S2G IN MAR 2019.

	EPA10	EPA10 HV	EPA14
L_{CPX} – dB	94.8	96.6	99.0
MPD – mm	1.23	1.42	1.76

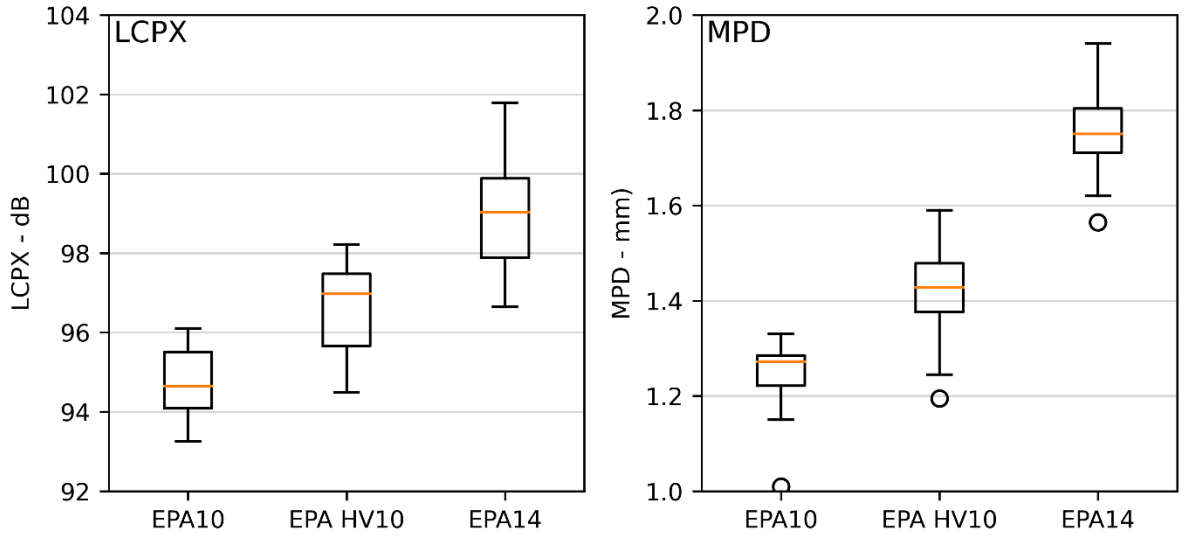

FIGURE 7. S2G TRIAL SITES. BOXPLOTS OF OVERALL L_{CPX} AND MPD.

3.3.2 Detailed Observations

The EPA10 was the quietest of the three surface types, followed by the EPA10 HV, and then EPA14. There were large intra-surface ranges (7 dB) in the overall L_{CPX}. Changes in L_{CPX} appeared to be dominated by surface texture. For all surface types, lane 1 was approximately 1 dB quieter, the reason cannot be explicitly determined with the available data but may have been due to increased mean thickness, construction processes, or other factors.

Figure 82 shows the relationship between L_{CPX} and MPD for all surfaces. There were no intra-surface correlations. The linear correlations were calculated separately for each lane. There was a positive correlation between L_{CPX} and MPD of 5.4 to 6.5 dB/mm. The lack of intra-surface correlations may be due to misalignment of MPD and CPX segments, dominant thickness variation effects, or other factors.

The A-weighted one-third octave band distributions are shown in Figure 81. All surface types were dominated by the 500 to 1000 Hz bands, with the peak in the 800 Hz band. Levels converged for all surfaces above 2500 Hz. There may have been a void-fraction effect in the 1600 Hz band. The EPA10 and EPA14 sections

had a greater (similar) level than the EPA10 HV section; this is in the approximate range of the second absorption peak for porous surfaces.

The one-third octave band correlations between L_{CPX} and MPD are shown in Figure 84. MPD had significant positive correlations with L_{CPX} in the 315 to 800 Hz bands, and a weak positive correlation in the 1,000 Hz band.

There may be a relationship between L_{CPX} and texture wavelength due to stone size; detailed texture data would be required to investigate this hypothesis.

3.3.3 Ageing

All results pertaining to ageing are in Figure 85 to Figure 90.

The overall L_{CPX} level and MPD are shown in Figure 85 and Figure 86, respectively. The L_{CPX} was decreasing with time for the EPA10 HV and EPA14 but was unchanged for EPA10. The MPD was decreasing for all surfaces with time, with a greater decreasing rate in lane 2. It is assumed the greater rate of decrease in lane 2 is due to higher traffic and more heavy vehicles.

The longitudinal variability is shown in Figure 87 to Figure 89. There was significant variation in the longitudinal rate of change for lane 1 in the EPA14 section. There was generally a stable rate throughout the mid-sections of the other surface types. It is hypothesised that the increasing rate at the upper end of the EPA10 section was due to debris tracking from the adjacent SMA section.

The one-third octave band rates of change with time are shown in Figure 90. For all surface types, the rate was negative in the 400 to 800 Hz bands, and positive in the 1,600 to 5,000 Hz bands. There was no consistent ageing effect in the 315 Hz band. There was no change in the 1,000 Hz band for EPA10, but negative rates for both the EPA10 HV and EPA14.

The decreasing rates in the 400 to 800 Hz bands were likely due to the reducing surface texture. This aligns with the EPA10 being stable with time, while the EPA10 HV and EPA14 are decreasing as they essentially have more texture to degrade with time.

The increasing rates in the 1,600 to 5,000 Hz bands may be attributable to decreasing void fraction due to debris collection. The EPA10 HV section was only less susceptible in the 1,250 Hz band. As these were not the current dominant frequency bands, they have little effect on the overall level.

It is not known why the 315 Hz band was not changing with time given it is correlated strongly with MPD. There may be a texture characteristic that was unchanged with time, such as wavelength. Given the minimal contribution of the 315 Hz band, this was not considered for further analysis.

3.4 Overall Thickness

Table 9 contains a summary of the change of overall L_{CPX} as a function of thickness. These are only for porous surfaces with a nominal void fraction of 20-25% and a nominal stone size of 7 mm. The first-order linear models are based on multi-variable fits with MPD. The second-order models are based on independent correlations with L_{CPX} and thickness.

TABLE 9. OVERALL L_{CPX} VS. THICKNESS.

	CNC		CSM2	
Thickness	1st Order	2nd Order	1st Order	2nd Order
		dB/10 mm		
30 mm	-1.50±0.34**	-3.57	-1.72 ±0.24**	-3.26
40 mm		-2.37		-1.66
50 mm		-1.17		-*

*50 mm is the upper limit of the available data.

**95% confidence interval.

The greatest benefit of increasing thickness occurred at 30 mm, with a marginal benefit at 50 mm. Increasing thickness offered a diminishing improvement in the overall L_{CPX}. The limited improvement in thickness likely arises from shifting the absorption peak of the porous surface outside of the maximum A-weighted frequency bands and the primary noise generation mechanisms. It should be noted that this is limited to the CPX measurement configuration only and further benefits may be realised in the actual application. The optimal maximum viable single-layer thickness may be 50-60 mm; this does not consider ageing effects.

For low-void (<10%) surfaces, there was a small benefit to increasing thickness in the 500 Hz band. For porous (>20%) surfaces, the benefit occurred in the 500 to 1,000 Hz bands. The levels in the 1,250 and 1,600 Hz bands were positively correlated with thickness; this was likely due to the absorption peak moving to lower frequencies with increasing thickness.

3.5 Overall MPD

Table 10 contains a summary of the rate of change of L_{CPX} as a function of MPD.

TABLE 10. OVERALL L_{CPX} VS. MPD.

	CNC	CSM2	S2G
Surface	SMA7	EPA7	EPA10/14/HV
MPD*	0.7-0.85 mm*	0.98-1.10 mm	1.00-2.00 mm
Slope - dB/mm	11.0±6.4** dB/mm	4.5±3.0** dB/mm	6.0±1.2** dB/mm

*CNC MPD sourced from the Road Science Hawkeye system.

** 95% confidence interval.

There appeared to be a stronger correlation between L_{CPX} and MPD for non-porous surfaces. The correlation was similar between the porous surfaces on CSM2 and S2G.

Low-void surfaces exhibited positive correlations in the lower frequency (<1,000 Hz) bands and negative correlations in the higher (>1,250 Hz) bands. Higher void fraction (>20%) surfaces only showed positive correlations in the lower frequency bands (<1,000 Hz) for S2G, with positive correlations in the 1,250 and 1,600 Hz bands for CSM2 and CNC.

There were only strong positive correlations in the lower frequency bands for surfaces with higher absolute MPD levels. This may be due to either the limited range of MPD for the smoother surfaces or there may be a physical phenomenon that requires further investigation to describe.

For non-porous surfaces, there may be an optimal MPD to achieve a minimum L_{CPX}; this does not account for other engineering requirements. For porous surfaces, L_{CPX} appeared to be positively correlated with MPD and had no observed lower limit; the porosity may be enabling the dispersion of air at the forward tyre-road interface.

4 Future Investigations

The following list summarises potential topics for future investigations.

- Determining the effect of construction parameters on final surface characteristics (e.g., paving speed and temperature, transfer vehicle, paving width, etc.).
- Determine the relationship between void fraction, thickness and L_{CPX}.
- Develop a methodology for in situ measurements of void fraction and/or surface absorption characteristics; this may be used for quantifying clogging and ageing effects.
- Determine the relationship between void fraction and macrotexture.
- Investigate long-term ageing effects (>5 years).
- Investigate ageing effects on non-porous surfaces.
- Characterise texture and its effect on noise generation. Review skid resistance requirements.
- Investigate and characterise noise generation mechanisms.
- Reprocess CNC trial sections with either HSD or CPX-laser data.

Given the opportunity for further trial sites, it is recommended to evaluate the following:

- High strength (void fraction 12-16%) surfaces with increased thickness and control surfaces:
  - EPA7 40 mm (control)
  - EPA7 HS 30 mm (duplicating initial result)
  - EPA7 HS 40 mm
  - EPA7 HS 50 mm
- EPA7 30 mm surface with minimum MPD (i.e., 0.7-0.8 mm).

5 Conclusions

The relationships between L_{CPX}, and MPD and thickness were explored for multiple projects and surface types. The parameters were explored independently and together for the overall level and one-third octave bands. Ageing effects were evaluated for several surface types.

Variations in thickness and MPD accounted for most of the measured changes in L_{CPX} for the evaluated projects. Multi-variable regressions between thickness, MPD, and L_{CPX} for CNC and CSM2 accounted for 79 and 74% of the longitudinal variability, respectively.

There was a strong relationship between thickness and the overall L_{CPX} for porous (>20%) surfaces. The correlation is negative and non-linear, and varied from -3.6 to -1.2 dB per 10 mm of thickness at 30 and 50 mm thicknesses, respectively.

MPD had a strong relationship with the overall L_{CPX}. The correlation is positive and linear and varies depending on the void fraction of the surface. The correlation was 11 dB per mm of MPD for a short section of SMA, and 6 dB per mm of MPD for surfaces with void fractions greater than 20% (S2G).

The high-strength porous asphalt on CNC demonstrated the best noise performance for comparable thicknesses – a review of skid resistance is required.

The 50 mm EPA7 on CNC demonstrated the best overall L_{CPX} at 92.1 dB. Limited improvements may be achieved through reducing MPD and a further increase in thickness. It is recommended that void fraction is explored in a future study to understand the underlying interactions with noise and any potential improvements.

6 References

Berengier, M., Hamet,, F., & Bar, P. (1990). *Acoustical properties of porous asphalts: theoretical and environmental aspects.* Transportation Research Record. (1265).

Bull, J. (2019). *Road surface noise research - Porous asphalt variability study.* Christchurch, New Zealand: Altissimo Consulting Ltd.

Bull, J., Wareing, R., Chiles, S., & Jackett, R. (2021). Investigating the effect of layer thickness on the variability of porous asphalt tyre/road noise. In N. a. Environmental Sustainability of Road Transport: Air Pollution (Ed.), *PIARC International Seminar.* Cluj-Napoca, Romania: PIARC International Seminar.

Hamet, J. F. (2004). *Reduction of tire road noise by acoustic absorption: Numerical evaluation of the pass-by noise level reduction using the normal incidence acoustic absorption coefficient.* Bron Cédex - France: Laboratoire Transport et Environnement.

Jackett, R. (2021). *Road Surface Noise Corrections - Part 1: Large CPX Survey of Road Surfaces.* Lower Hutt, New Zealand: WSP Research.

Peeters, B., & Kuijpers, A. (2008). The effect of porous road surfaces on radiation and propagation of tyre noise. *Journal of the Acoustical Society of America*, 123(5), 3673-3673.

Wareing, R. (2022). Canterbury Road Surface Noise 2022 Measurement Summary.

Wareing, R., Bull, J., Chiles, S., & Jackett, R. (2021). Optimising New Zealand's State highway low-noise road surface. *Environmental Sustainability of Road Transport: Air Pollution, Noise and Relationship with Energy Transition and Climate Change.* Cluj-Napoca, Romania: PIARC International Seminar.

7 Appendix A - Detailed Results

7.1 Christchurch Northern Corridor (CNC)

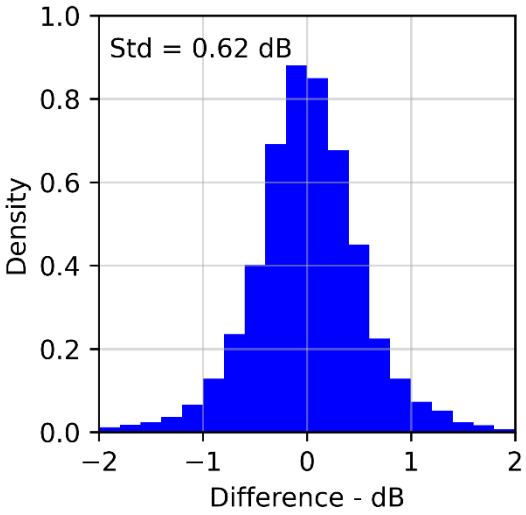

FIGURE 8. DISTRIBUTION OF DIFFERENCE BETWEEN 4 M L_{CPX} AND 20 M L_{CPX} FOR ALL CNC DATA.

7.1.1 SMA7

TABLE 11. SMA7 ON CNC. SUMMARY OF RESULTS.

	L_{CPX}	Thickness	MPD
Samples	212	26	212
Mean	96.2 dB	27.1 mm	0.82 mm
Std	0.96 dB	2.56 mm	0.05 mm

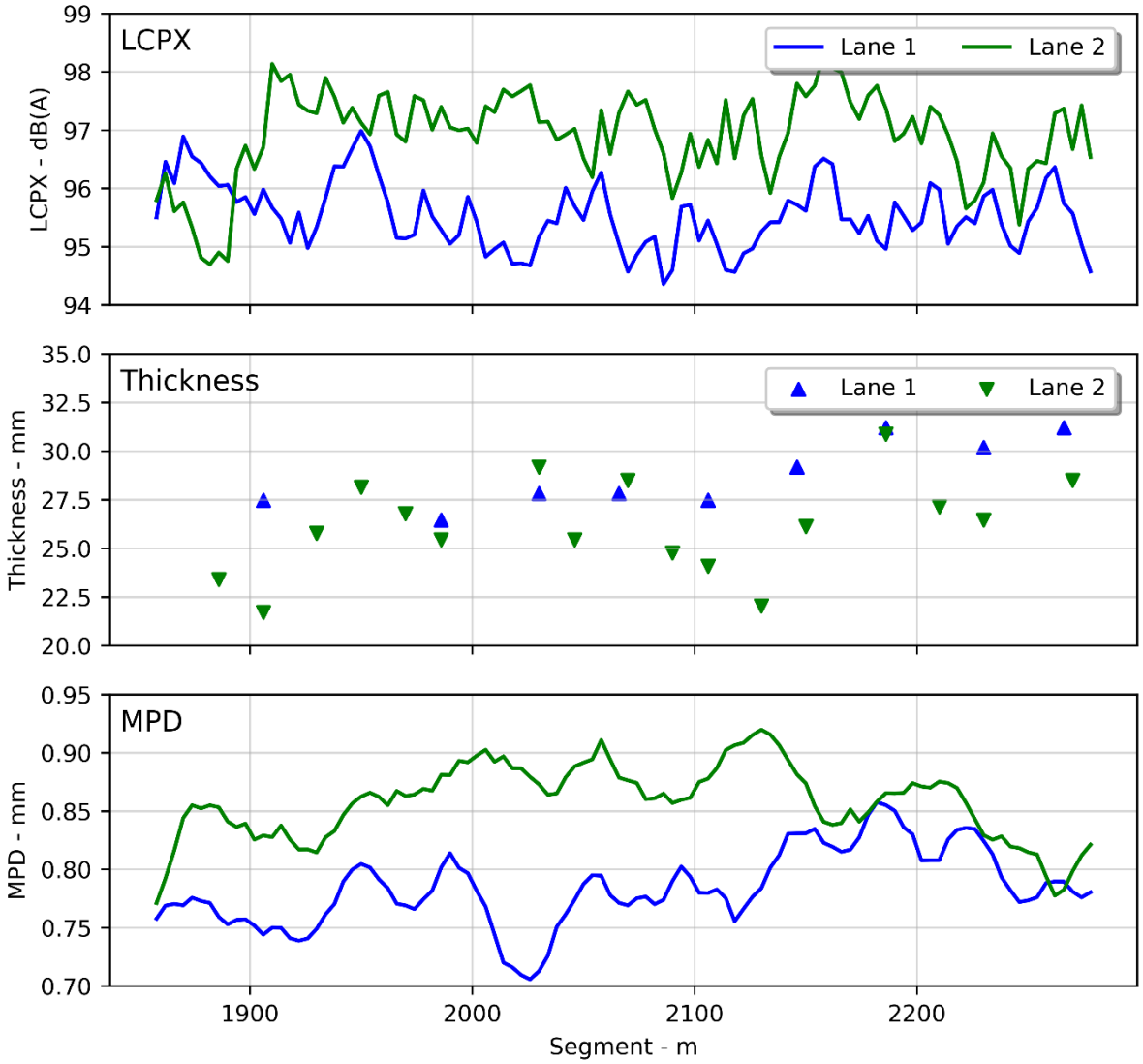

FIGURE 9. SMA7 ON CNC. LONGITUDINAL PLOTS OF L_{CPX}, THICKNESS, AND MPD.

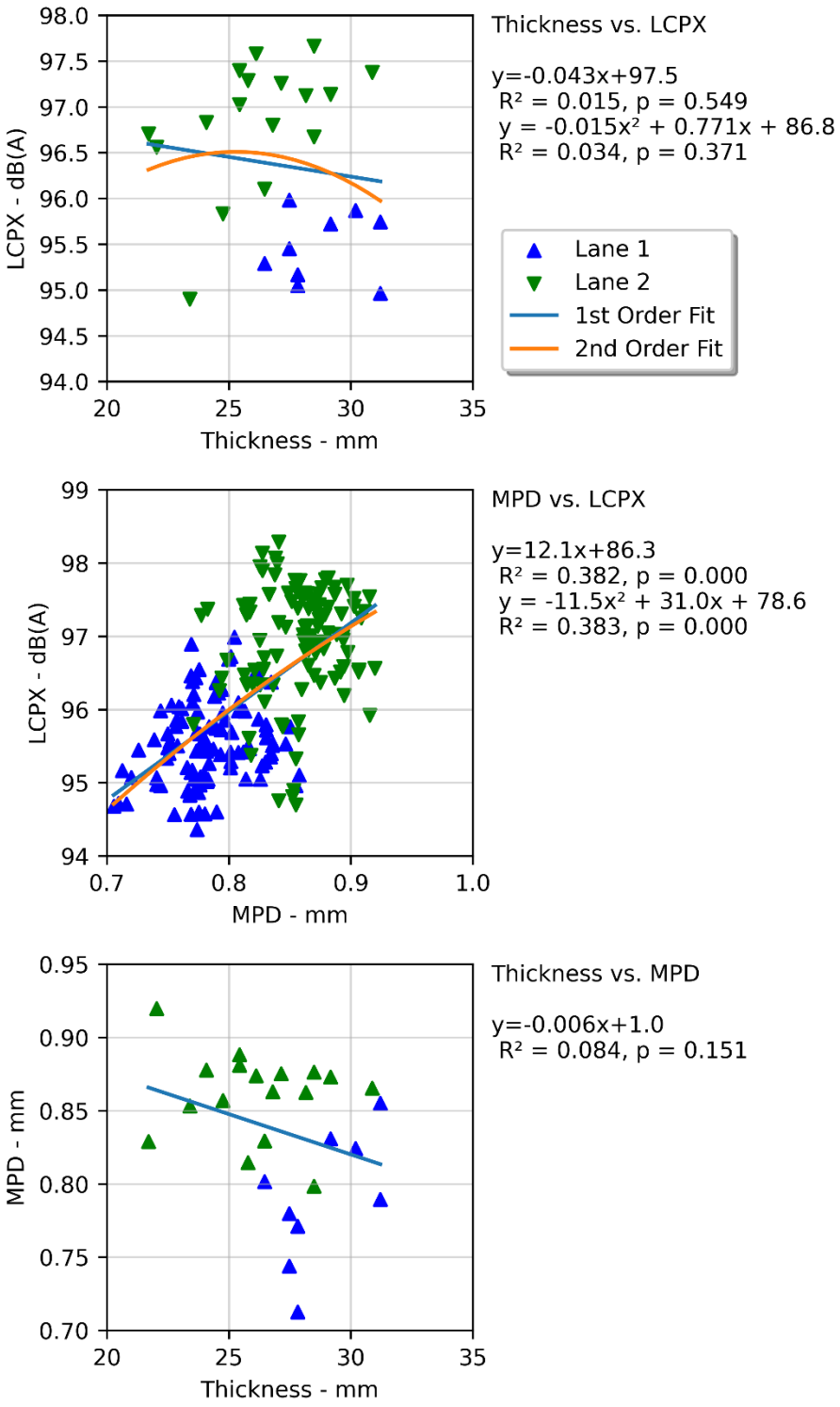

FIGURE 10. SMA7 ON CNC. L_{CPX} VS. THICKNESS, L_{CPX} VS. MPD, AND MPD VS. THICKNESS.

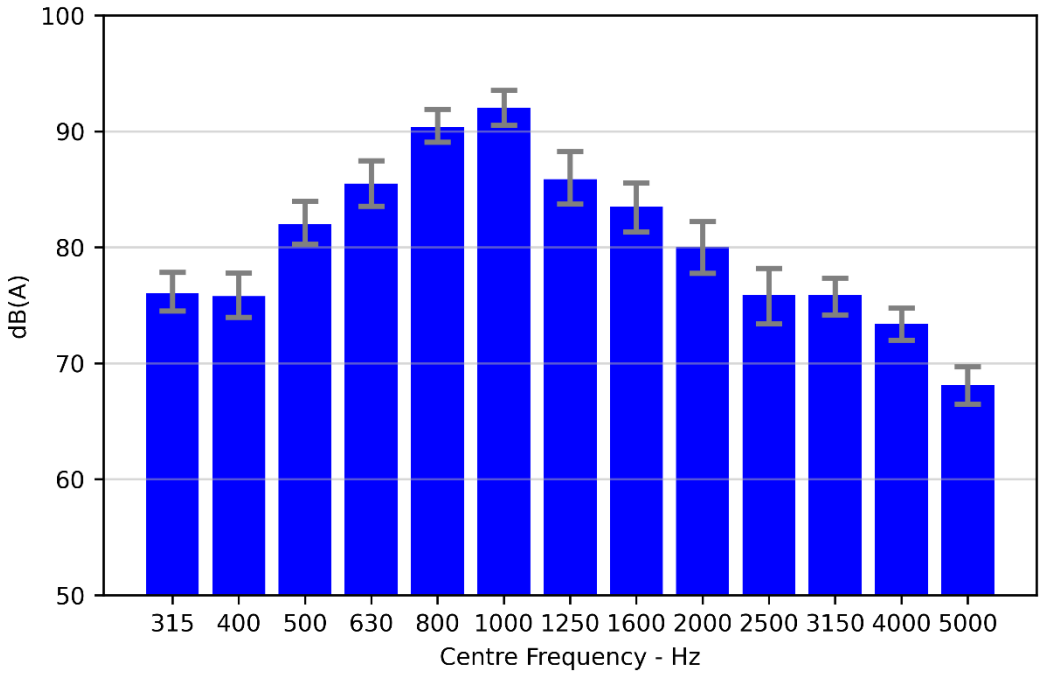

FIGURE 11. SMA7 ON CNC. ONE-THIRD OCTAVE BAND DISTRIBUTION WITH 10-90TH PERCENTILE VARIATION.

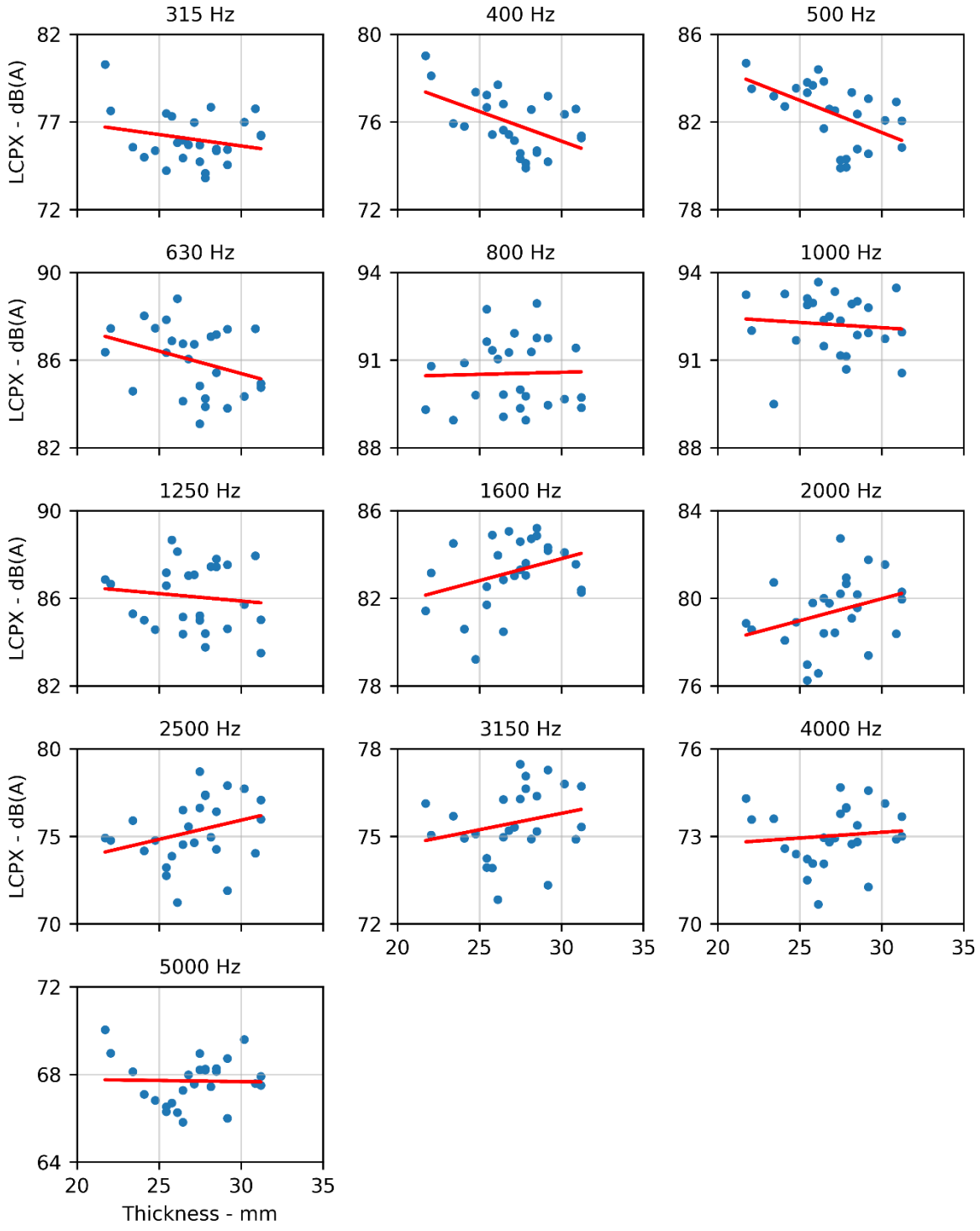

FIGURE 12. SMA7 ON CNC. ONE-THIRD OCTAVE BAND L_{CPX} VS. THICKNESS.

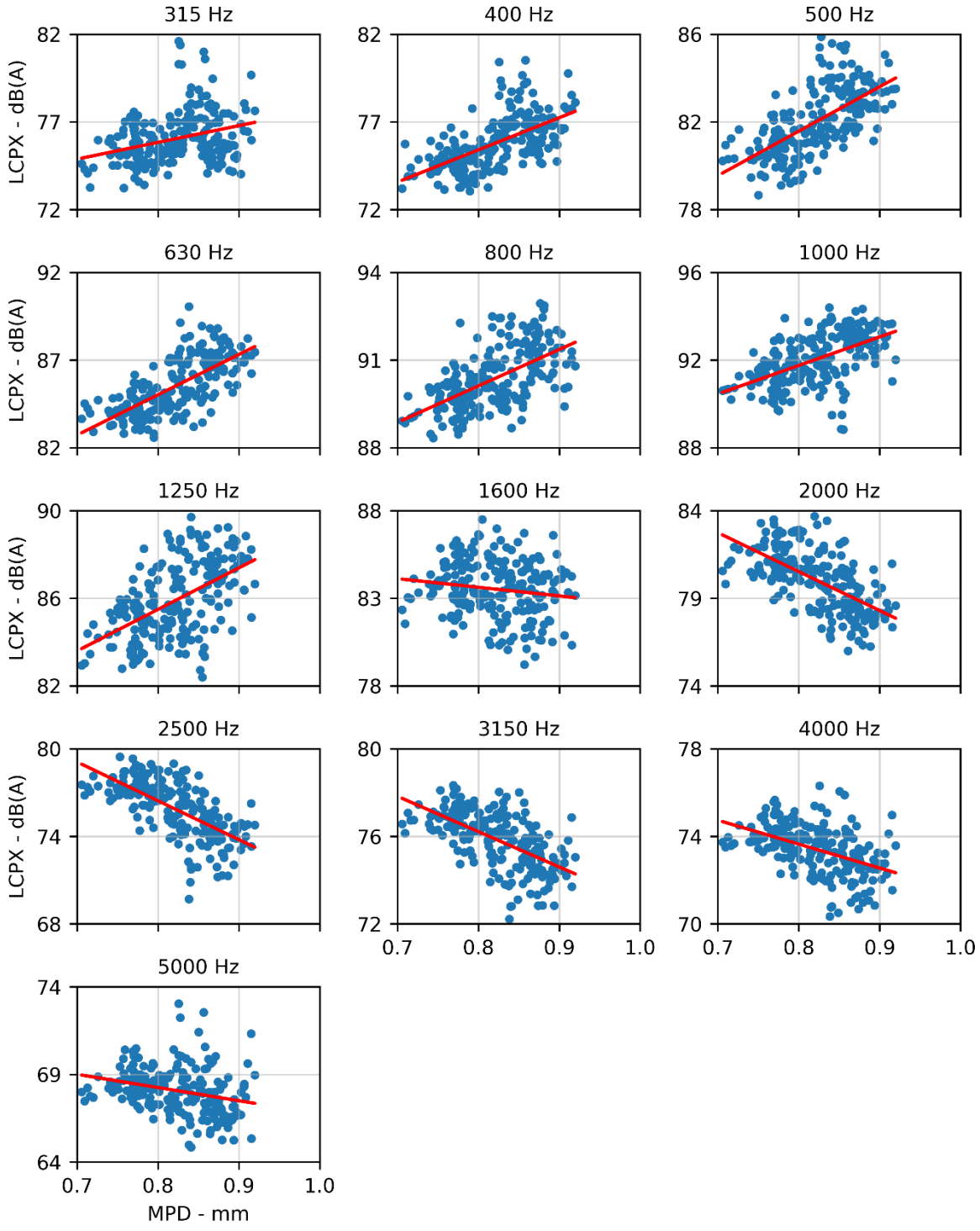

FIGURE 13. SMA7 ON CNC. ONE-THIRD OCTAVE BAND L_{CPX} VS. MPD.

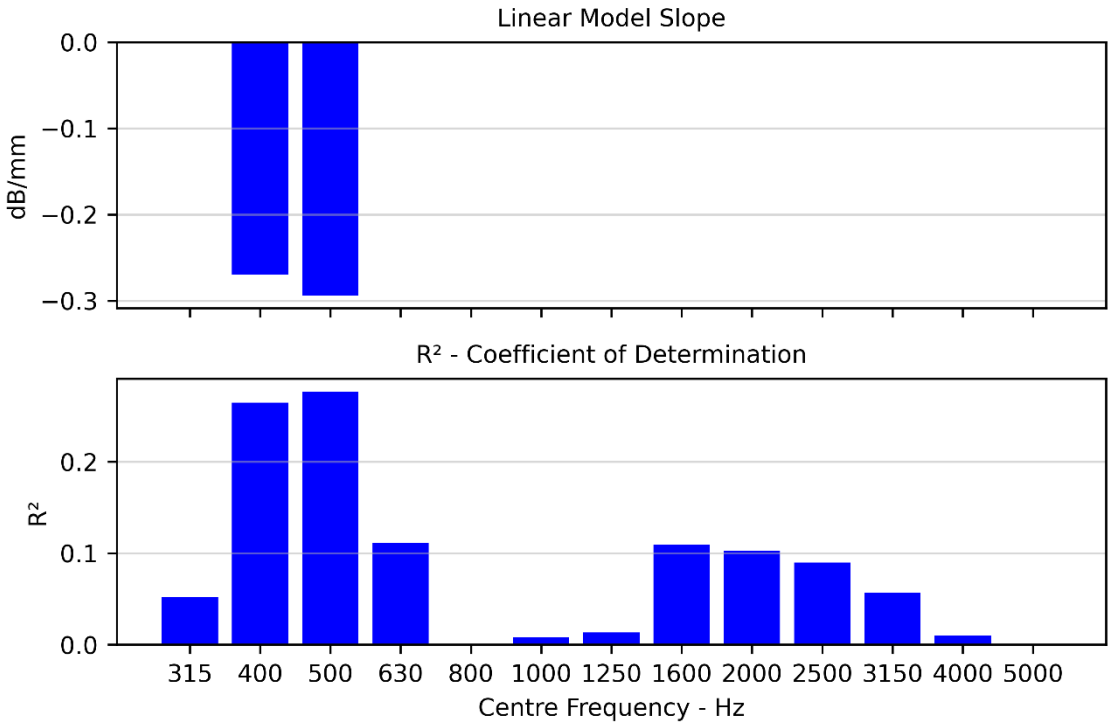

FIGURE 14. SMA7 ON CNC. ONE-THIRD OCTAVE BAND L_{CPX} AND THICKNESS CORRELATIONS. TOP CHART IS THE LINEAR FIT SLOPE AND BOTTOM CHART IS COEFFICIENT OF DETERMINATION (R^2). MAXIMUM P-VALUE OF 0.025.

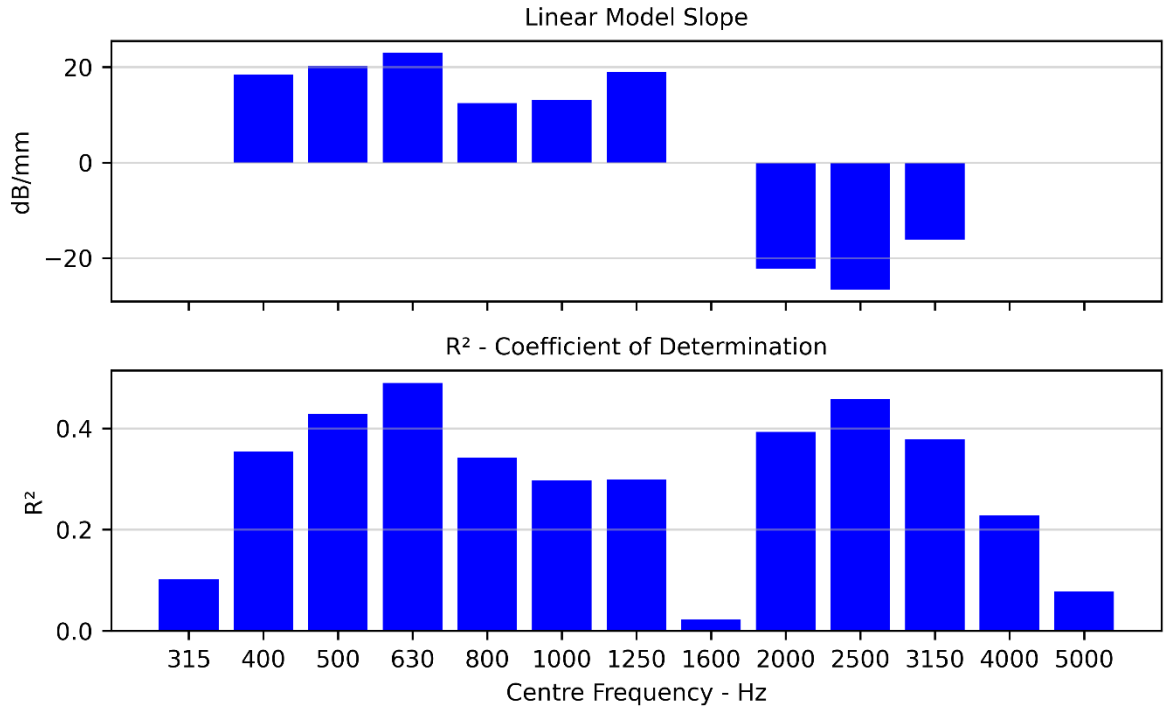

FIGURE 15. SMA7 ON CNC. ONE-THIRD OCTAVE BAND L_{CPX} AND MPD CORRELATIONS. TOP CHART IS THE LINEAR FIT SLOPE AND BOTTOM CHART IS COEFFICIENT OF DETERMINATION (R^2). MAXIMUM P-VALUE OF 0.025.

TABLE 12. SMA7 ON CNC. MULTI-VARIABLE LINEAR REGRESSION BETWEEN L_{CPX}, MPD, AND THICKNESS.

R^2	0.35	
Adj. R^2	0.29	
Thickness	-	p = 0.773
MPD	11.0 dB/mm	p = 0.002

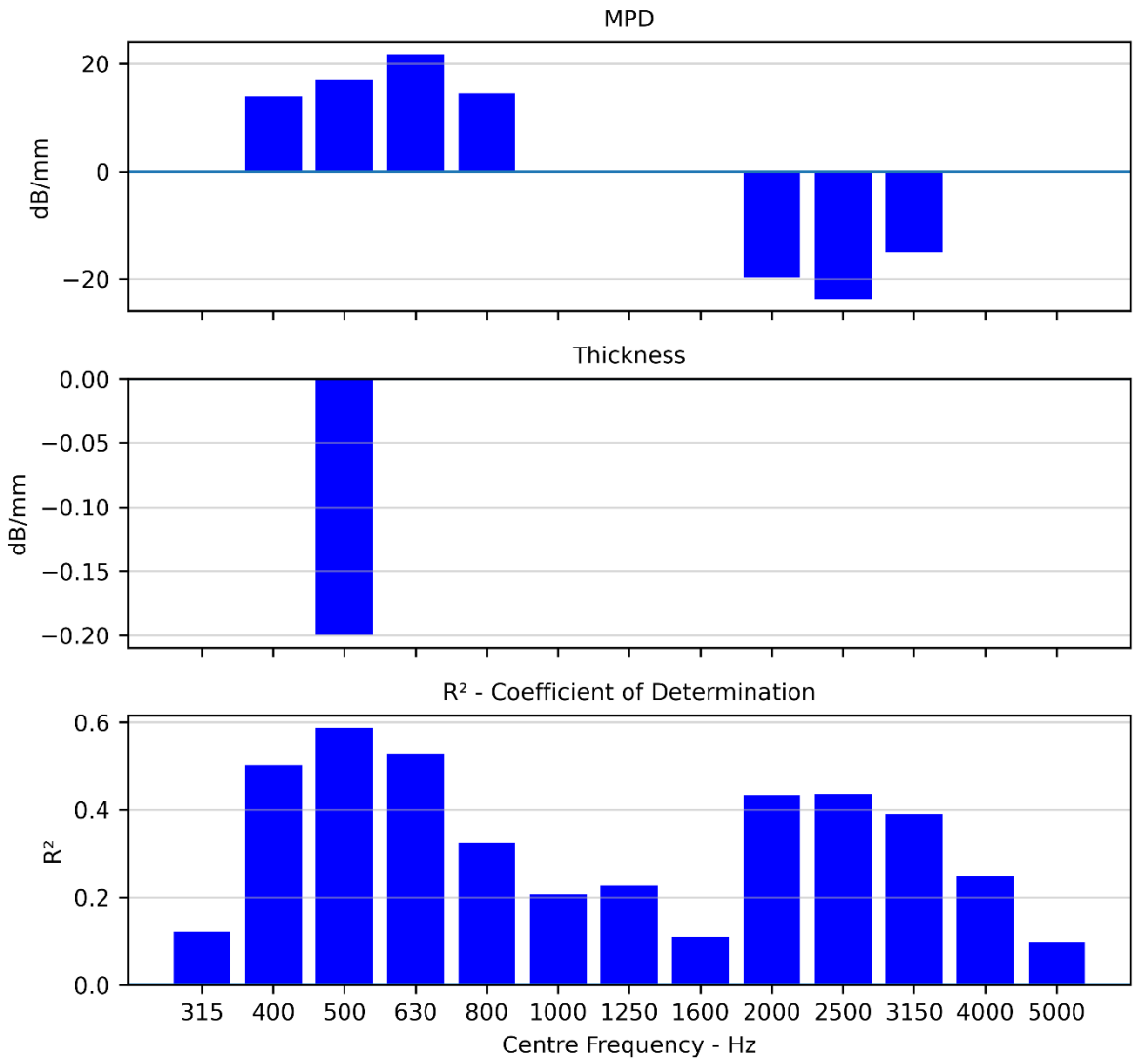

FIGURE 16. SMA7 ON CNC. ONE-THIRD OCTAVE BAND L_{CPX} VS. MPD AND THICKNESS CORRELATIONS. MAXIMUM P-VALUE OF 0.025.

7.1.2 PA7 LV

TABLE 13. PA7 LV ON CNC. SUMMARY OF RESULTS.

	L_{CPX}	Thickness	MPD
Samples	180	23	180
Mean	94.7 dB	30.1 mm	0.75 mm
Std	0.8 dB	3.3 mm	0.04 mm

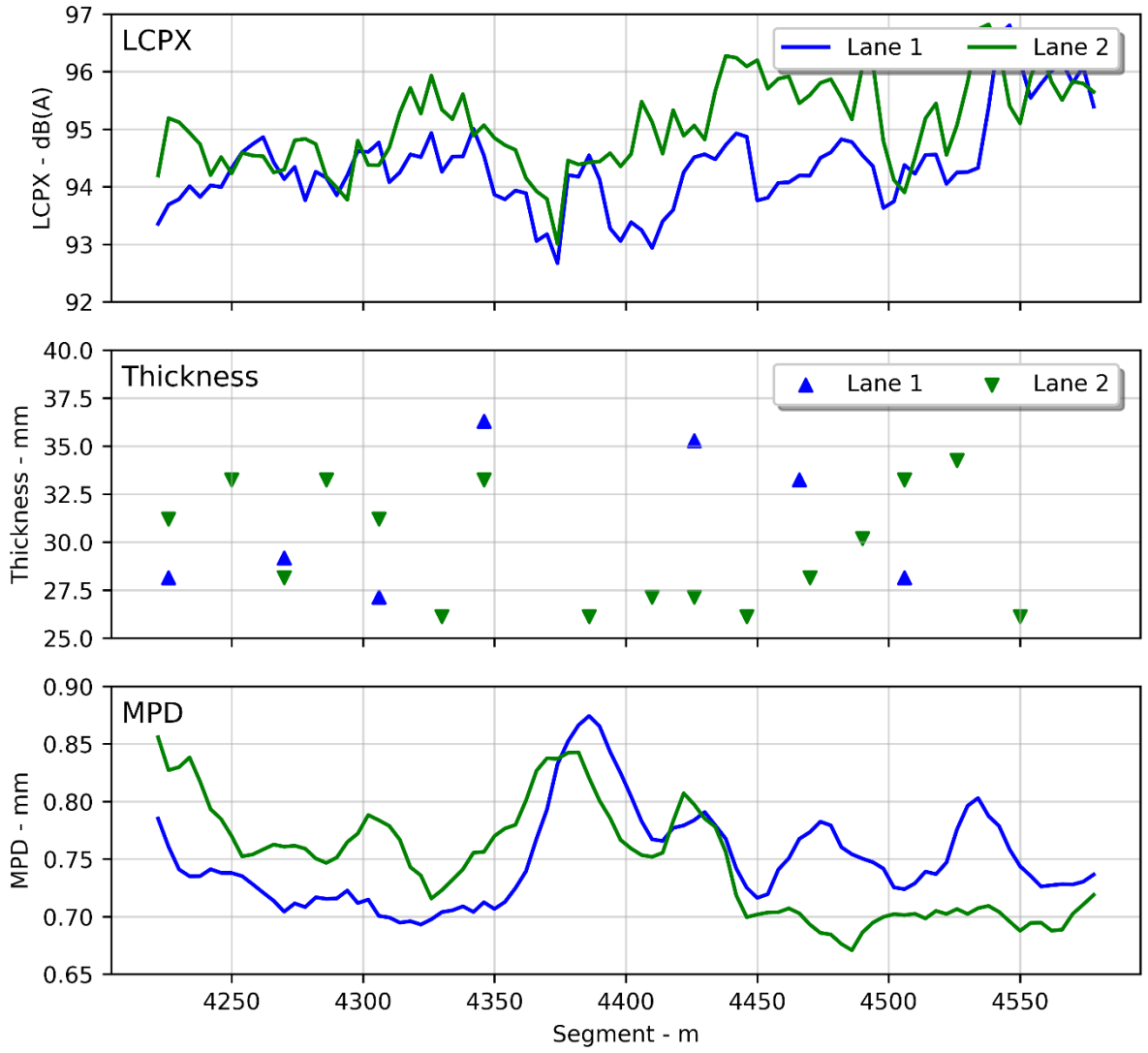

FIGURE 17. PA7 LV ON CNC. LONGITUDINAL PLOTS OF L_{CPX}, THICKNESS, AND MPD.

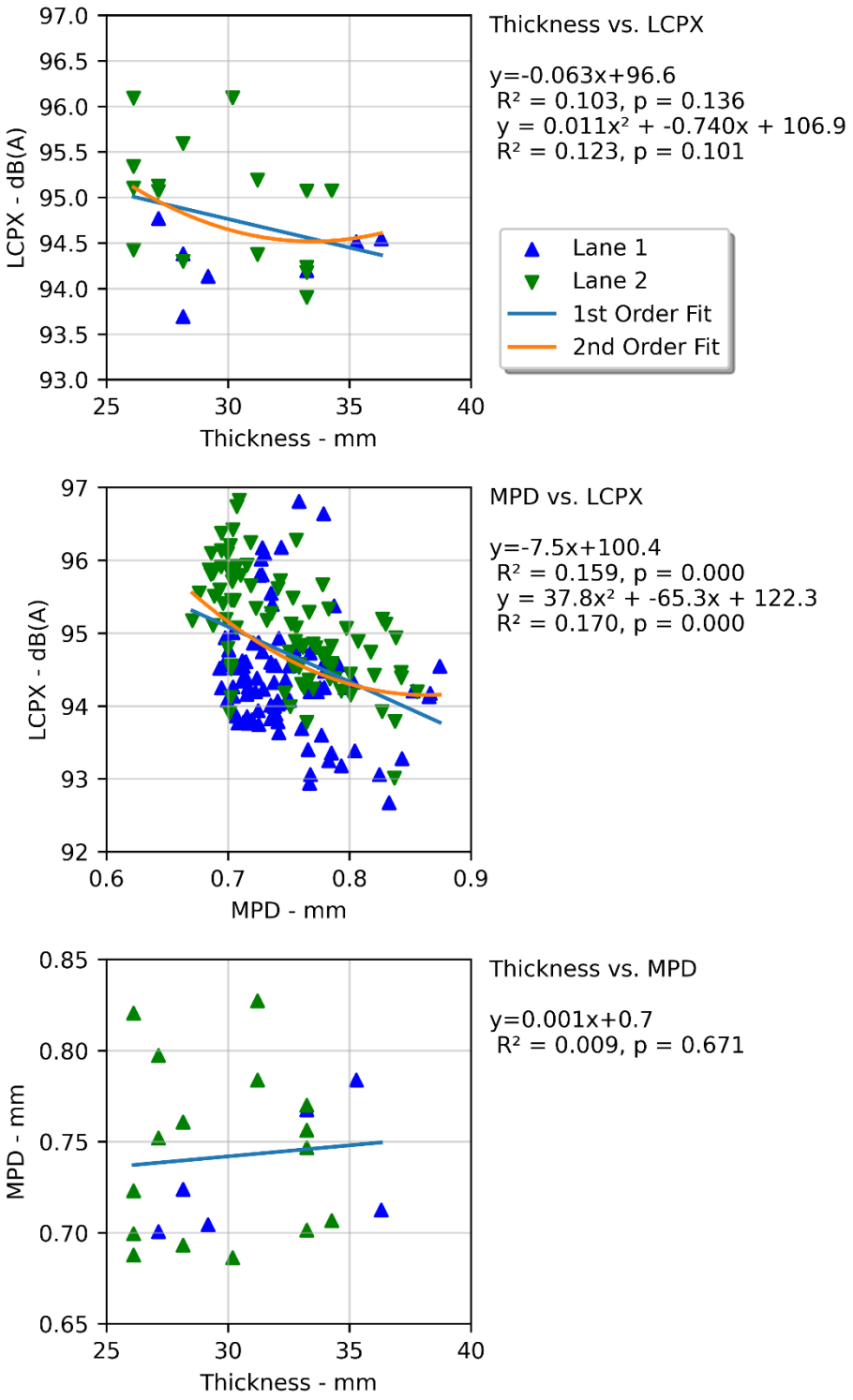

FIGURE 18. PA7 LV ON CNC. L_{CPX} VS. THICKNESS, L_{CPX} VS. MPD, AND MPD VS. THICKNESS.

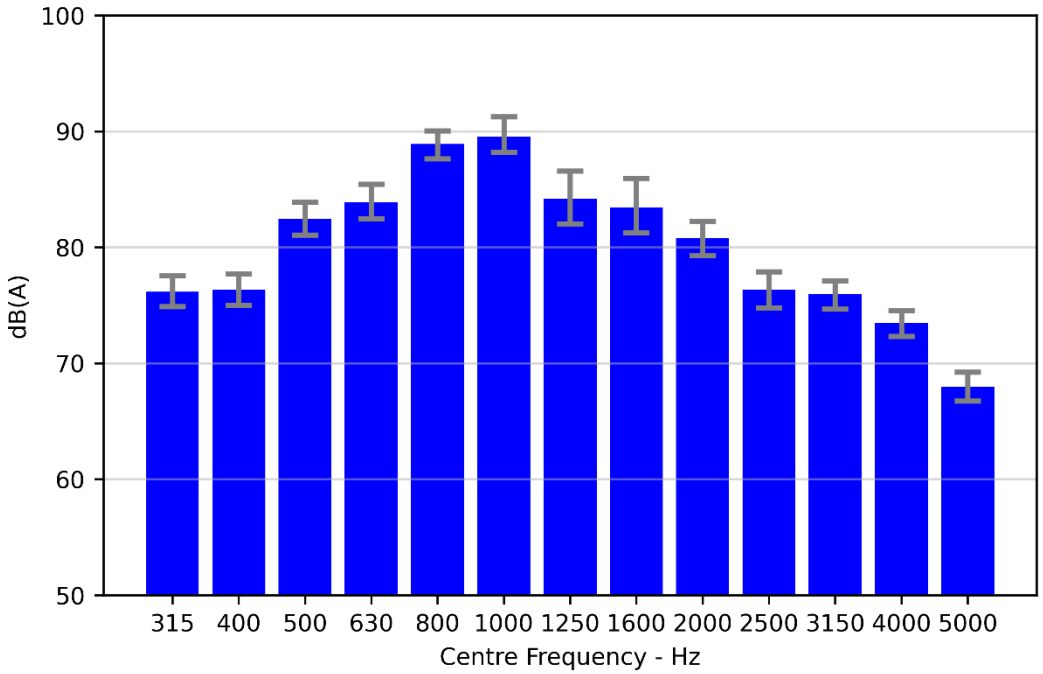

FIGURE 19. PA7 LV ON CNC. ONE-THIRD OCTAVE BAND DISTRIBUTION WITH 10-90TH PERCENTILE VARIATION.

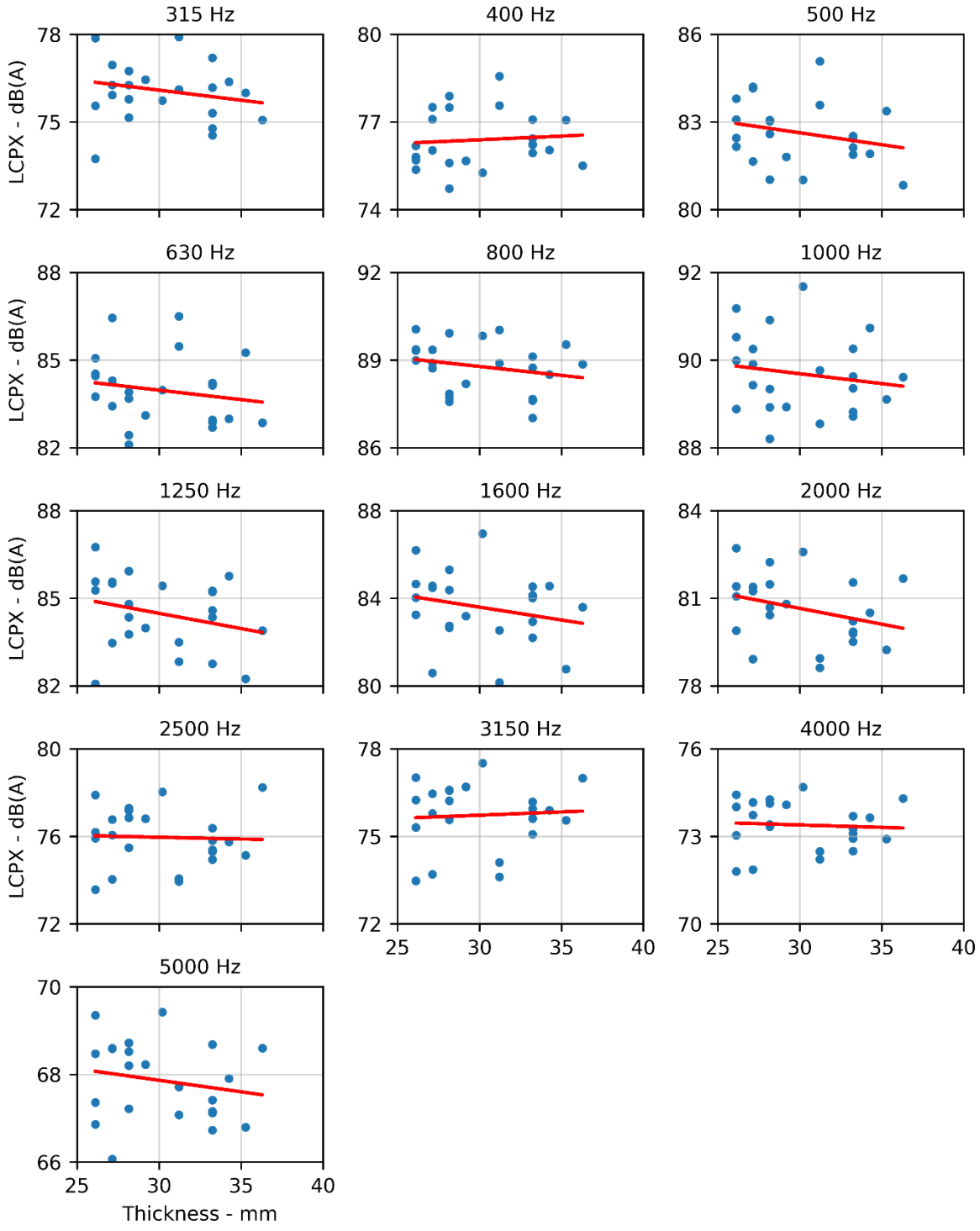

FIGURE 20. PA7 LV ON CNC. ONE-THIRD OCTAVE BAND L_{CPX} VS. THICKNESS.

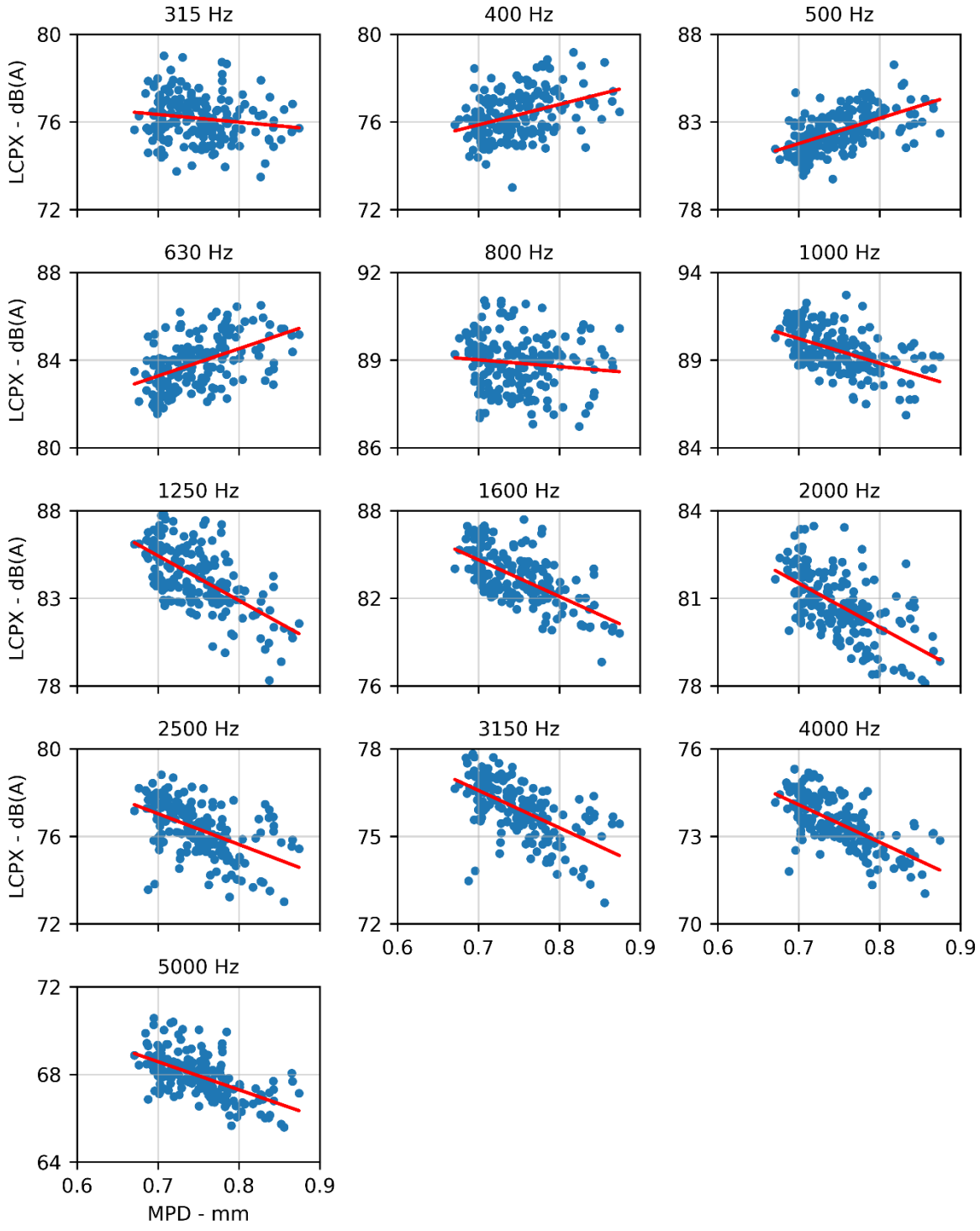

FIGURE 21. PA7 LV ON CNC. ONE-THIRD OCTAVE BAND LCPX VS. MPD.

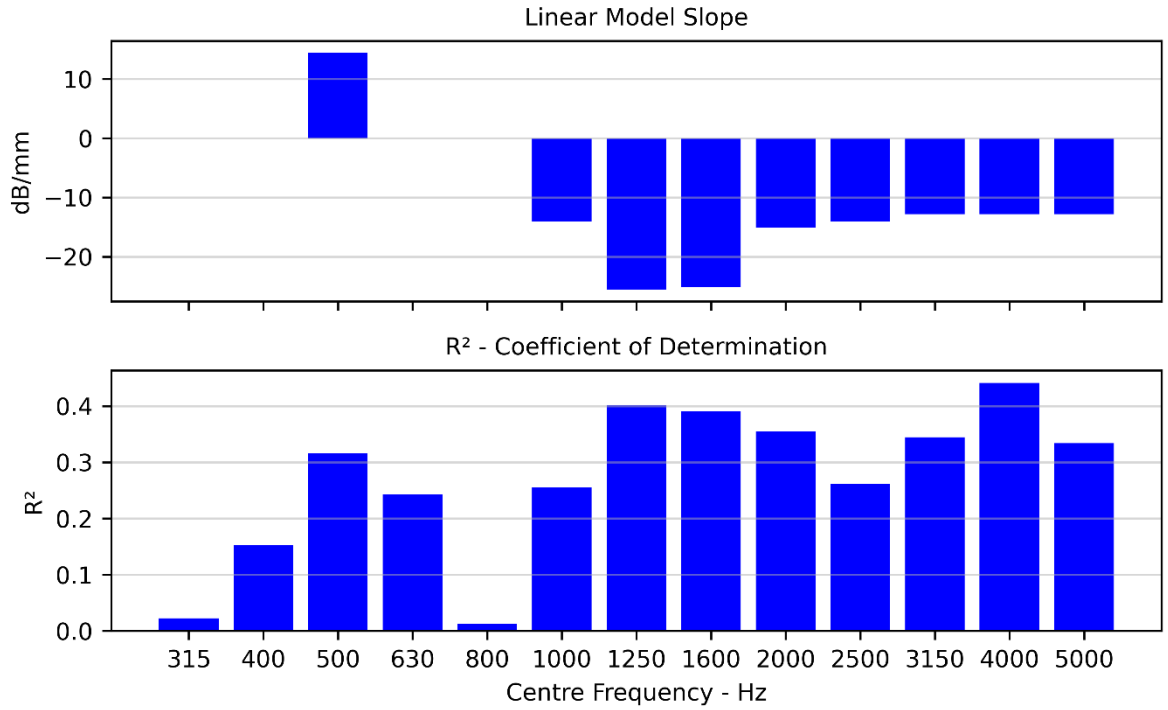

FIGURE 22. PA7 LV ON CNC. ONE-THIRD OCTAVE BAND L_{CPX} AND THICKNESS CORRELATIONS. TOP CHART IS THE LINEAR FIT SLOPE AND BOTTOM CHART IS COEFFICIENT OF DETERMINATION (R^2). MAXIMUM P-VALUE OF 0.025.

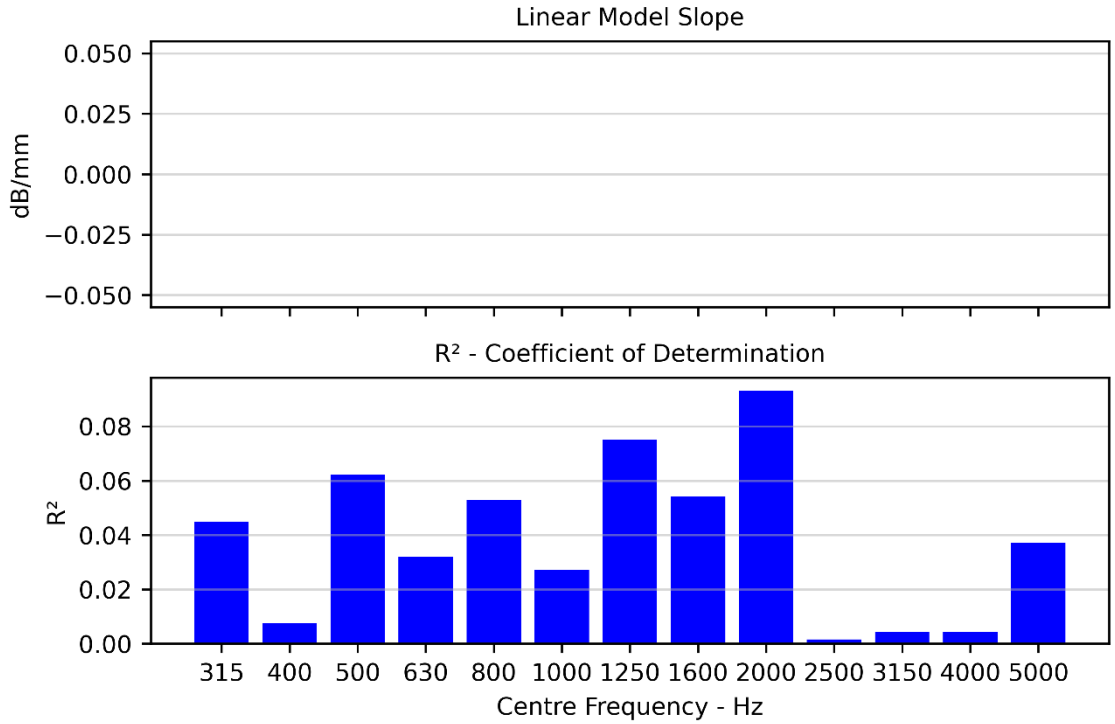

FIGURE 23. PA7 LV ON CNC. ONE-THIRD OCTAVE BAND L_{CPX} AND MPD CORRELATIONS. TOP CHART IS THE LINEAR FIT SLOPE AND BOTTOM CHART IS COEFFICIENT OF DETERMINATION (R^2). MAXIMUM P-VALUE OF 0.025.

TABLE 14. PA7 LV ON CNC. MULTI-VARIABLE LINEAR REGRESSION BETWEEN L_{CPX}, MPD, AND THICKNESS.

R^2		0.19
Adj. R^2		0.10
Thickness	-	p = 0.171
MPD	-	p = 0.164

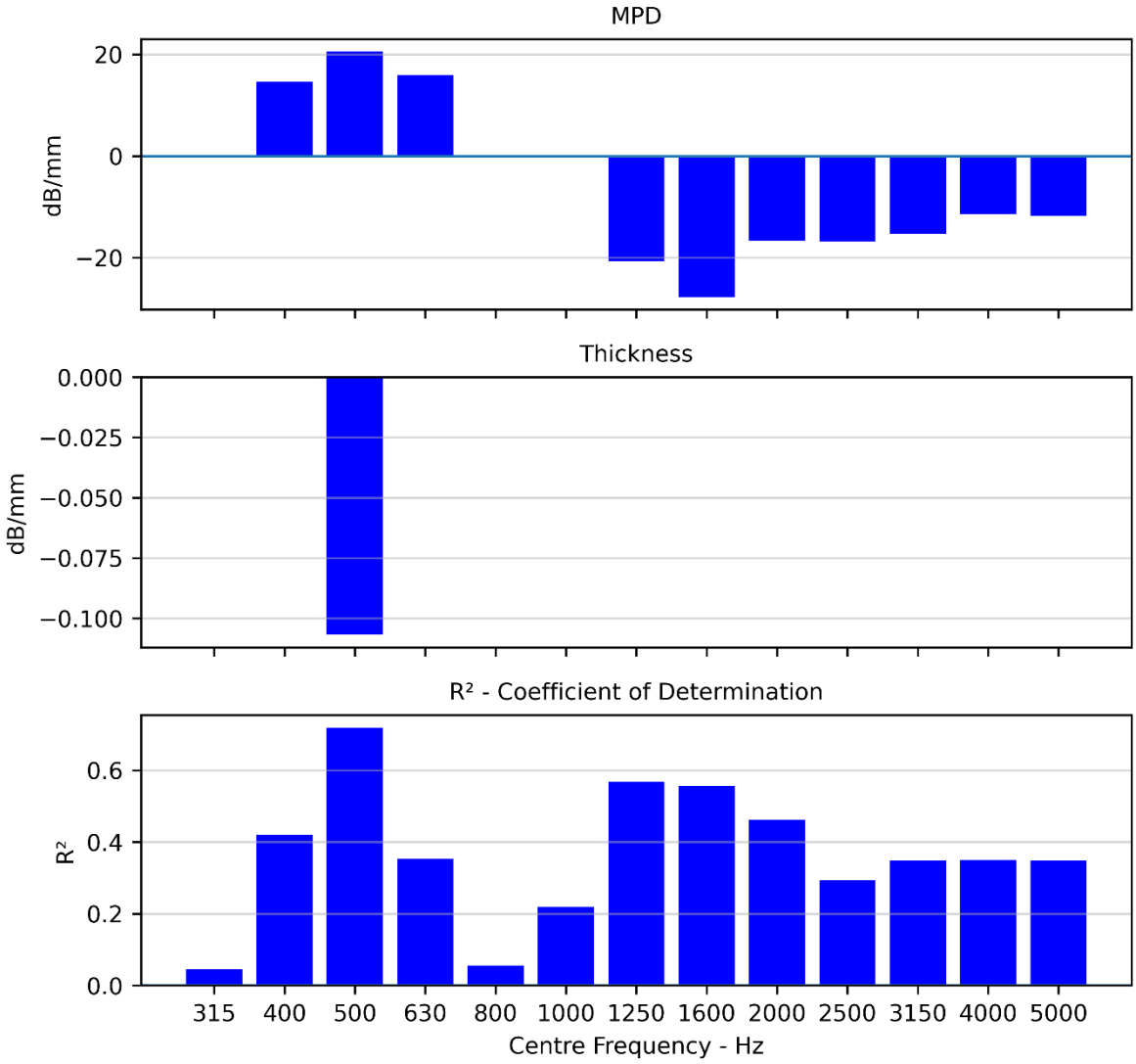

FIGURE 24. PA7 LV ON CNC. ONE-THIRD OCTAVE BAND L_{CPX} VS. MPD AND THICKNESS CORRELATIONS. MAXIMUM P-VALUE OF 0.025.

7.1.3 PA7 HS

TABLE 15. PA7 HS ON CNC. SUMMARY OF RESULTS.

	L_{CPX}	Thickness	MPD
Samples	161	23	161
Mean	93.4 dB	33.1 mm	0.74 mm
Std	0.8 dB	3.5 mm	0.03 mm

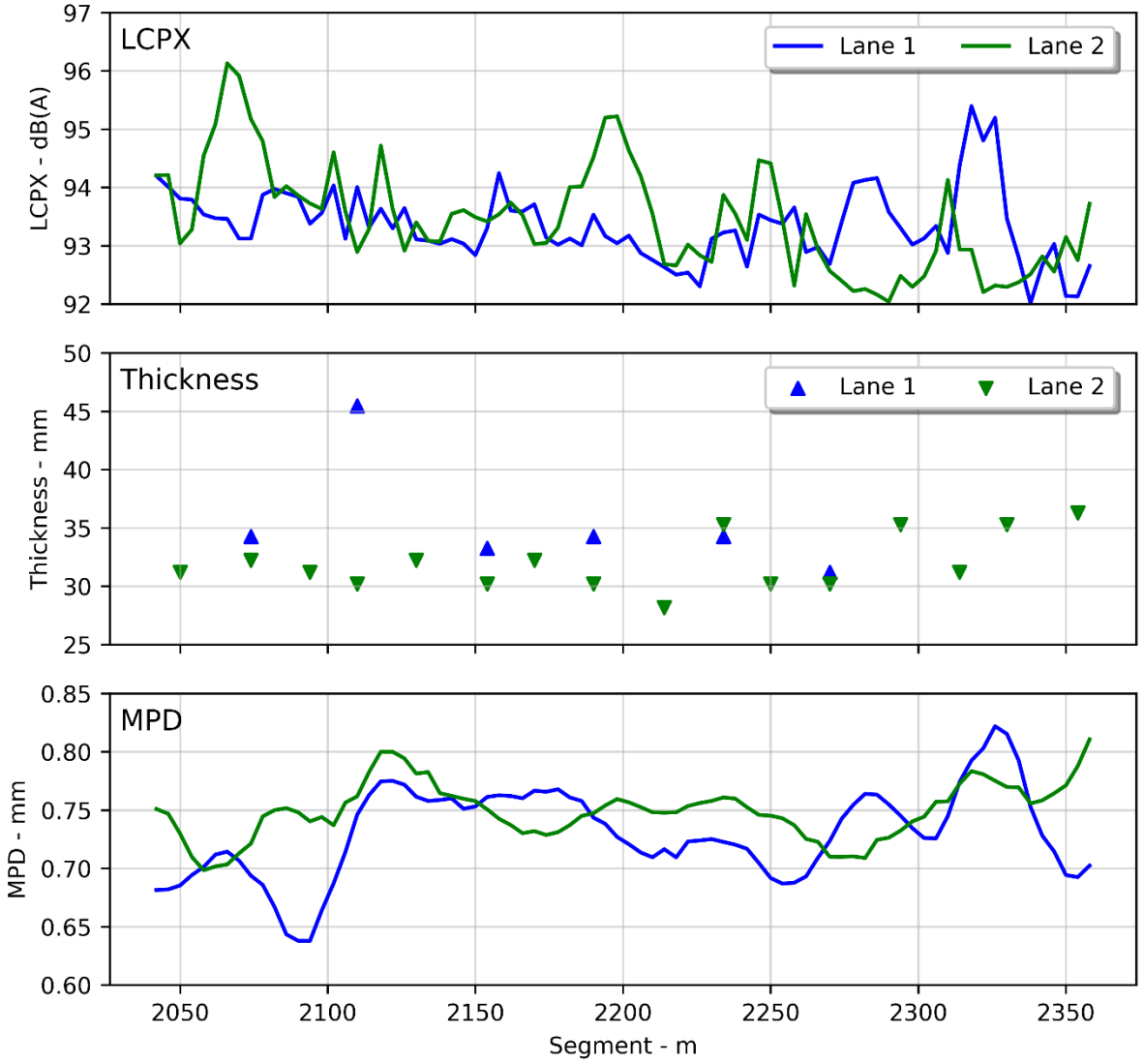

FIGURE 25. PA7 HS ON CNC. LONGITUDINAL PLOTS OF L_{CPX}, THICKNESS, AND MPD.

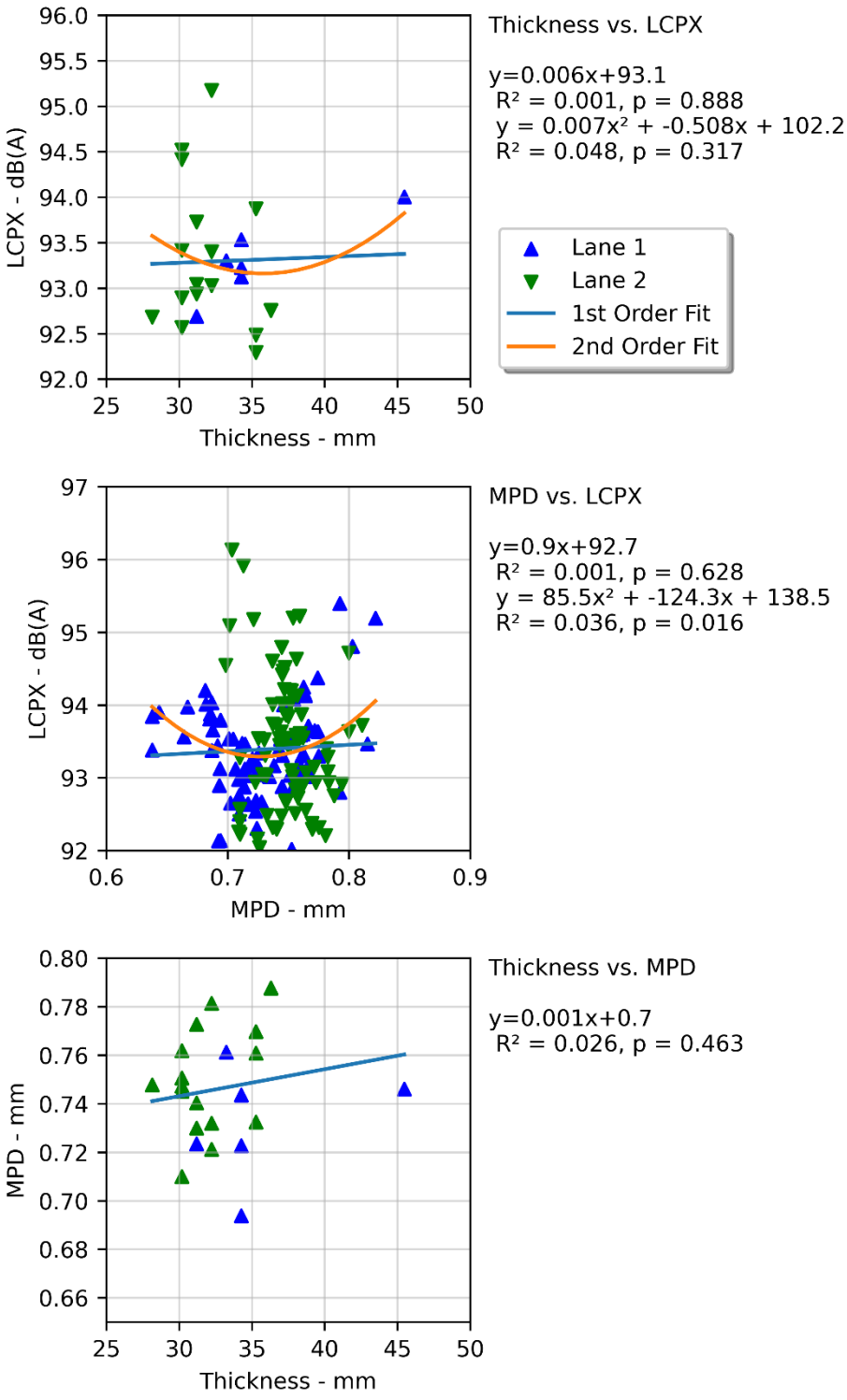

FIGURE 26. PA7 HS ON CNC. L_{CPX} VS. THICKNESS, L_{CPX} VS. MPD, AND MPD VS. THICKNESS.

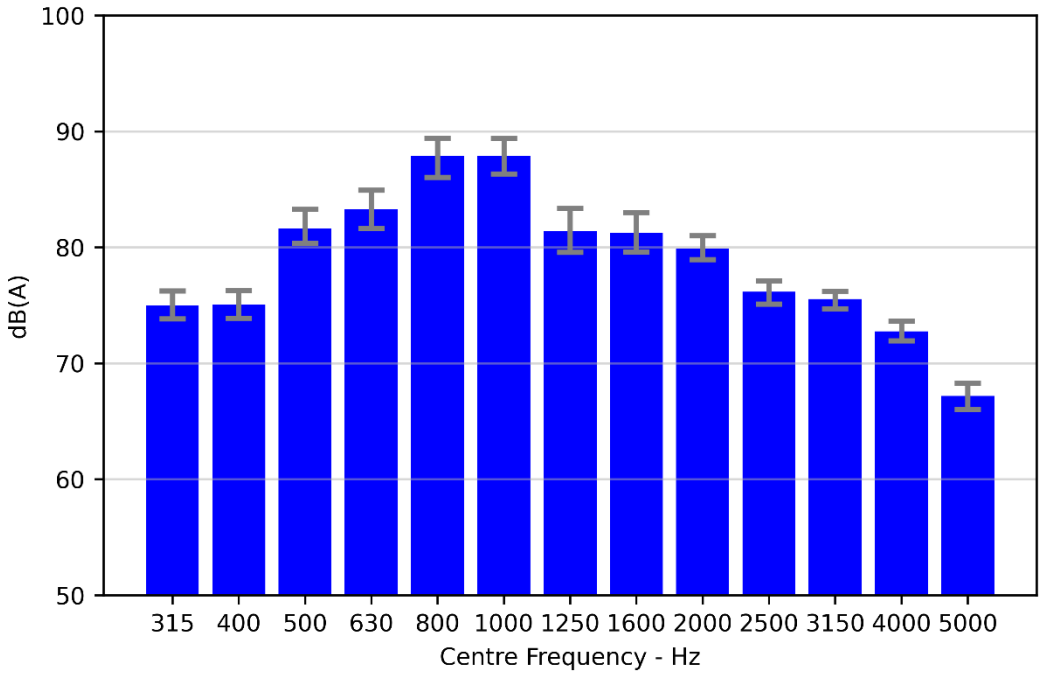

FIGURE 27. PA7 HS ON CNC. ONE-THIRD OCTAVE BAND DISTRIBUTION WITH 10-90TH PERCENTILE VARIATION.

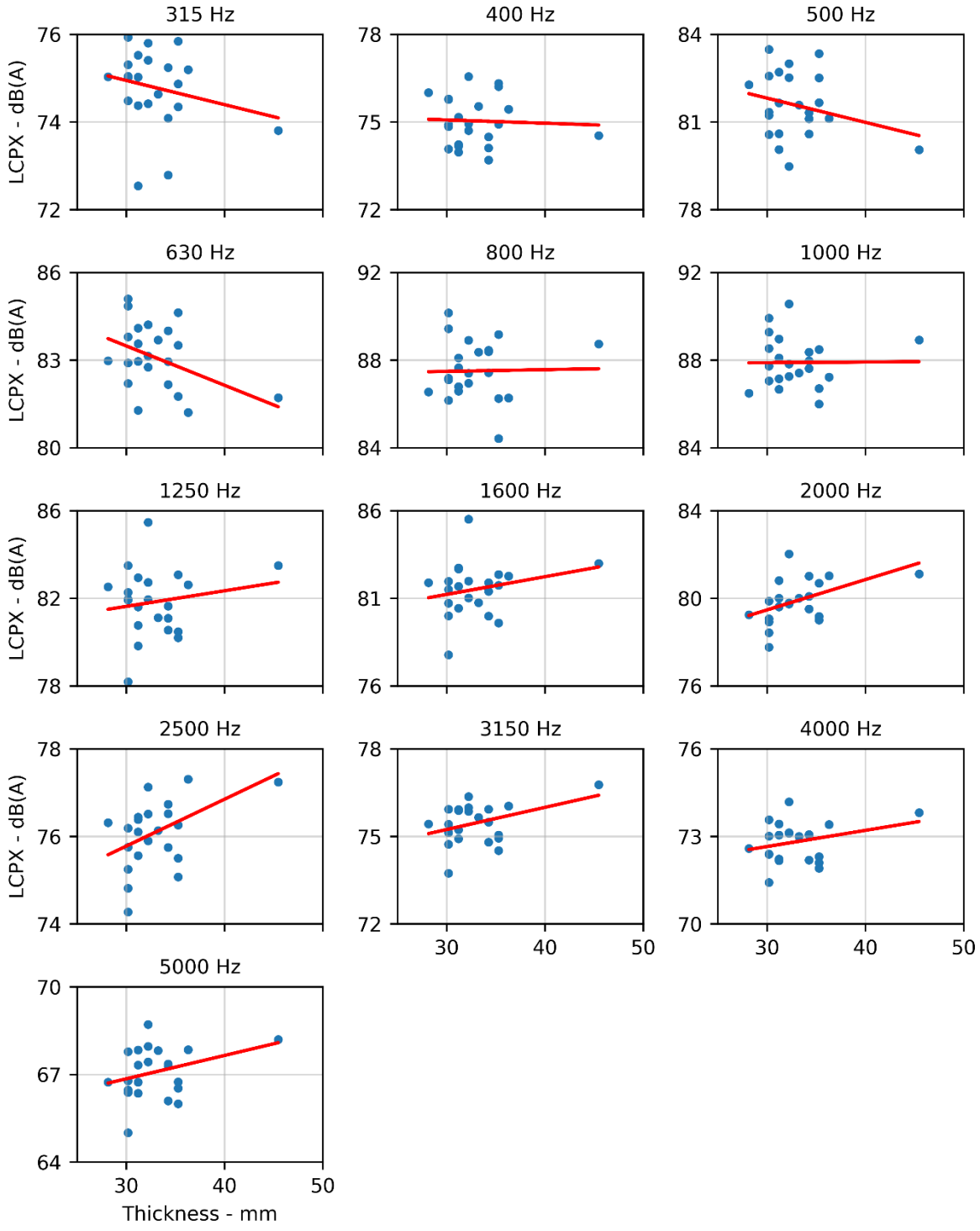

FIGURE 28. PA7 HS ON CNC. ONE-THIRD OCTAVE BAND L_{CPX} VS. THICKNESS.

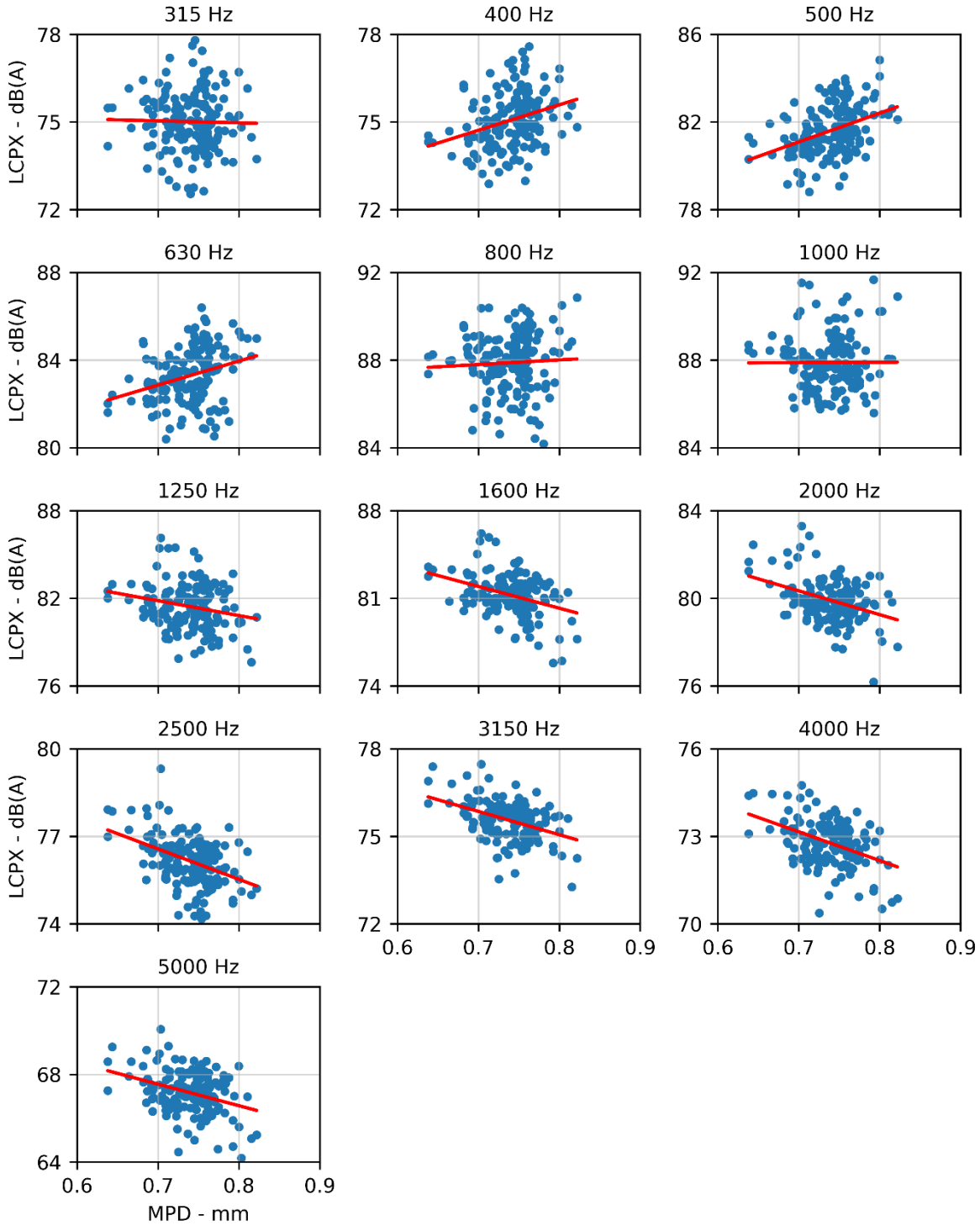

FIGURE 29. PA7 HS ON CNC. ONE-THIRD OCTAVE BAND L_{CPX} VS. MPD.

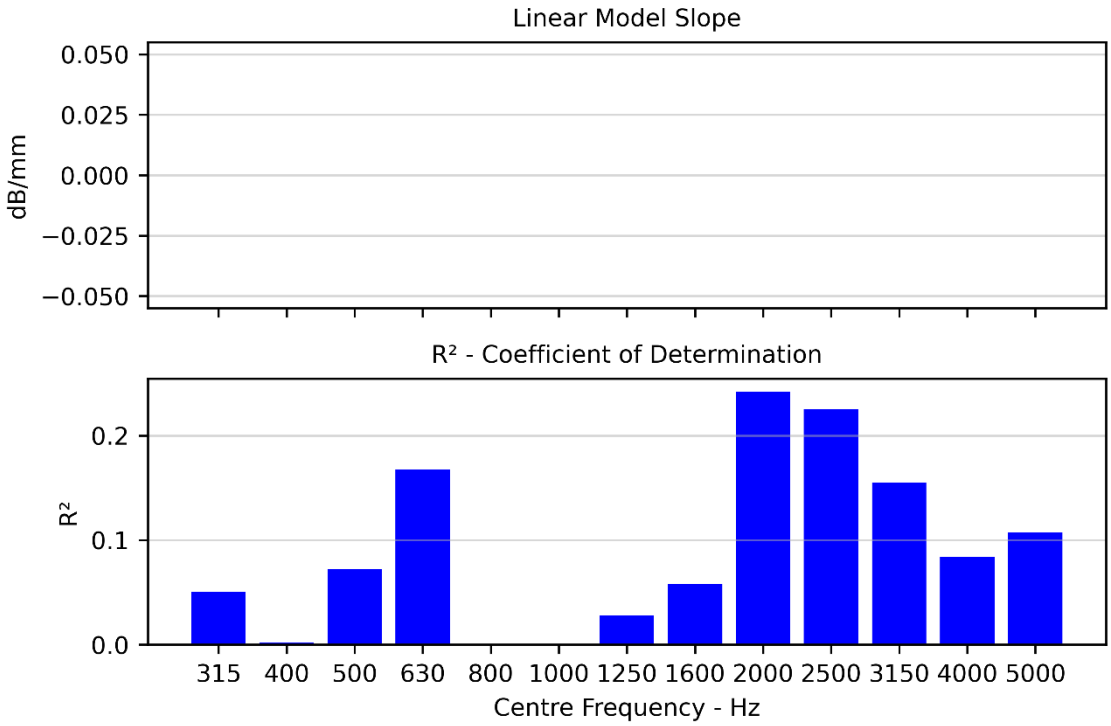

FIGURE 30. PA7 HS ON CNC. ONE-THIRD OCTAVE BAND LCPX AND THICKNESS CORRELATIONS. TOP CHART IS THE LINEAR FIT SLOPE AND BOTTOM CHART IS COEFFICIENT OF DETERMINATION (R^2). MAXIMUM P-VALUE OF 0.025.

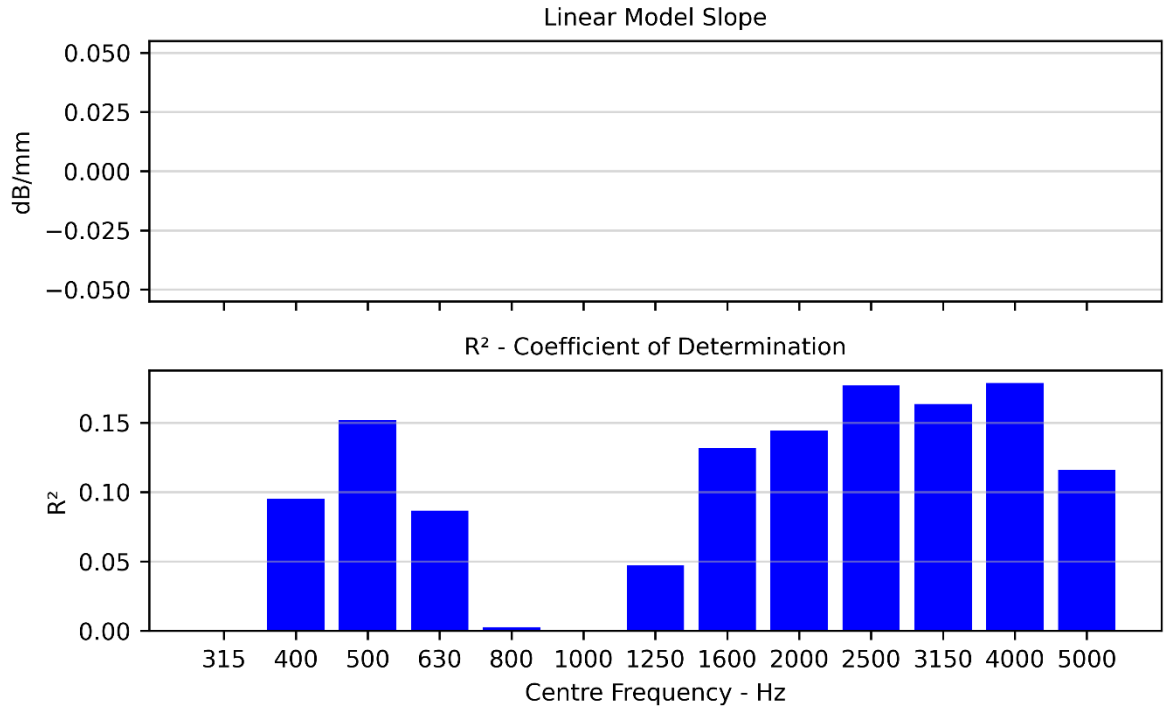

FIGURE 31. PA7 HS ON CNC. ONE-THIRD OCTAVE BAND L_{CPX} AND MPD CORRELATIONS. TOP CHART IS THE LINEAR FIT SLOPE AND BOTTOM CHART IS COEFFICIENT OF DETERMINATION (R^2). MAXIMUM P-VALUE OF 0.025.

TABLE 16. PA7 HS ON CNC. MULTI-VARIABLE LINEAR REGRESSION BETWEEN L_{CPX}, MPD, AND THICKNESS.

R^2		0.02
Adj. R^2		-0.08
Thickness	-	p = 0.81
MPD	-	p = 0.52

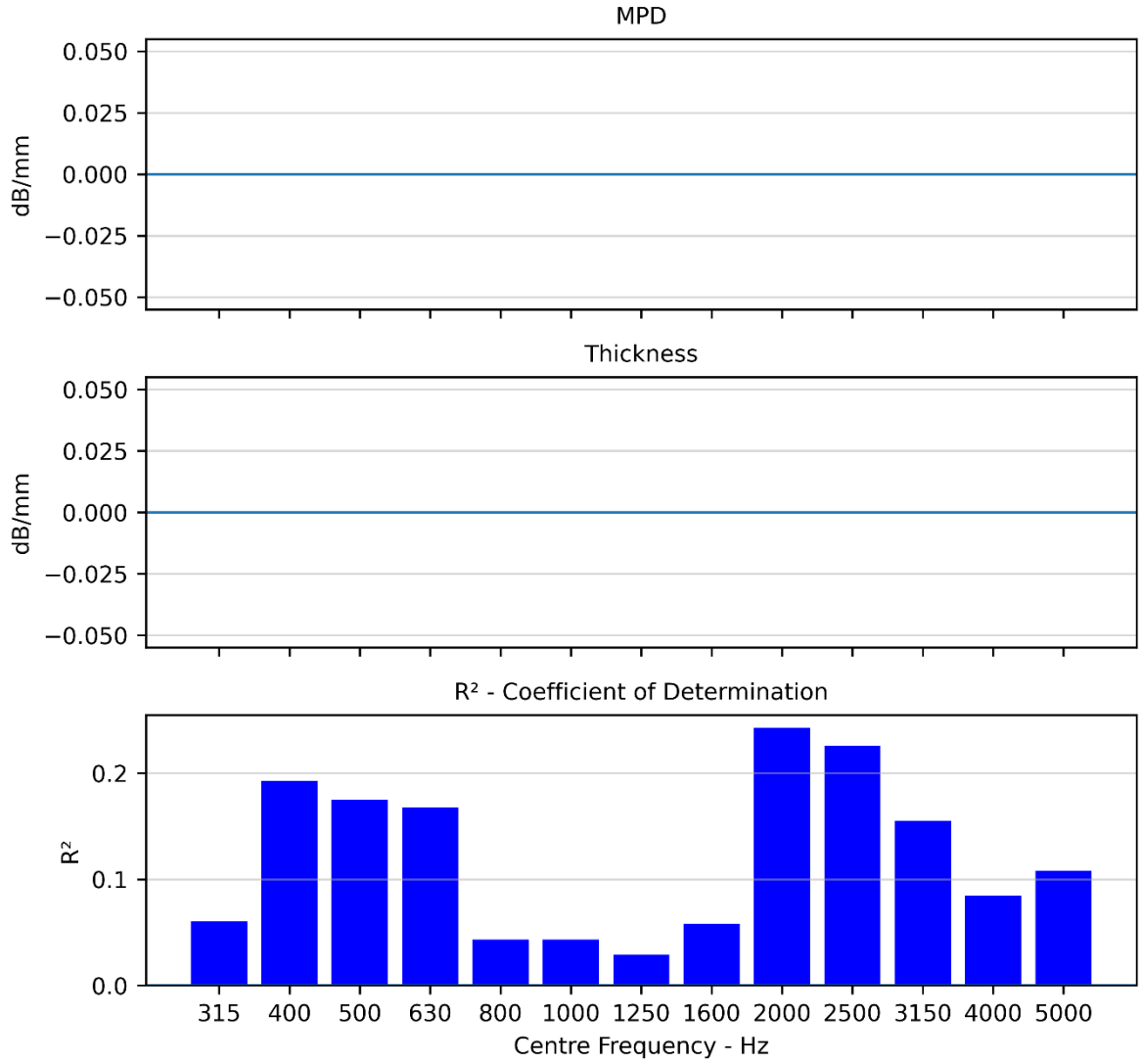

FIGURE 32. PA7 HS ON CNC. ONE-THIRD OCTAVE BAND L_{CPX} VS. MPD AND THICKNESS CORRELATIONS. MAXIMUM P-VALUE OF 0.025.

7.1.4 PA7

TABLE 17. PA7 ON CNC. SUMMARY OF RESULTS.

	L_{CPX}	Thickness	MPD
Samples	168	22	168
Mean	96.57 dB	32.1 mm	0.93 mm
Std	0.63 dB	3.5 mm	0.02 mm

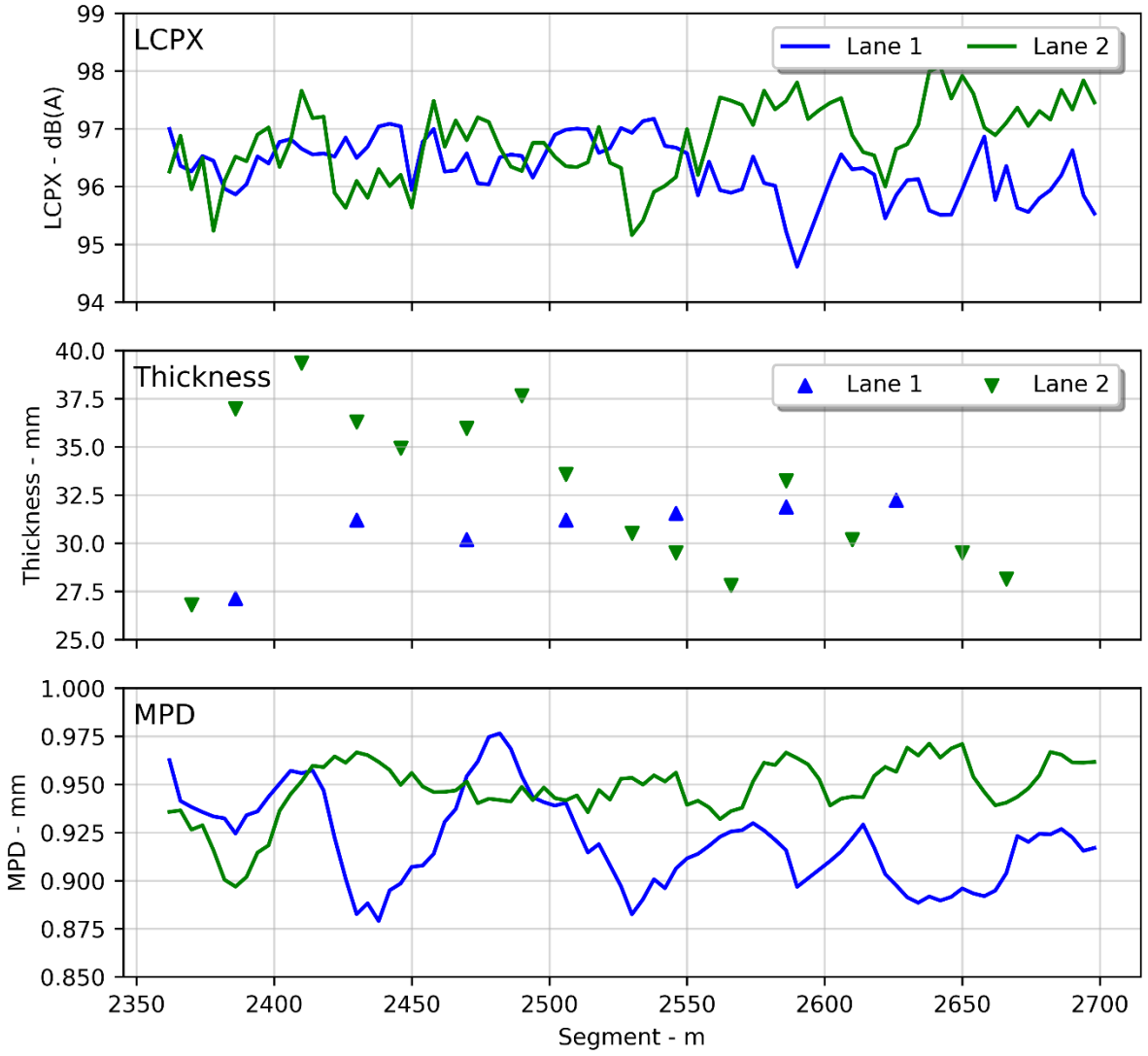

FIGURE 33. PA7 ON CNC. LONGITUDINAL PLOTS OF L_{CPX}, THICKNESS, AND MPD.

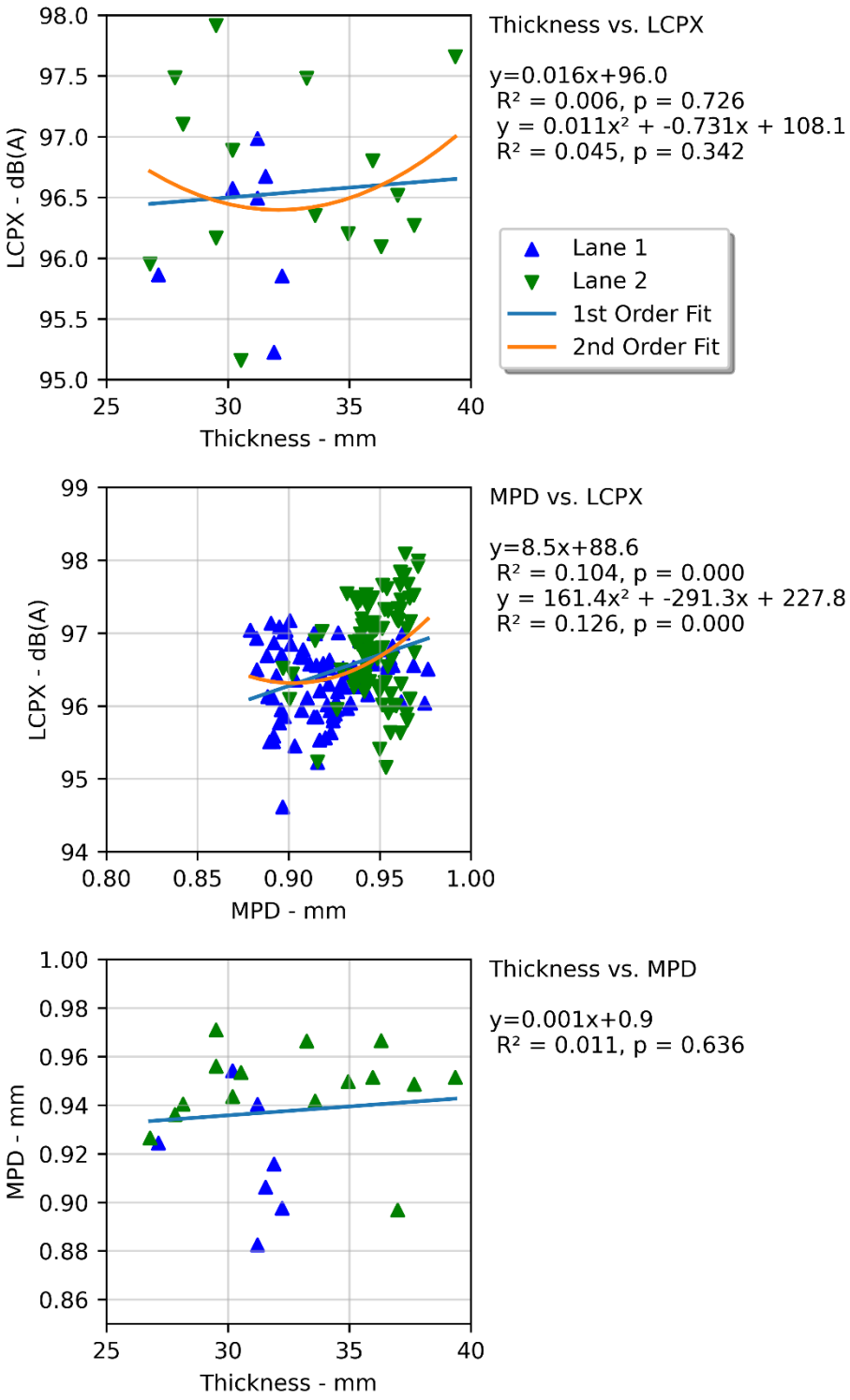

FIGURE 34. PA7 ON CNC. L_{CPX} VS. THICKNESS, L_{CPX} VS. MPD, AND MPD VS. THICKNESS.

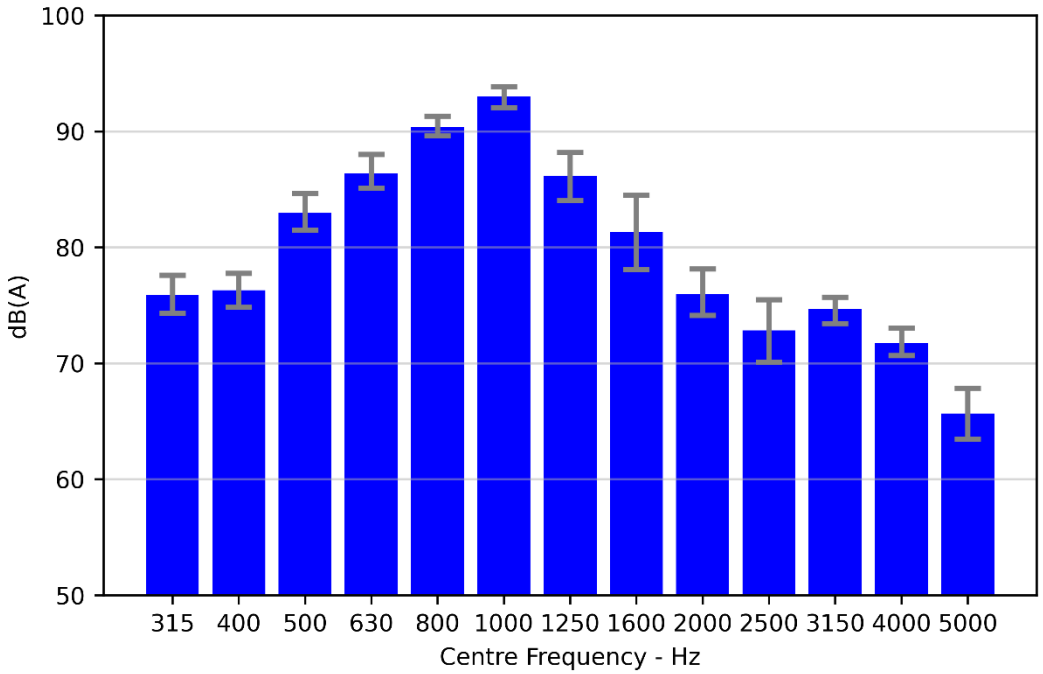

FIGURE 35. PA7 ON CNC. ONE-THIRD OCTAVE BAND DISTRIBUTION WITH 10-90TH PERCENTILE VARIATION.

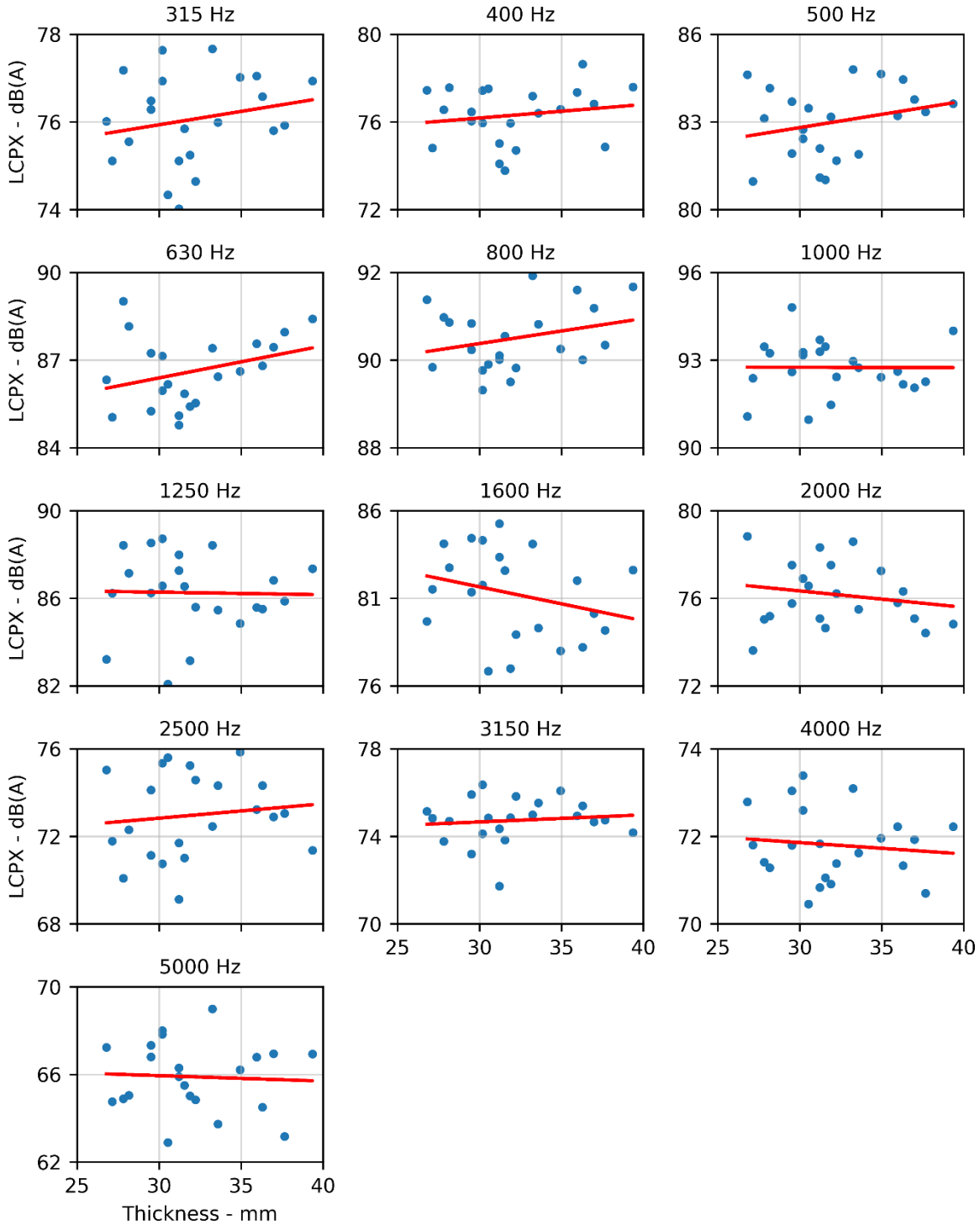

FIGURE 36. PA7 ON CNC. ONE-THIRD OCTAVE BAND L_{CPX} VS. THICKNESS.

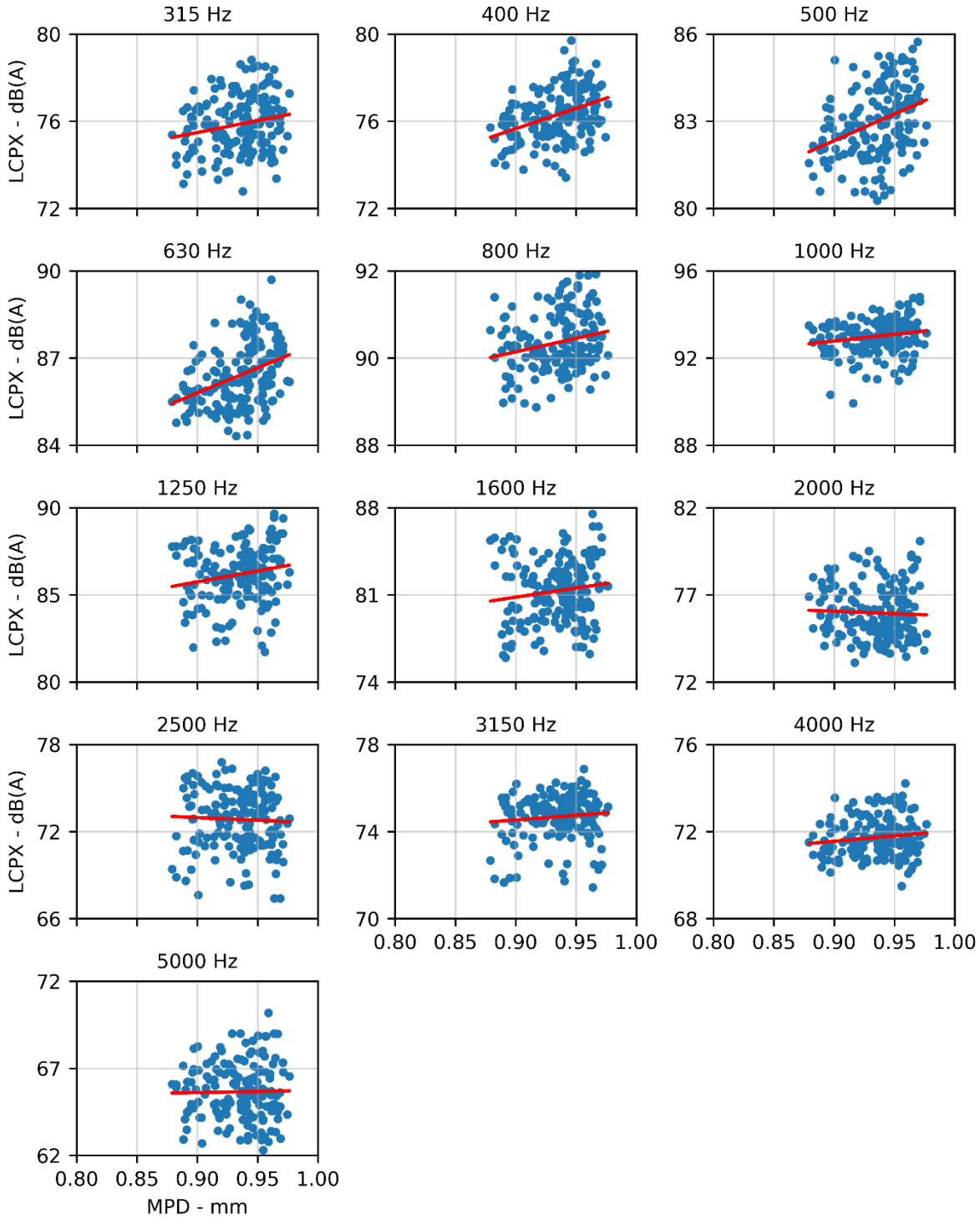

FIGURE. PA7 ON CNC. ONE-THIRD OCTAVE BAND L_{CPX} VS. MPD.

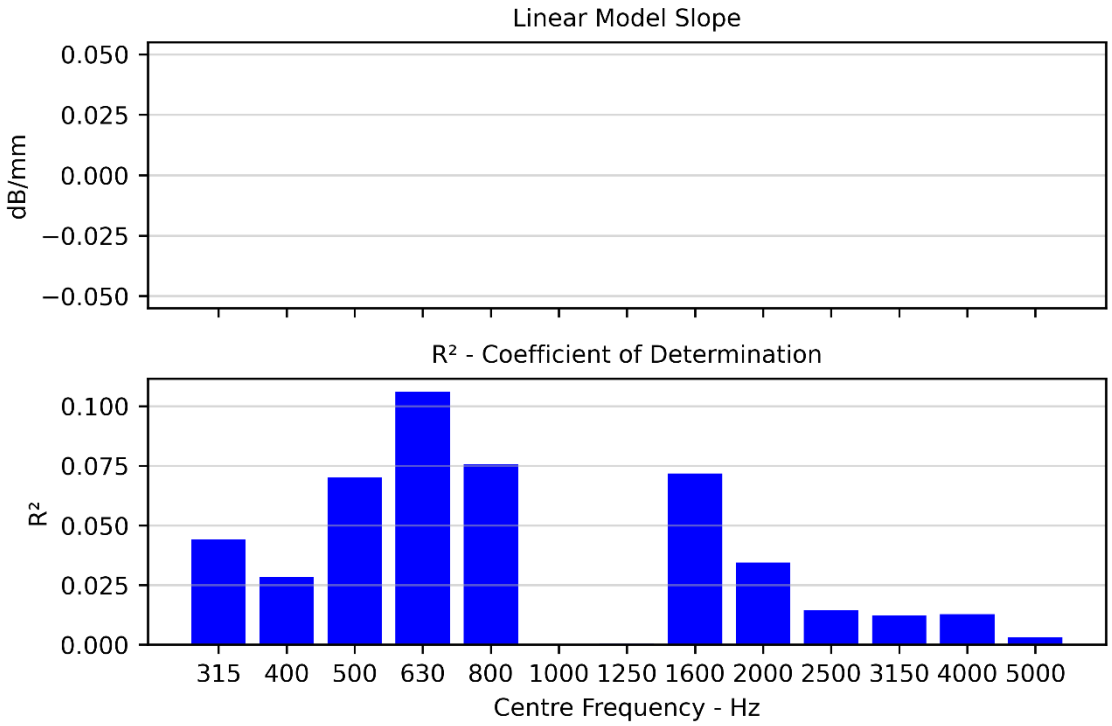

FIGURE 37. PA7 ON CNC. ONE-THIRD OCTAVE BAND LCPX AND THICKNESS CORRELATIONS. TOP CHART IS THE LINEAR FIT SLOPE AND BOTTOM CHART IS COEFFICIENT OF DETERMINATION (R^2). MAXIMUM P-VALUE OF 0.025.

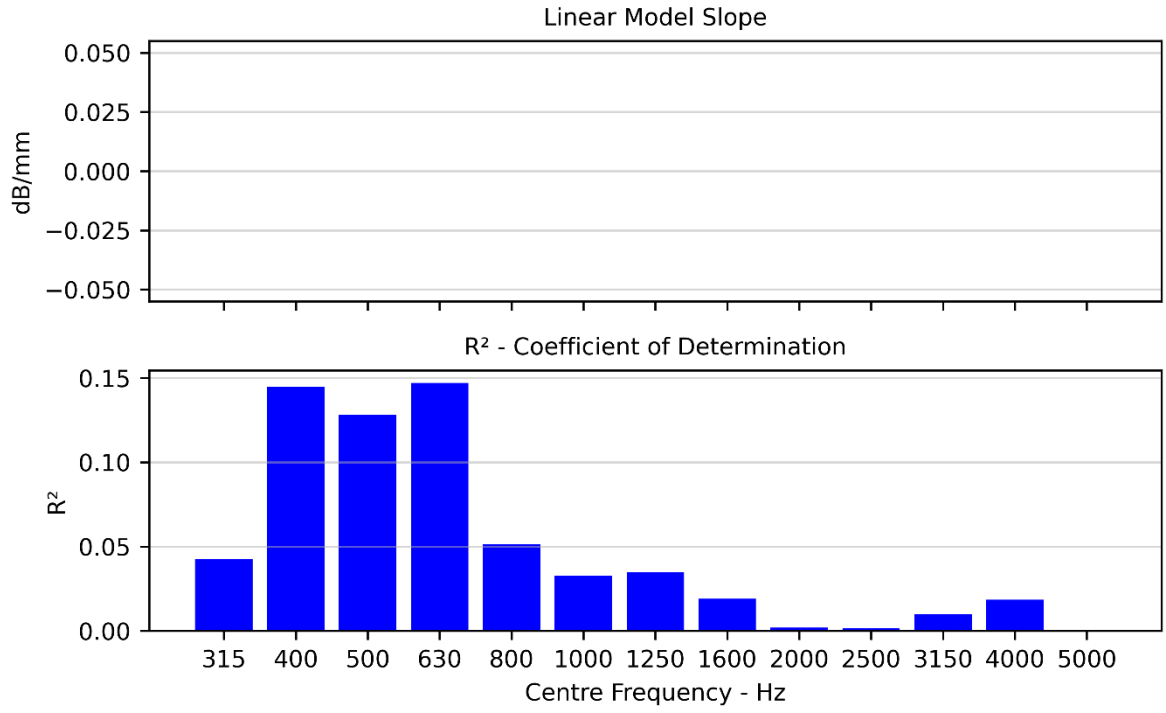

FIGURE 38. PA7 ON CNC. ONE-THIRD OCTAVE BAND L_{CPX} AND MPD CORRELATIONS. TOP CHART IS THE LINEAR FIT SLOPE AND BOTTOM CHART IS COEFFICIENT OF DETERMINATION (R^2). MAXIMUM P-VALUE OF 0.025.

TABLE 18. PA7 ON CNC. MULTI-VARIABLE LINEAR REGRESSION BETWEEN L_{CPX}, MPD, AND THICKNESS.

R^2		0.10
Adj. R^2		0.01
Thickness	-	p = 0.84
MPD	-	p = 0.17

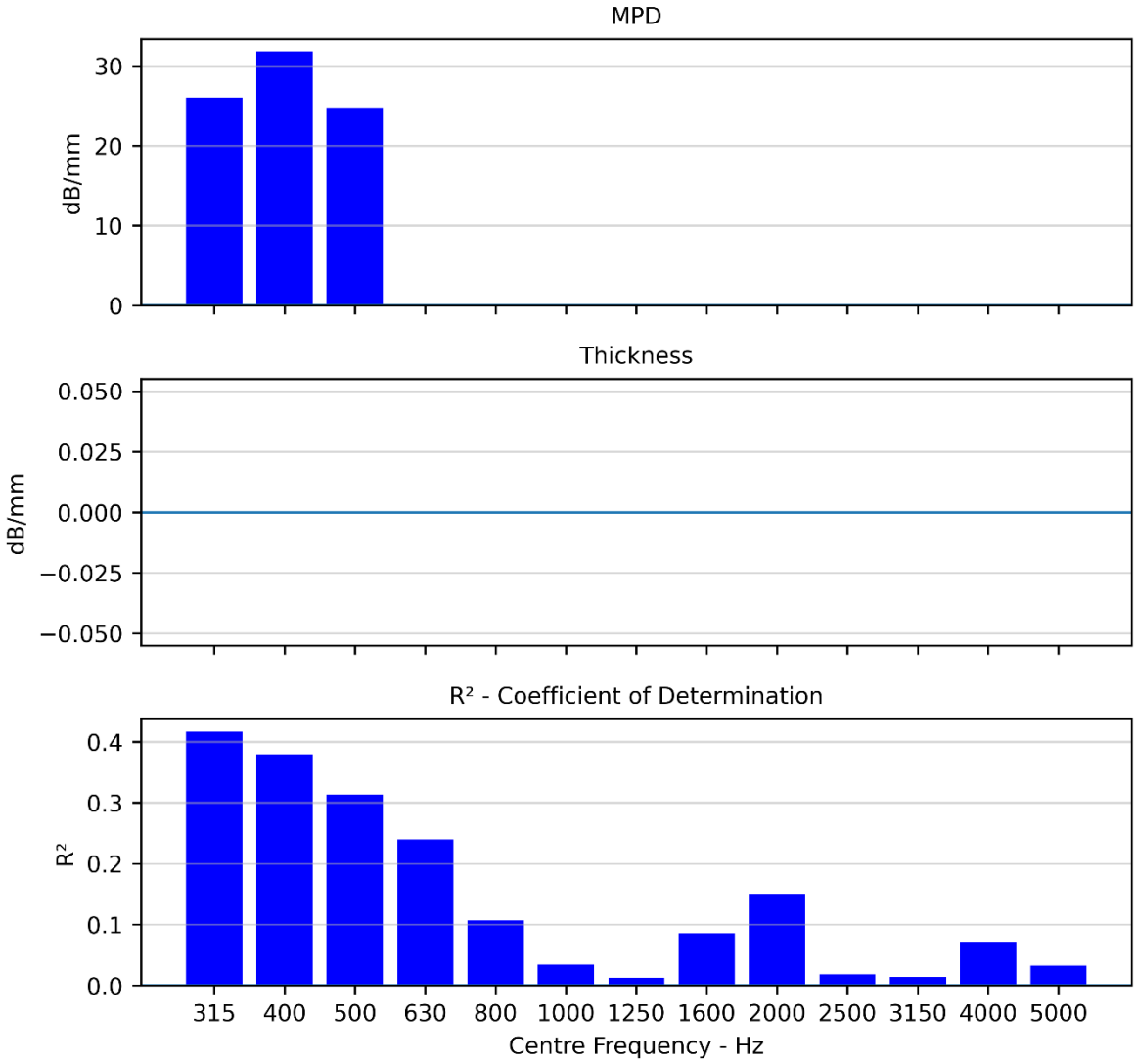

FIGURE 39. PA7 ON CNC. ONE-THIRD OCTAVE BAND L_{CPX} VS. MPD AND THICKNESS CORRELATIONS. MAXIMUM P-VALUE OF 0.025.

7.1.5 PA10

TABLE 19. PA10 ON CNC. SUMMARY OF RESULTS.

	L_{CPX}	Thickness	MPD
Samples	188	26	188
Mean	96.1 dB	36.2 mm	1.14 mm
Std	1.8 dB	7.3 mm	0.08 mm

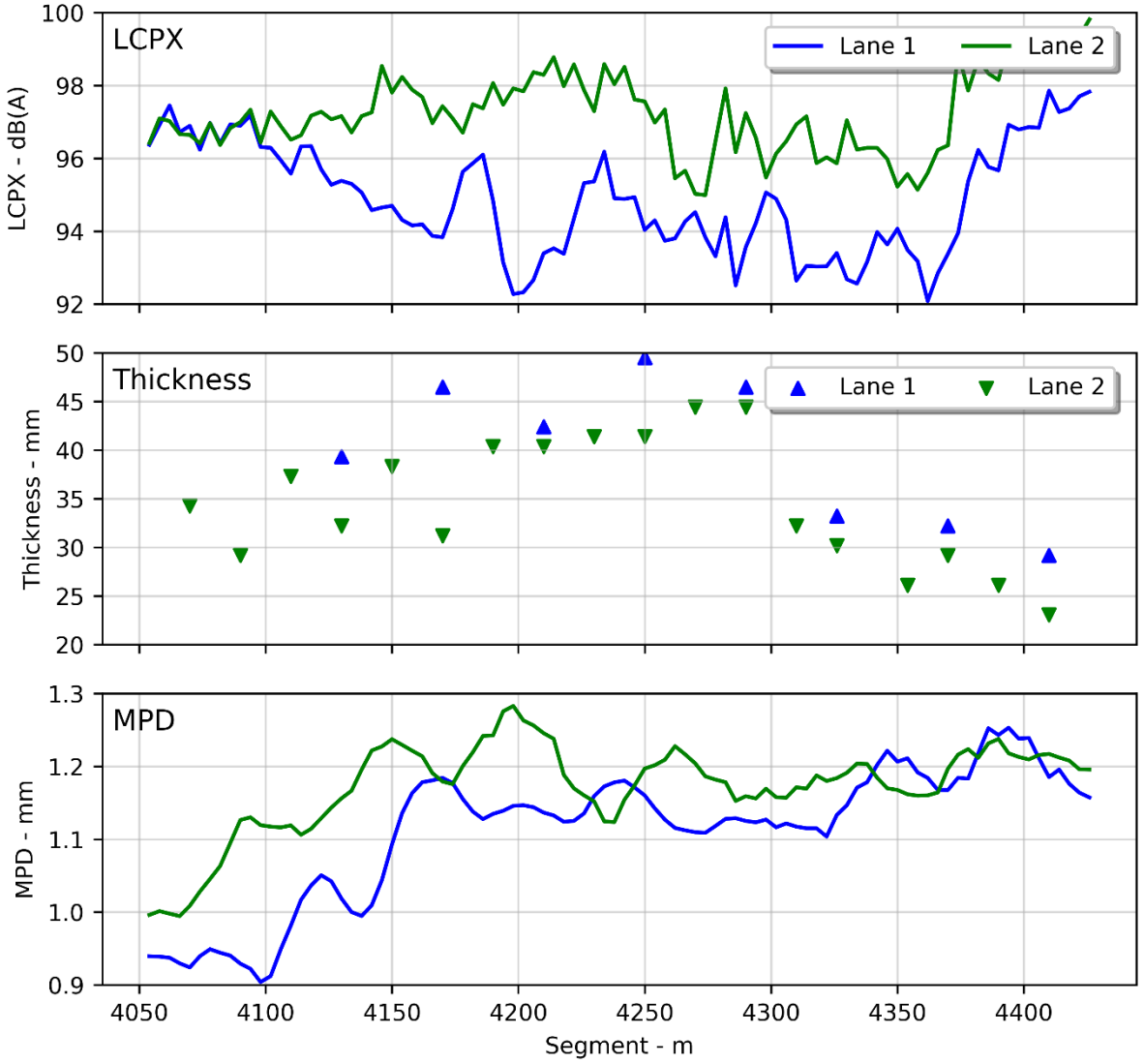

FIGURE 40. PA10 ON CNC. LONGITUDINAL PLOTS OF L_{CPX}, THICKNESS, AND MPD.

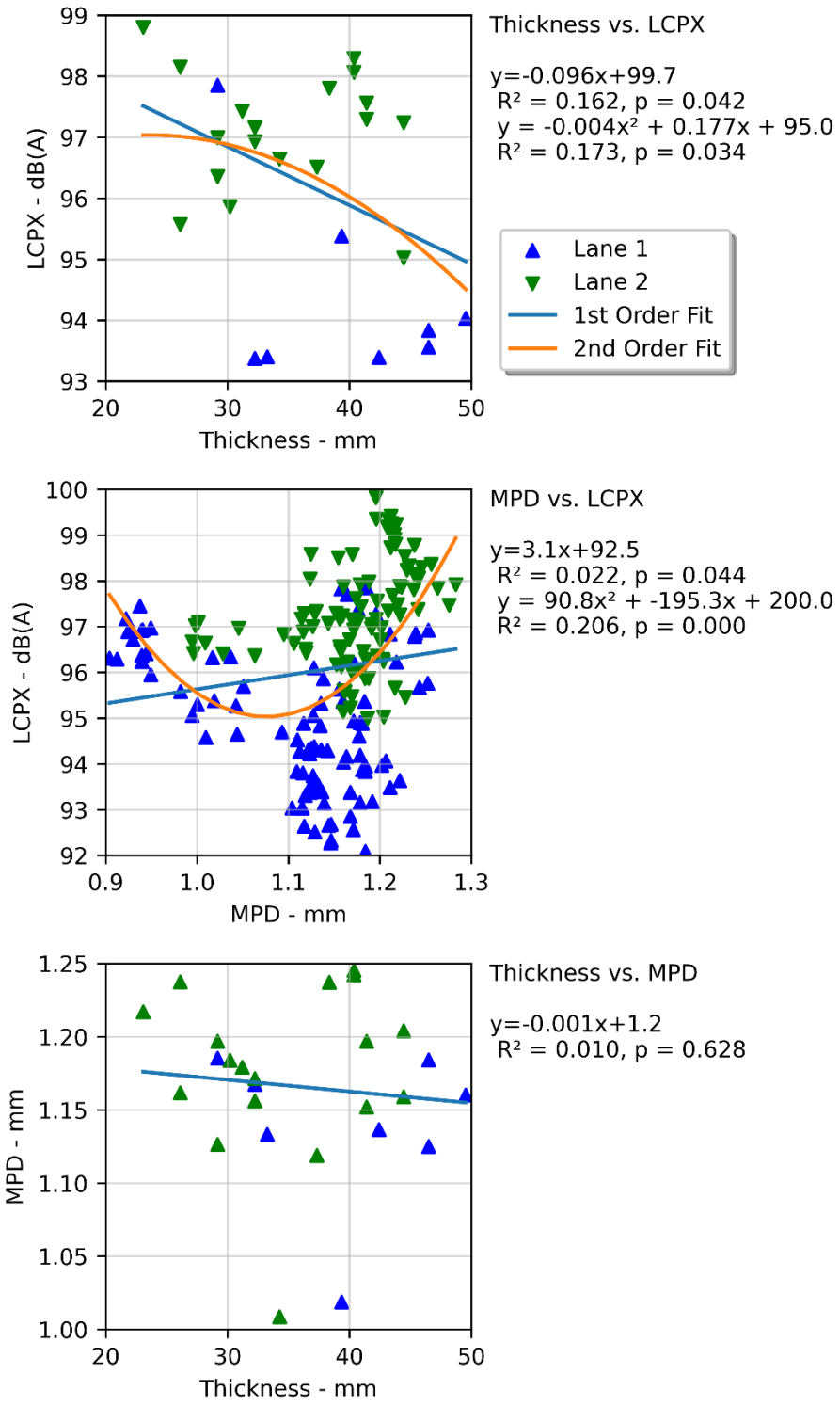

FIGURE 41. PA10 ON CNC. L_{CPX} VS. THICKNESS, L_{CPX} VS. MPD, AND MPD VS. THICKNESS.

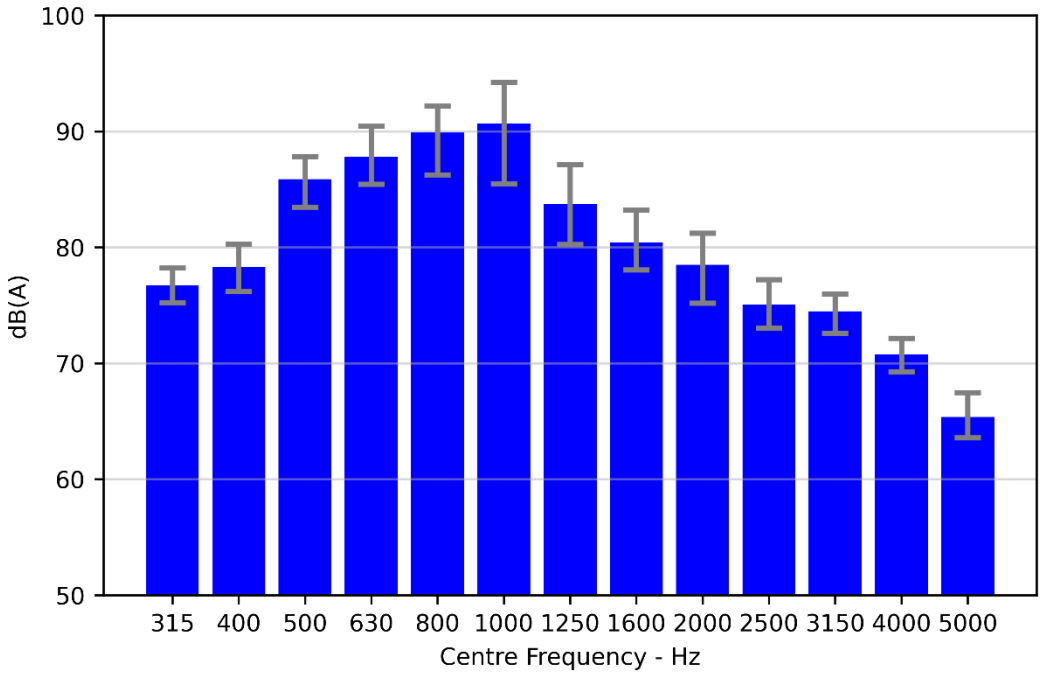

FIGURE 42. PA10ON CNC. ONE-THIRD OCTAVE BAND DISTRIBUTION WITH 10-90TH PERCENTILE VARIATION.

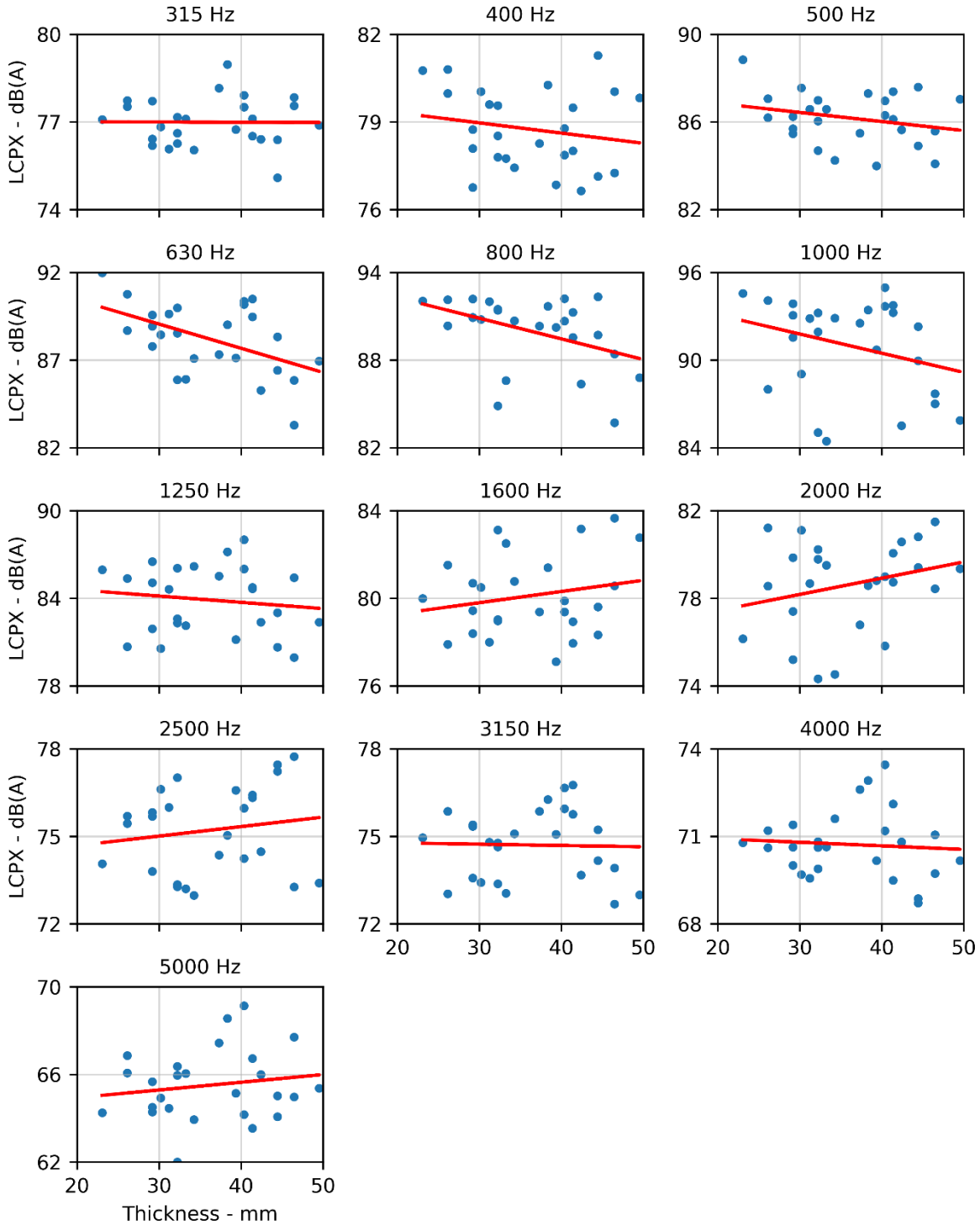

FIGURE 43. PA10 ON CNC. ONE-THIRD OCTAVE BAND L_{CPX} VS. THICKNESS.

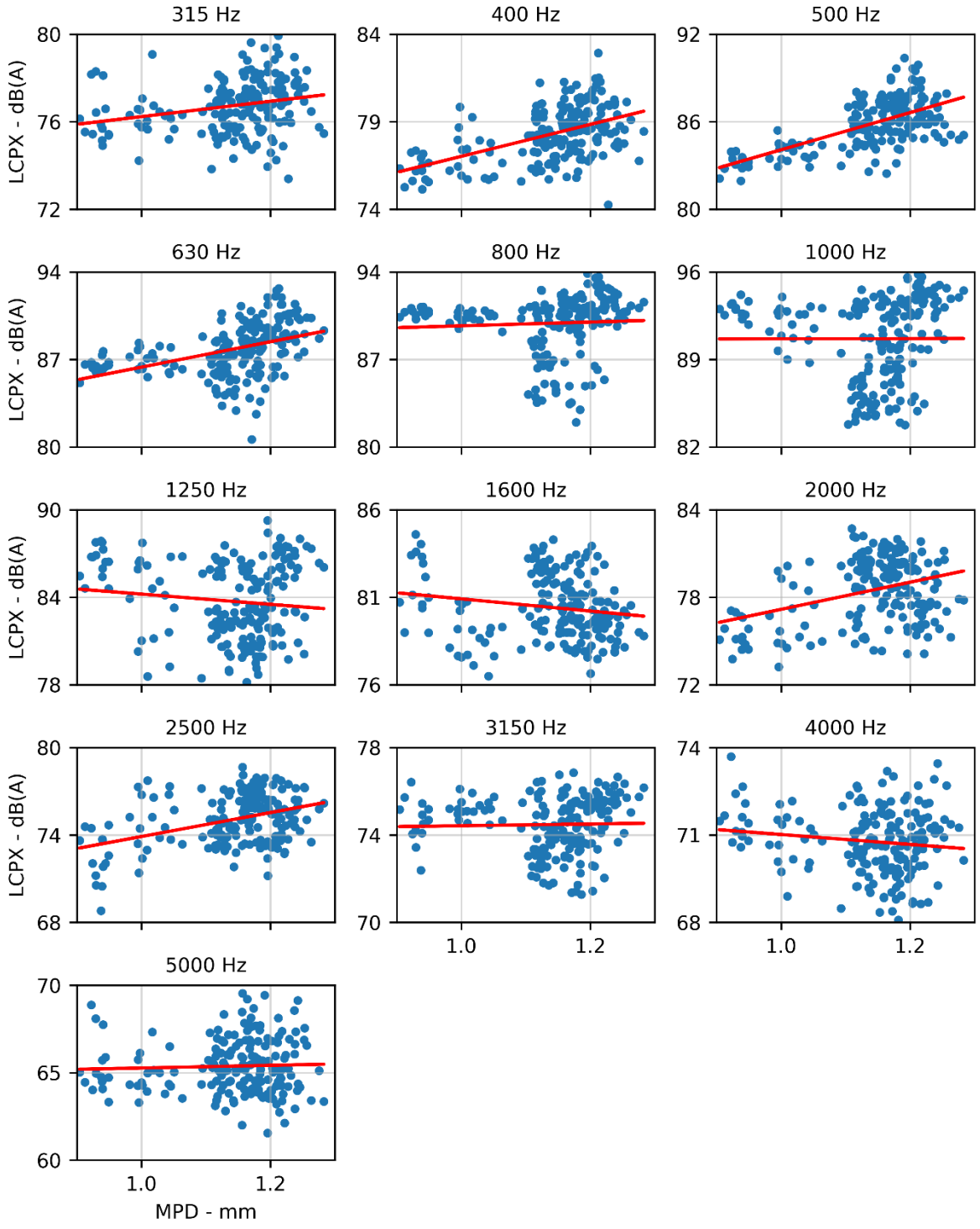

FIGURE 44. PA10 ON CNC. ONE-THIRD OCTAVE BAND LCPX VS. MPD.

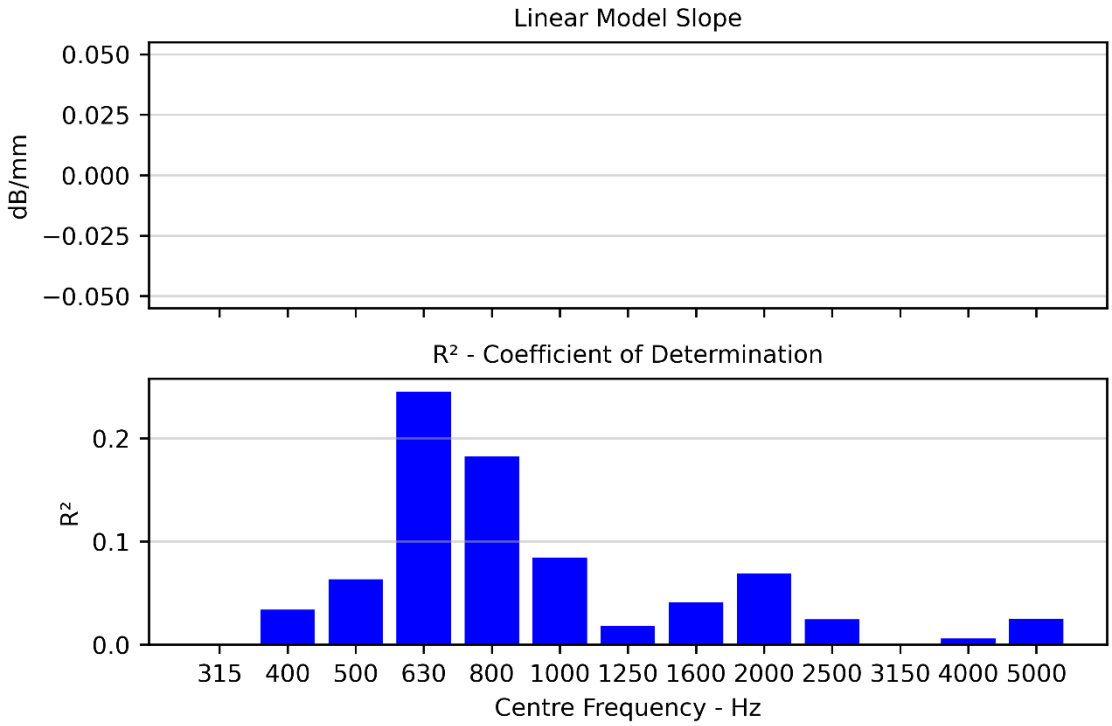

FIGURE 45. PA10 ON CNC. ONE-THIRD OCTAVE BAND LCPX AND THICKNESS CORRELATIONS. TOP CHART IS THE LINEAR FIT SLOPE AND BOTTOM CHART IS COEFFICIENT OF DETERMINATION (R^2).

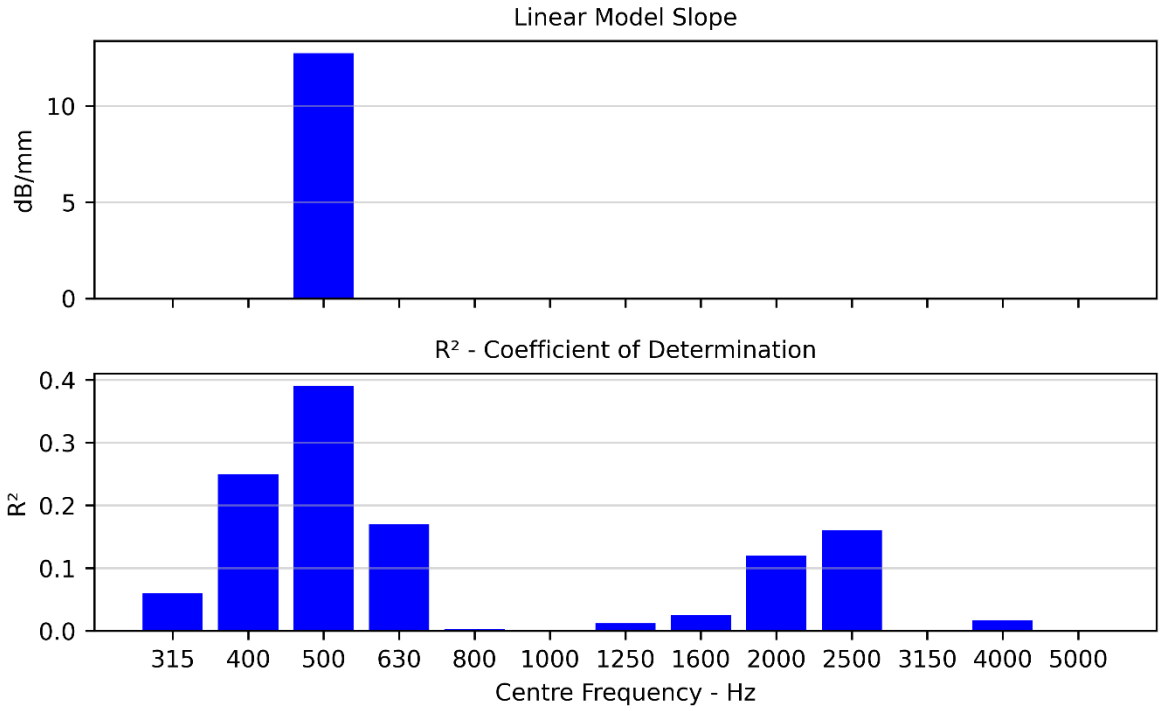

FIGURE 46. PA10 ON CNC. ONE-THIRD OCTAVE BAND L_{CPX} AND MPD CORRELATIONS. TOP CHART IS THE LINEAR FIT SLOPE AND BOTTOM CHART IS COEFFICIENT OF DETERMINATION (R^2).

TABLE 20. PA10 ON CNC. MULTI-VARIABLE LINEAR REGRESSION BETWEEN L_{CPX}, MPD, AND THICKNESS.

R^2	0.28	
Adj. R^2	0.22	
Thickness	-0.09 dB/mm	p = 0.05
MPD	-	p = 0.06

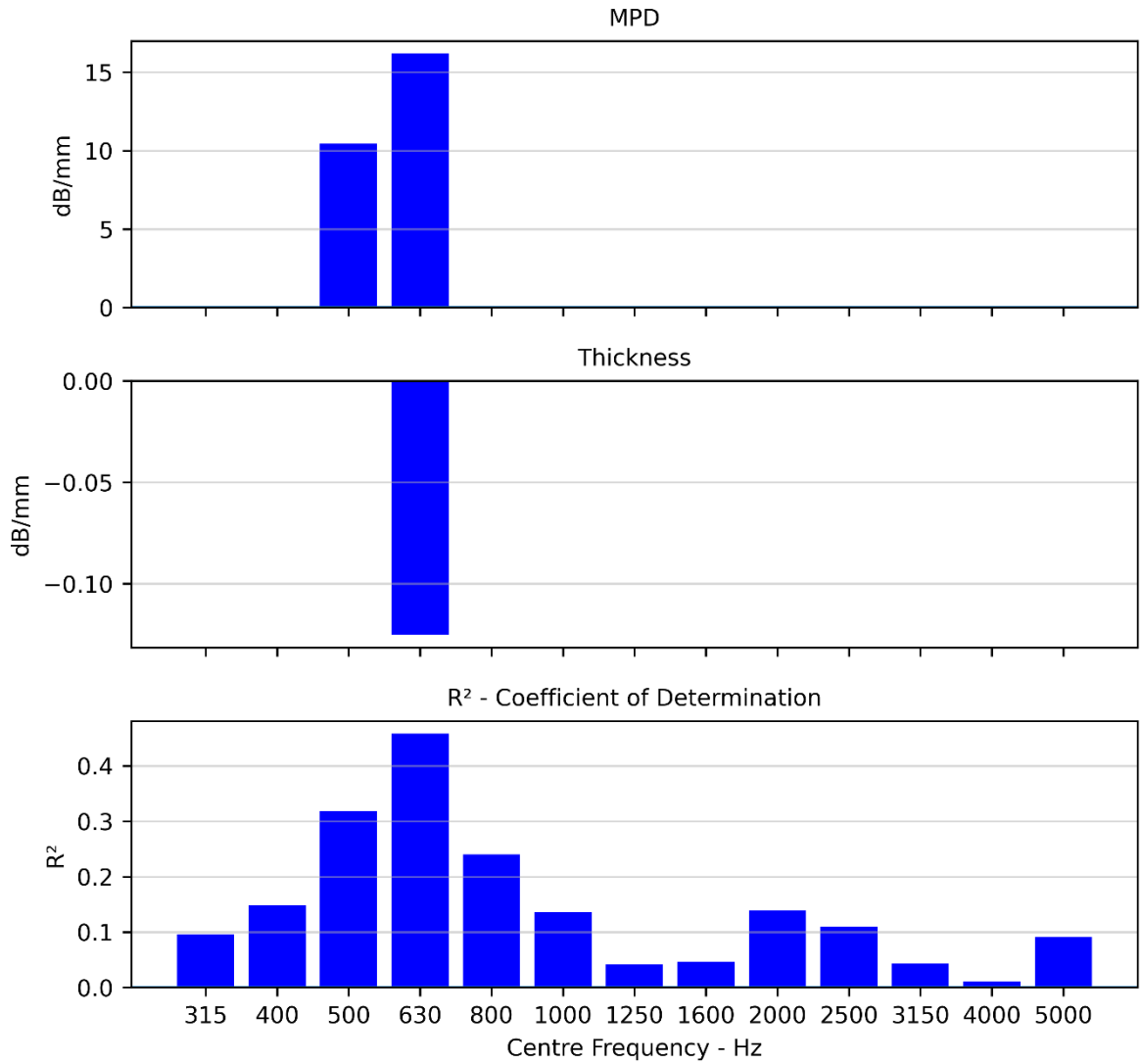

FIGURE 47. PA10 ON CNC. ONE-THIRD OCTAVE BAND L_{CPX} VS. MPD AND THICKNESS CORRELATIONS. MAXIMUM P-VALUE OF 0.025.

7.1.6 EPA7-50 mm

TABLE 21. EPA7-50 MM ON CNC. SUMMARY OF RESULTS.

	L_{CPX}	Thickness	MPD
Samples	550	43	550
Mean	92.1 dB	48.1 mm	0.83 mm
Std	0.9 dB	6.6 mm	0.04 mm

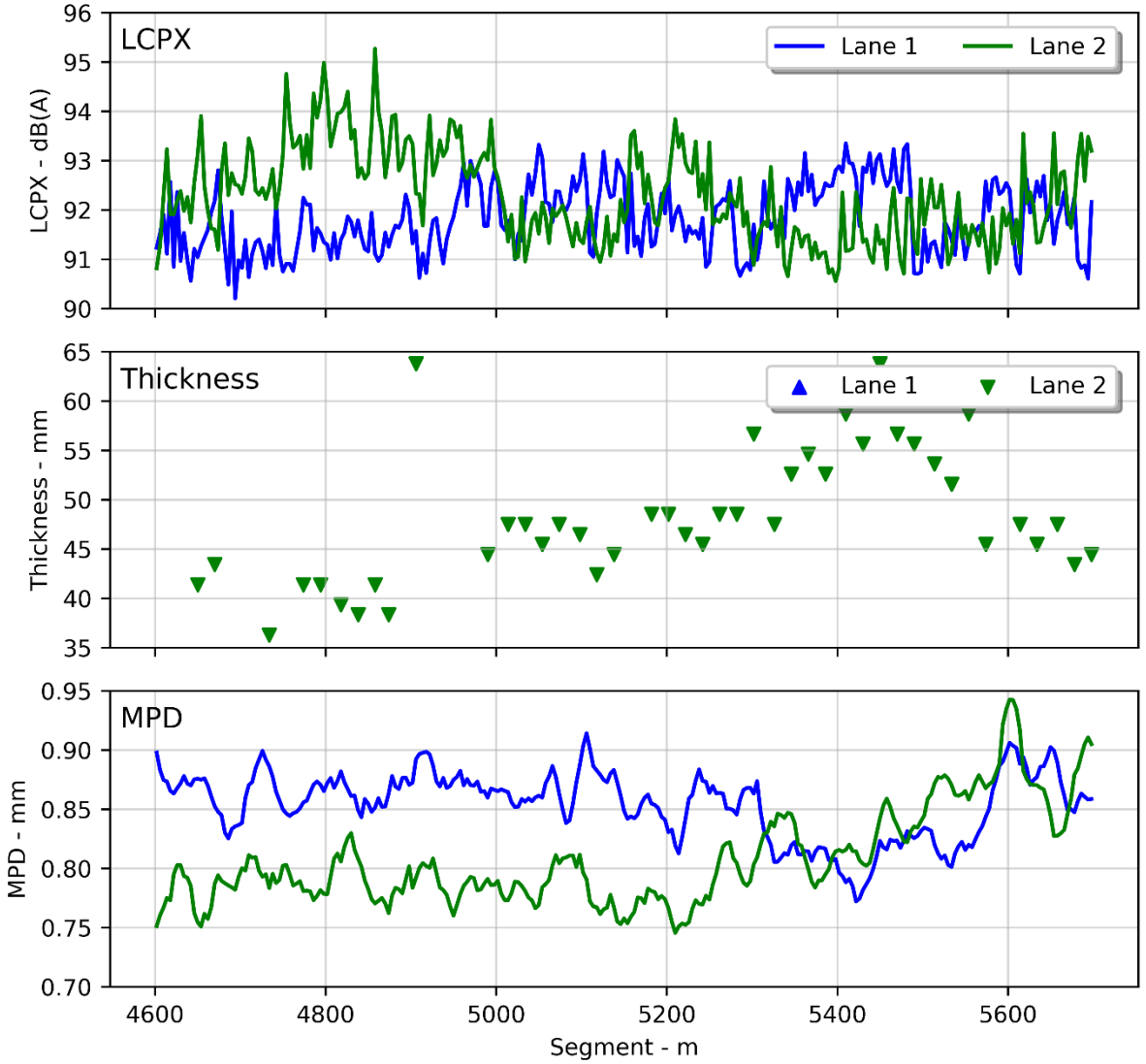

FIGURE 48. EPA7-50 MM ON CNC. LONGITUDINAL PLOTS OF L_{CPX}, THICKNESS, AND MPD.

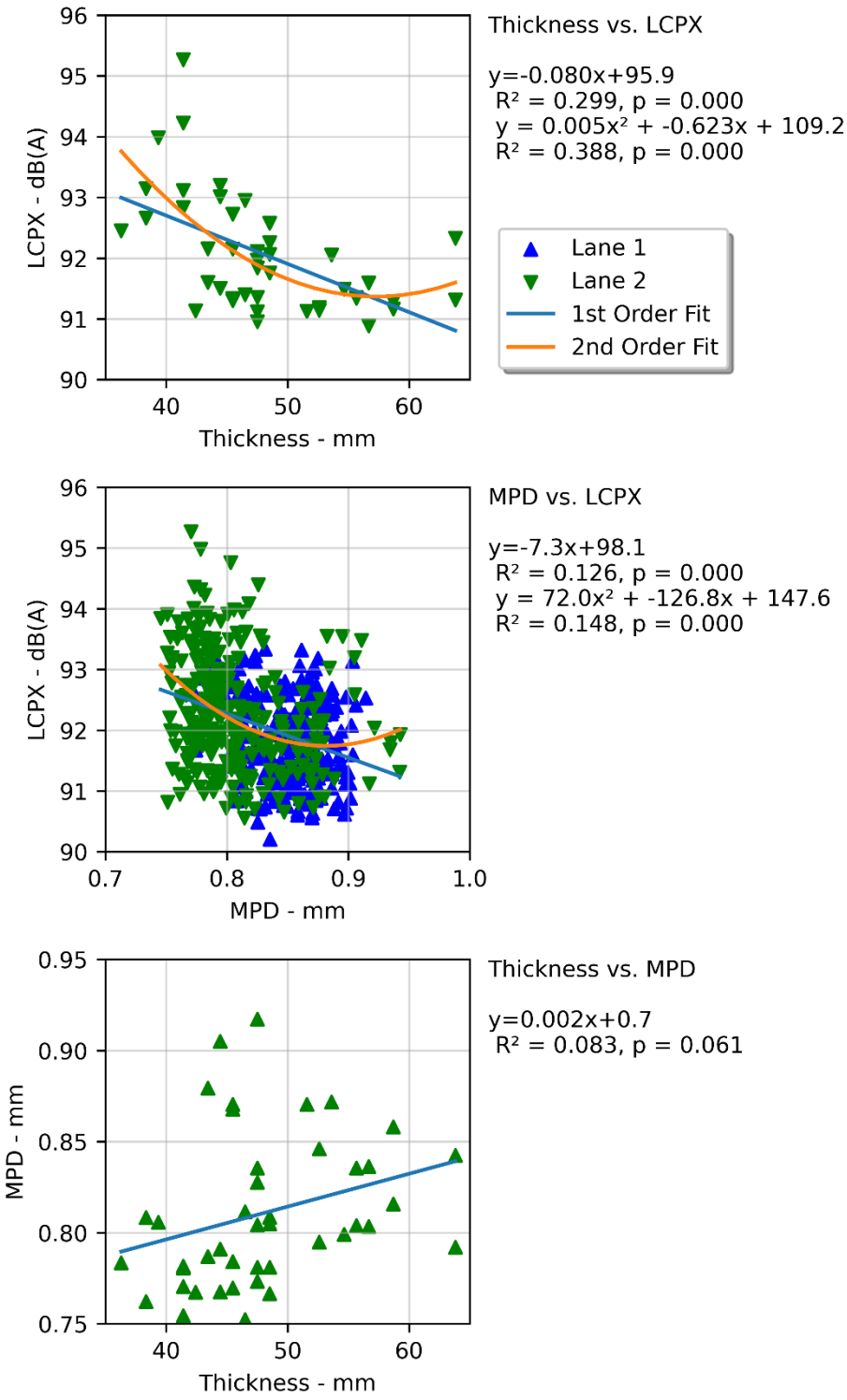

FIGURE 49. EPA7-50 MM ON CNC. L_{CPX} VS. THICKNESS, L_{CPX} VS. MPD, AND MPD VS. THICKNESS.

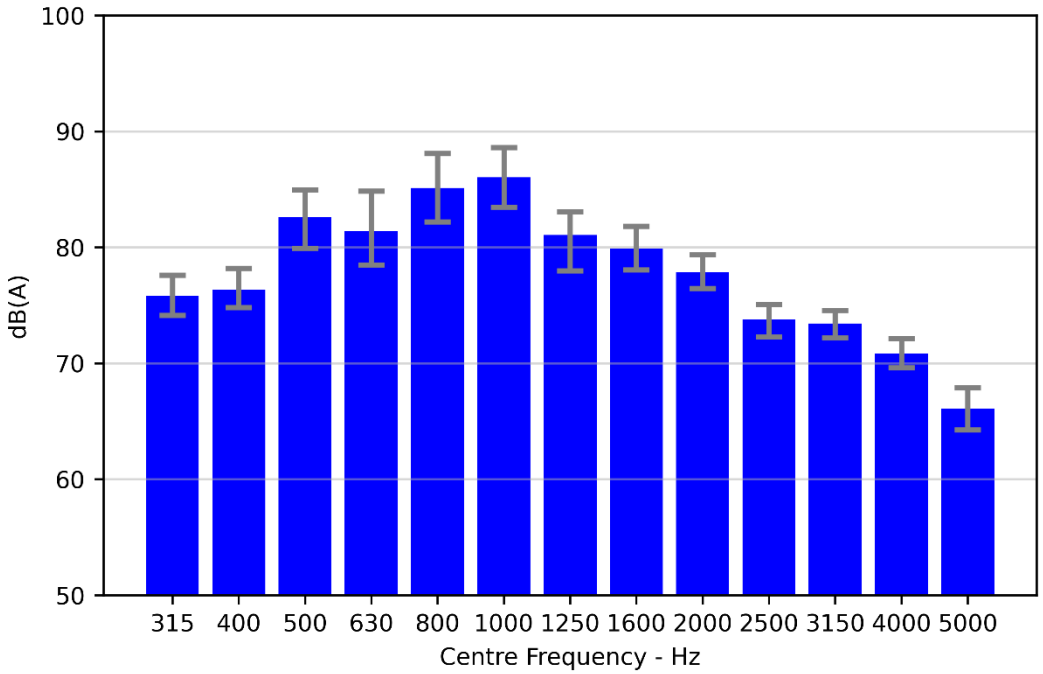

FIGURE 50. EPA7-50 MM ON CNC. ONE-THIRD OCTAVE BAND DISTRIBUTION WITH 10-90TH PERCENTILE VARIATION.

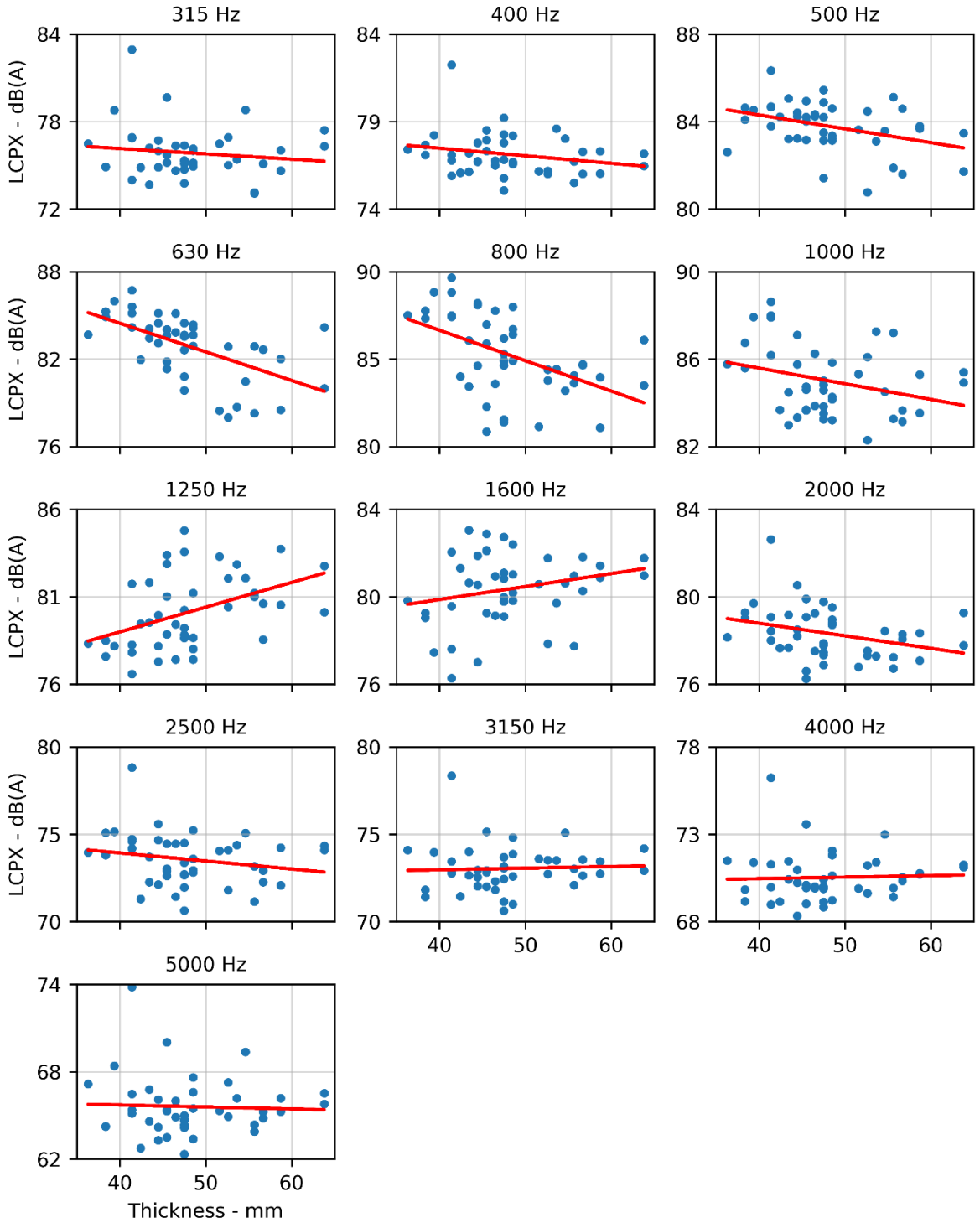

FIGURE 51. EPA7-50 MM ON CNC. ONE-THIRD OCTAVE BAND L_{CPX} VS. THICKNESS.

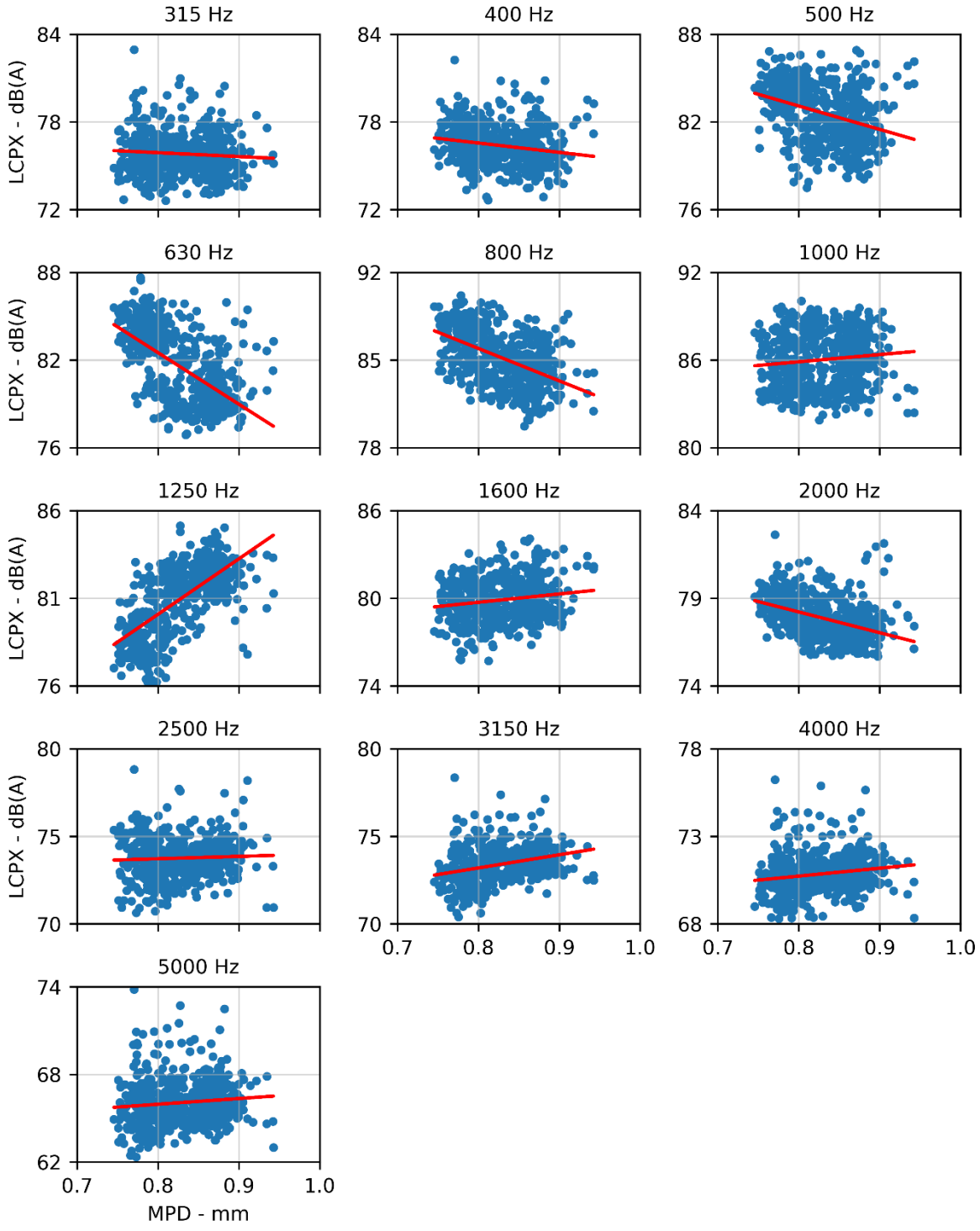

FIGURE 52. EPA7-50 MM ON CNC. ONE-THIRD OCTAVE BAND L_{CPX} VS. MPD.

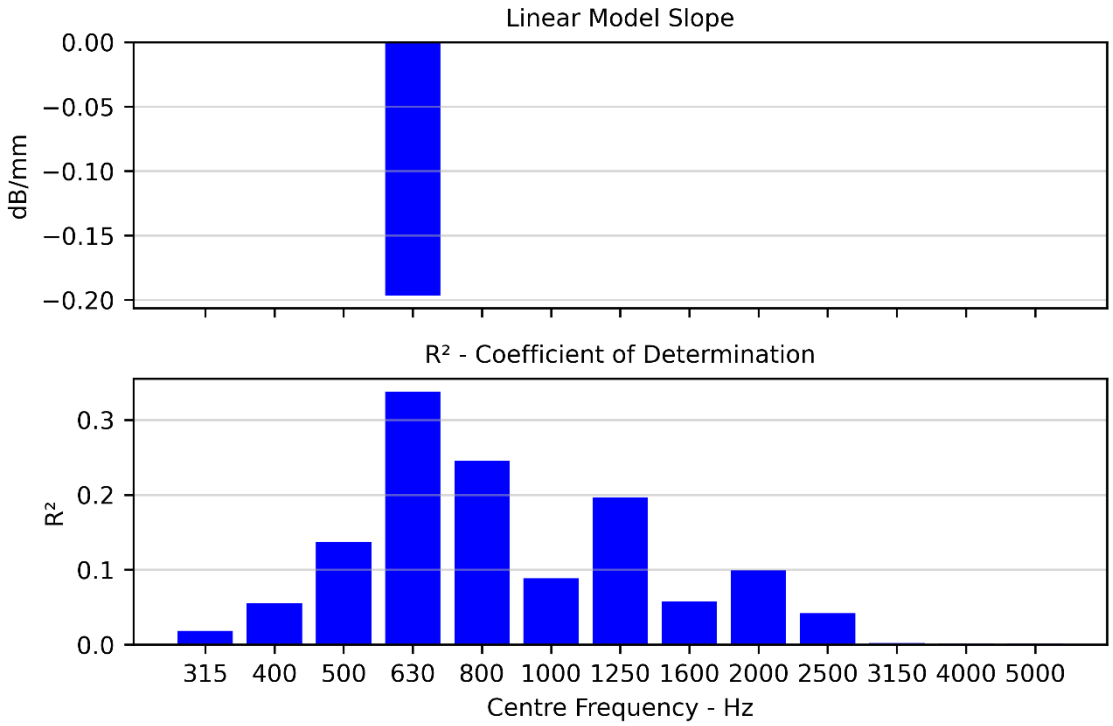

FIGURE 53. EPA7-50 MM ON CNC. ONE-THIRD OCTAVE BAND L_{CPX} AND THICKNESS CORRELATIONS. TOP CHART IS THE LINEAR FIT SLOPE AND BOTTOM CHART IS COEFFICIENT OF DETERMINATION (R^2).

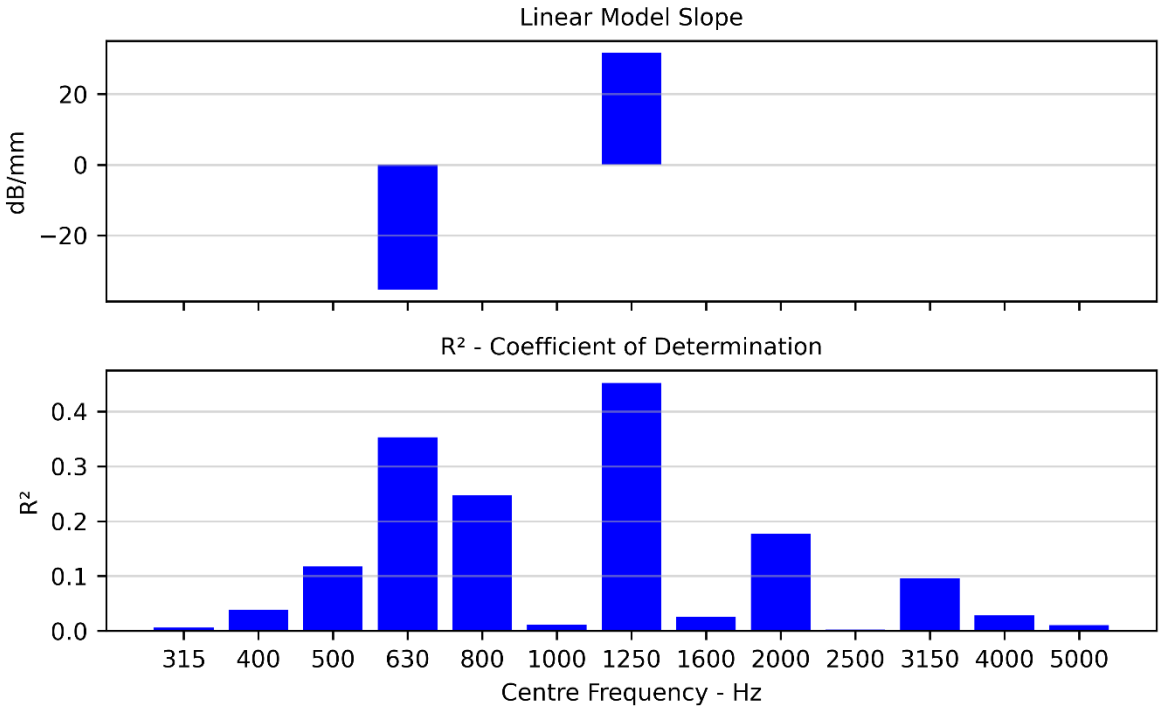

FIGURE 54. EPA7-50 MM ON CNC. ONE-THIRD OCTAVE BAND L_{CPX} AND MPD CORRELATIONS. TOP CHART IS THE LINEAR FIT SLOPE AND BOTTOM CHART IS COEFFICIENT OF DETERMINATION (R^2).

Table 22. EPA7-50 mm on CNC. Multi-variable linear regression between L_{CPX}, MPD, and thickness.

R^2	0.34	
Adj. R^2	0.30	
Thickness	-0.07 dB/mm	p = 0.001
MPD	-	p = 0.14

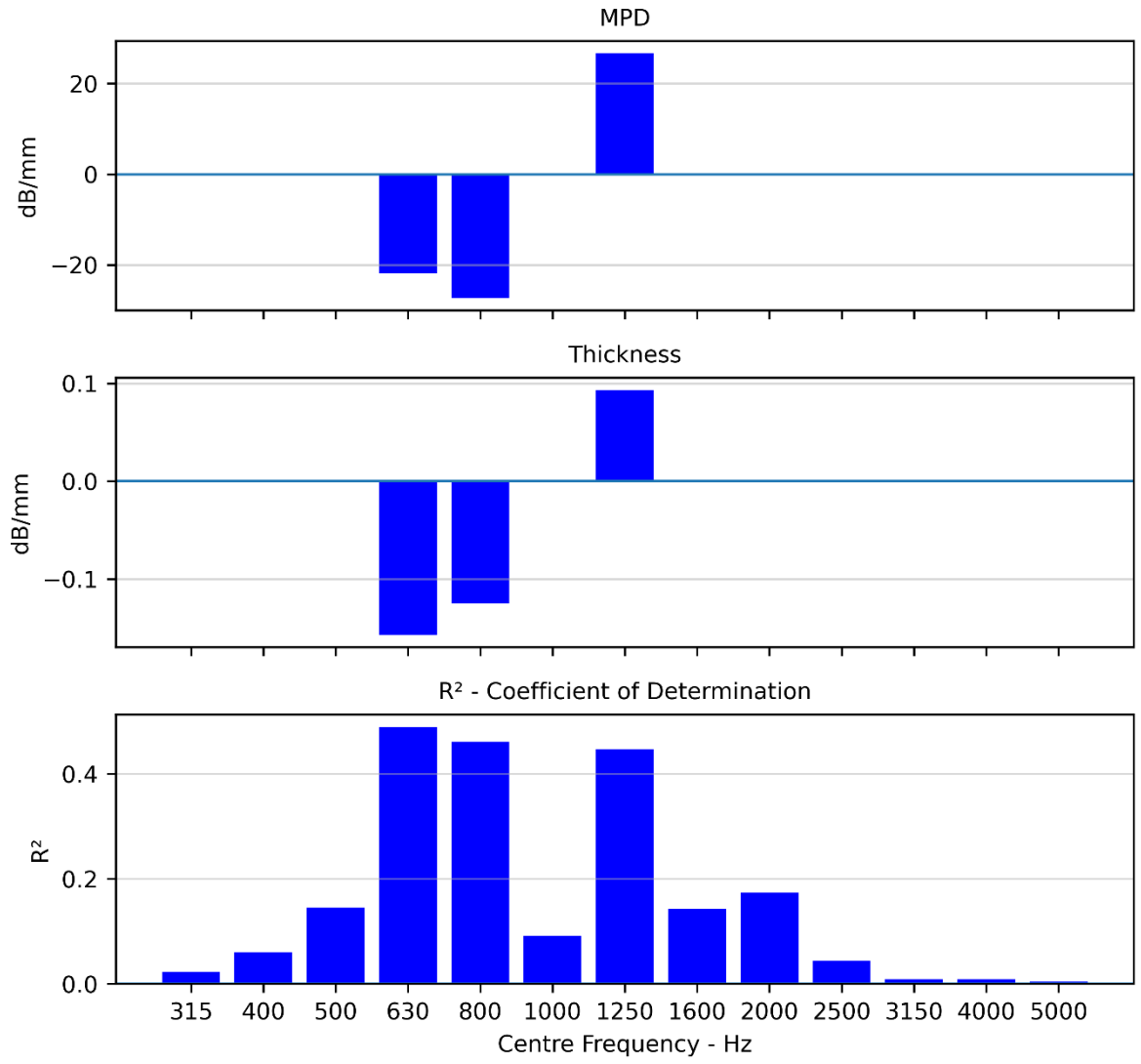

Figure 55. EPA7-50 mm on CNC. One-third octave band L_{CPX} vs. MPD and thickness correlations. Maximum p-value of 0.025.

7.1.7 PA7 and PA10

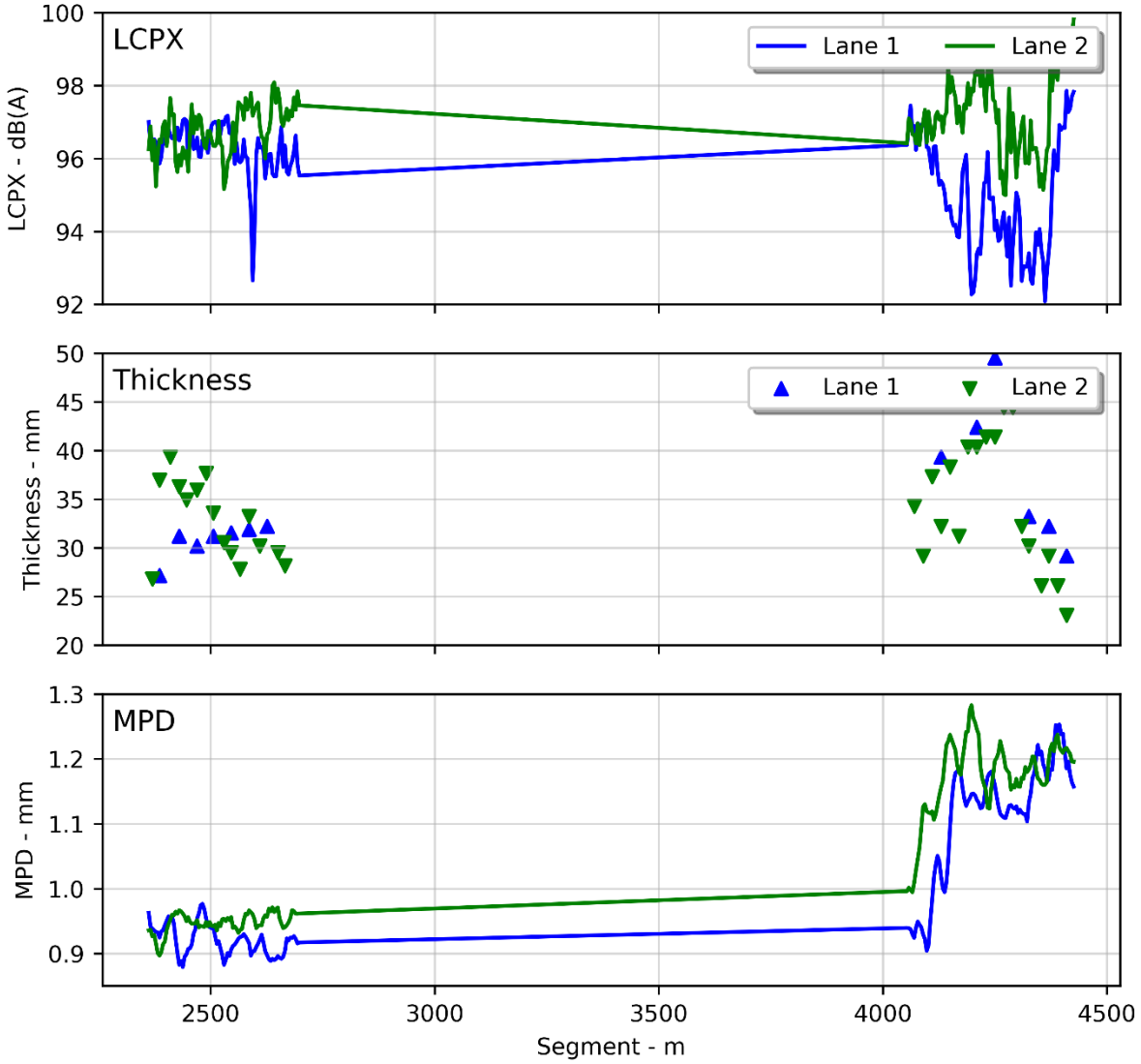

FIGURE 56. PA7 (LEFT) AND PA10 (RIGHT) ON CNC. LONGITUDINAL PLOTS OF L_{CPX}, THICKNESS, AND MPD.

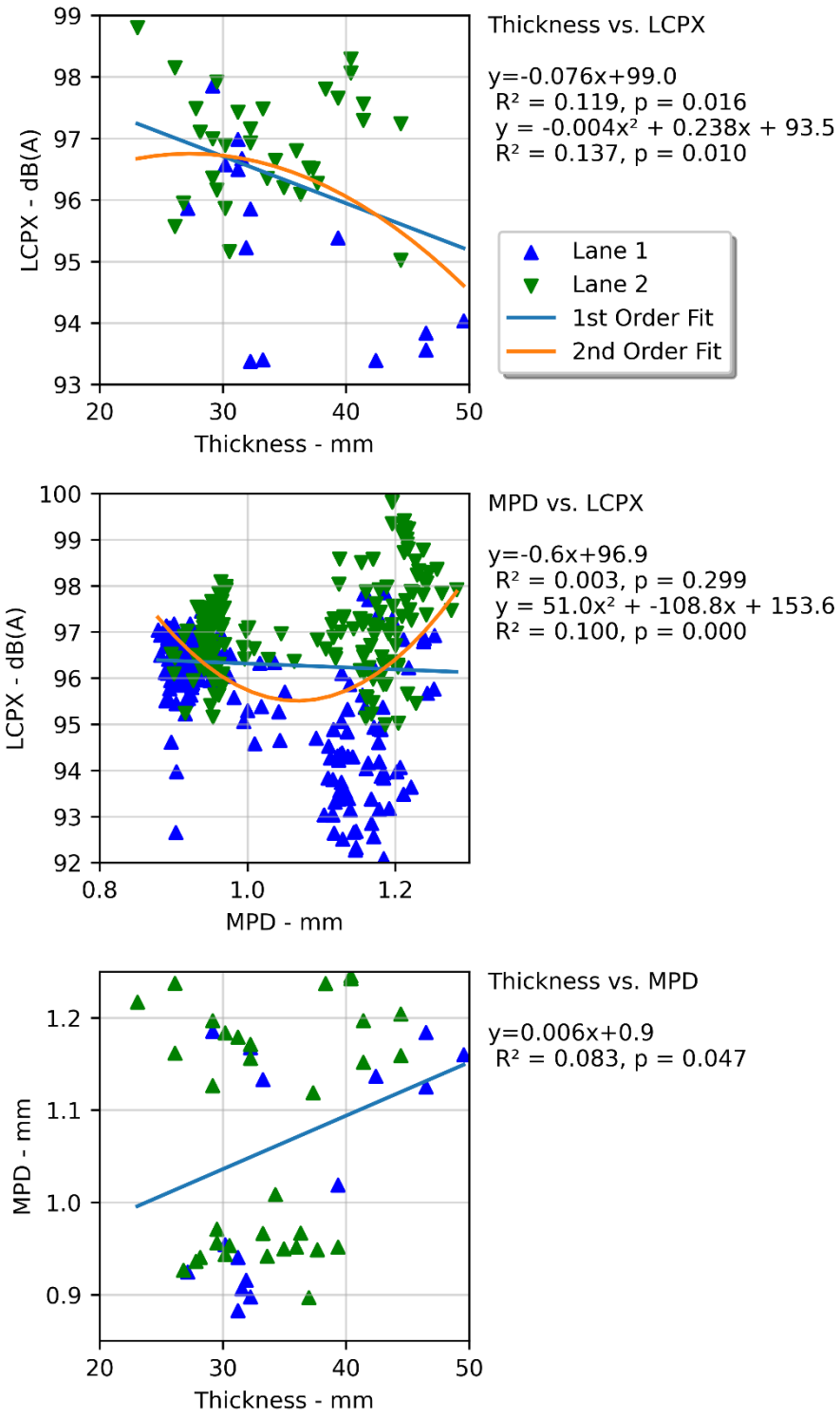

FIGURE 57. PA7 AND PA10ON CNC. L_{CPX} VS. THICKNESS, L_{CPX} VS. MPD, AND MPD VS. THICKNESS.

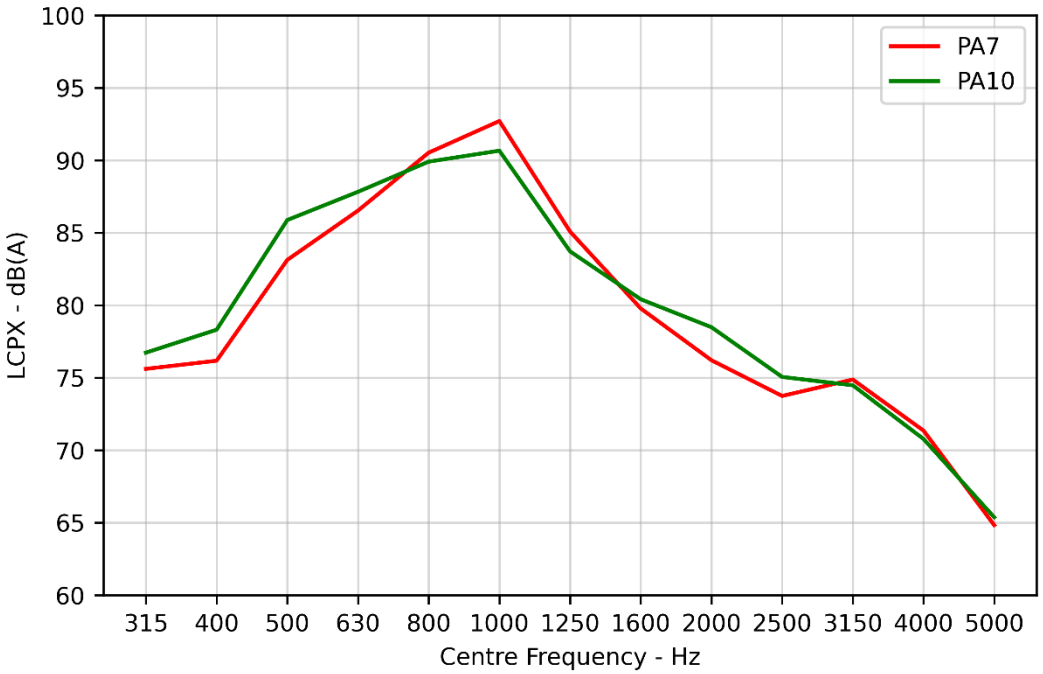

FIGURE 58. PA7 AND PA10 ON CNC. ONE-THIRD OCTAVE BAND DISTRIBUTIONS.

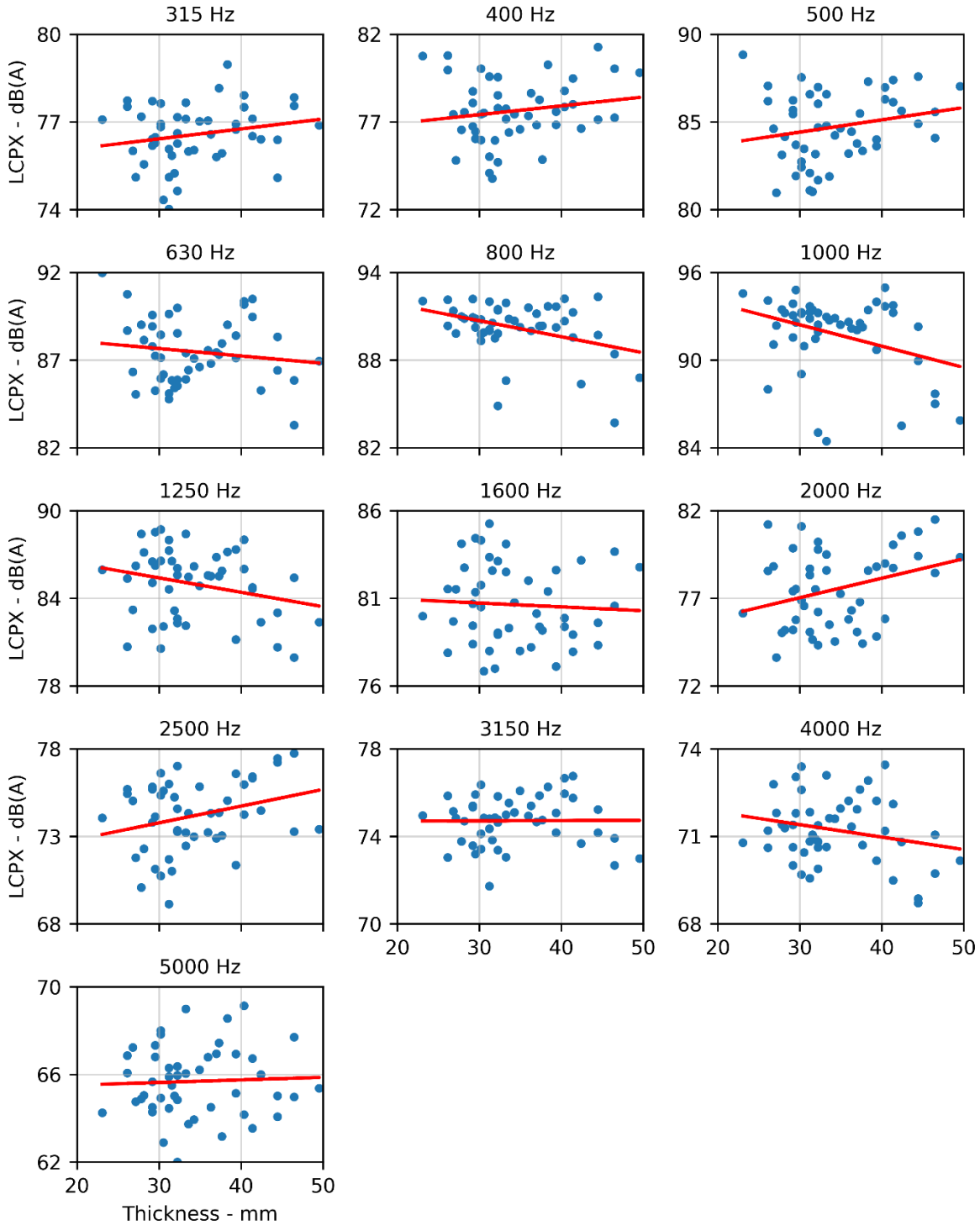

FIGURE 59. PA7 AND PA10 ON CNC. ONE-THIRD OCTAVE BAND L_{CPX} VS. THICKNESS.

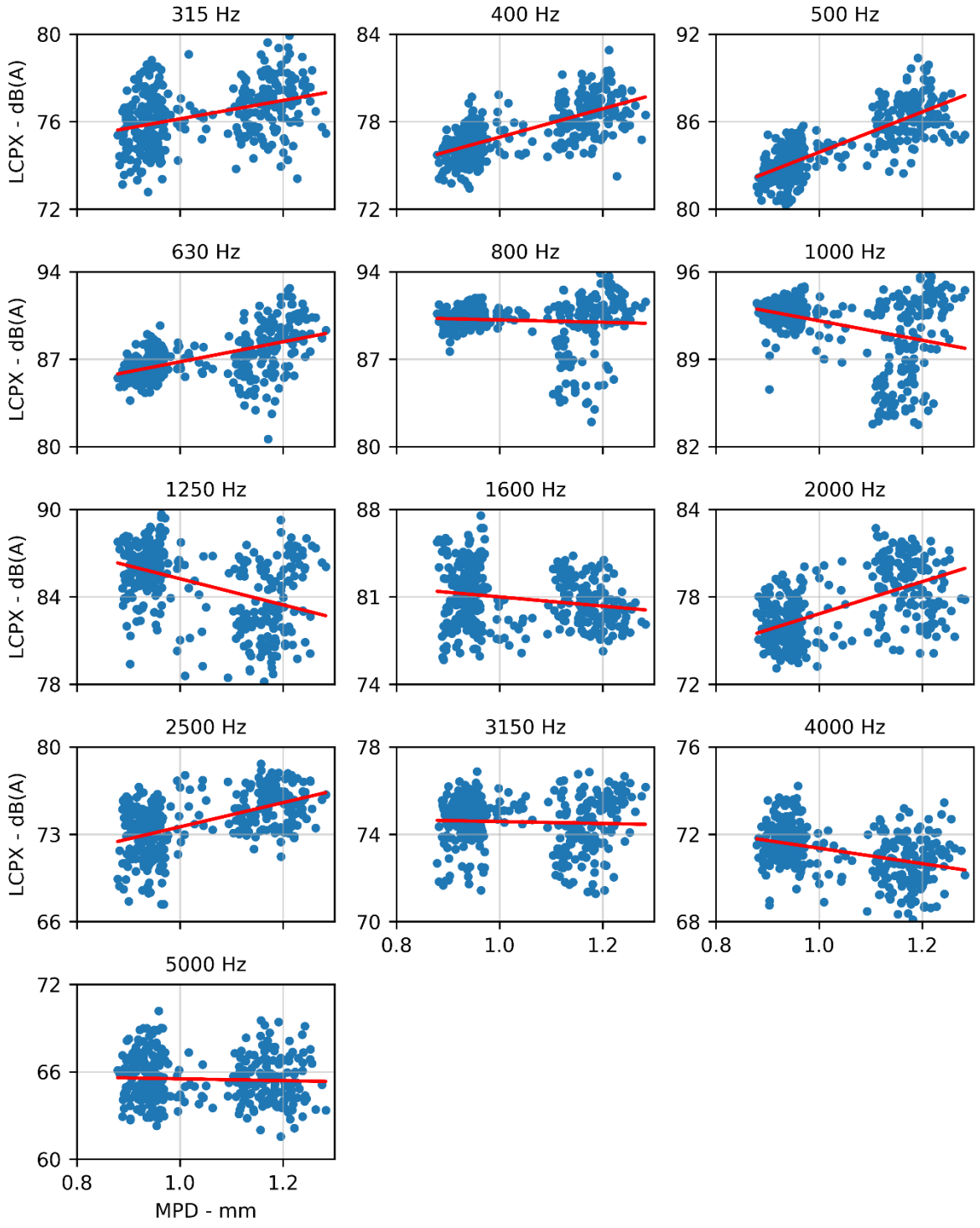

FIGURE 60. PA7 AND PA10 ON CNC. ONE-THIRD OCTAVE BAND L_{CPX} VS. MPD.

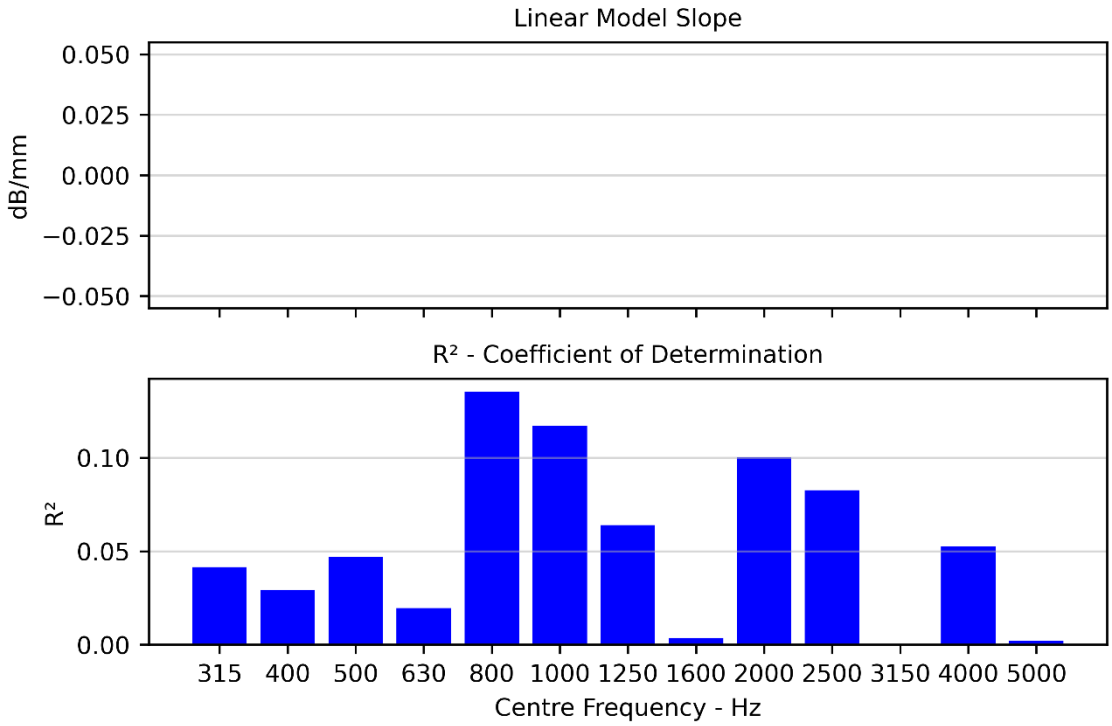

FIGURE 61. PA7 AND PA10 ON CNC. ONE-THIRD OCTAVE BAND L_{CPX} AND THICKNESS CORRELATIONS. TOP CHART IS THE LINEAR FIT SLOPE AND BOTTOM CHART IS COEFFICIENT OF DETERMINATION (R^2).

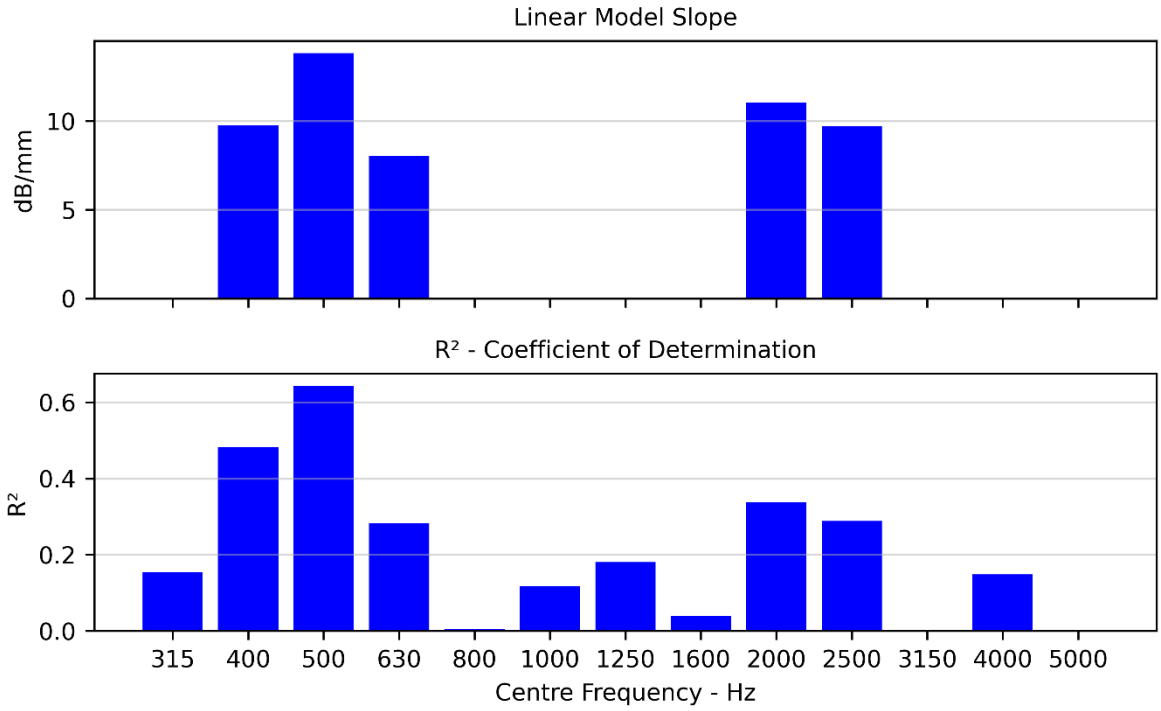

FIGURE 62. PA7 AND PA10 ON CNC. ONE-THIRD OCTAVE BAND L_{CPX} AND MPD CORRELATIONS. TOP CHART IS THE LINEAR FIT SLOPE AND BOTTOM CHART IS COEFFICIENT OF DETERMINATION (R^2).

TABLE 23. PA7 AND PA10ON CNC. MULTI-VARIABLE LINEAR REGRESSION BETWEEN L_{CPX}, MPD, AND THICKNESS.

R^2	0.14	
Adj. R^2	0.10	
Thickness	-0.009 dB/mm	p = 0.01
MPD	-	p = 0.30

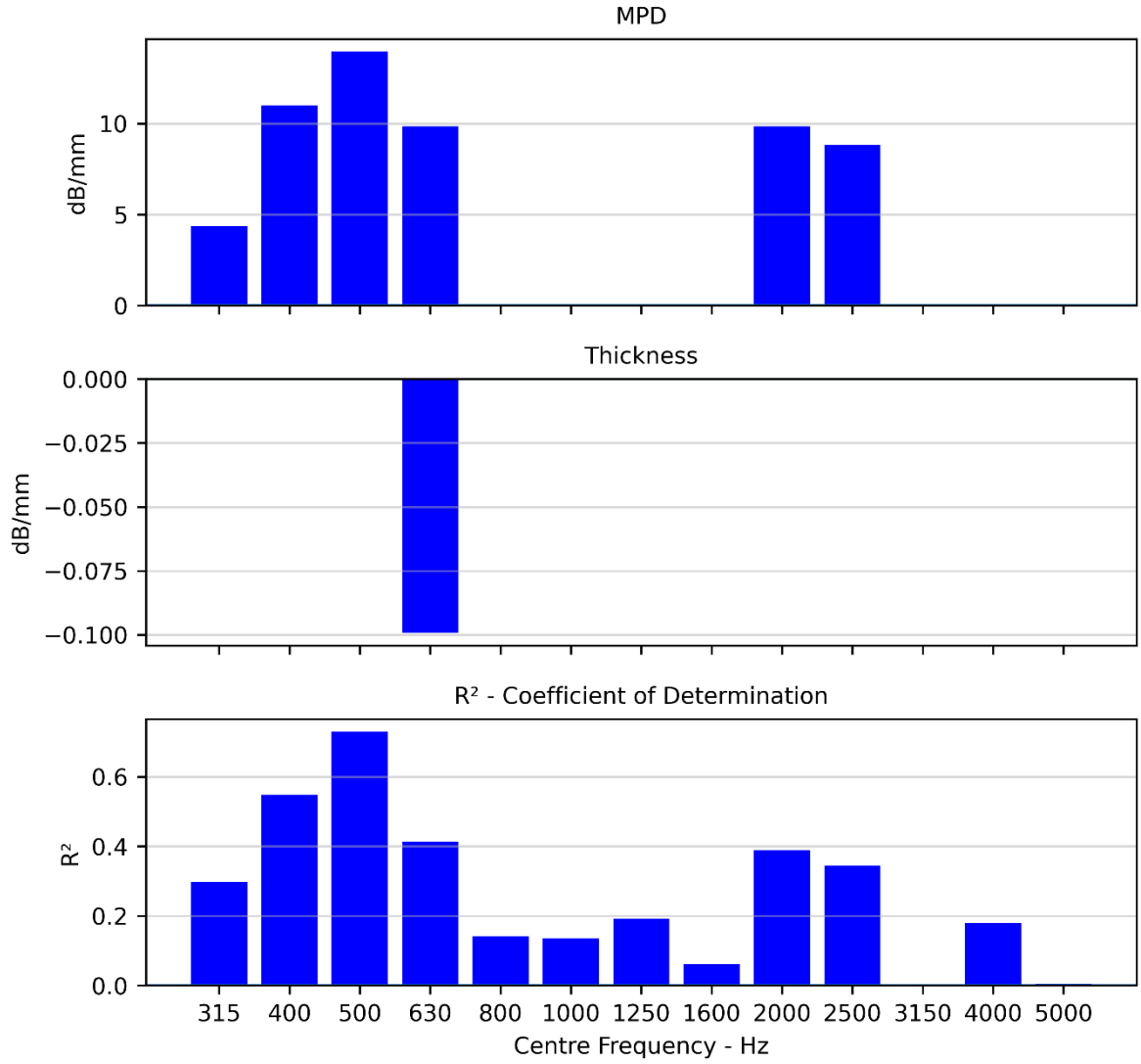

FIGURE 63. PA7 AND PA10 ON CNC. ONE-THIRD OCTAVE BAND L_{CPX} VS. MPD AND THICKNESS CORRELATIONS. MAXIMUM P-VALUE OF 0.025.

7.1.8 PA7-30 mm and EPA7-50 mm

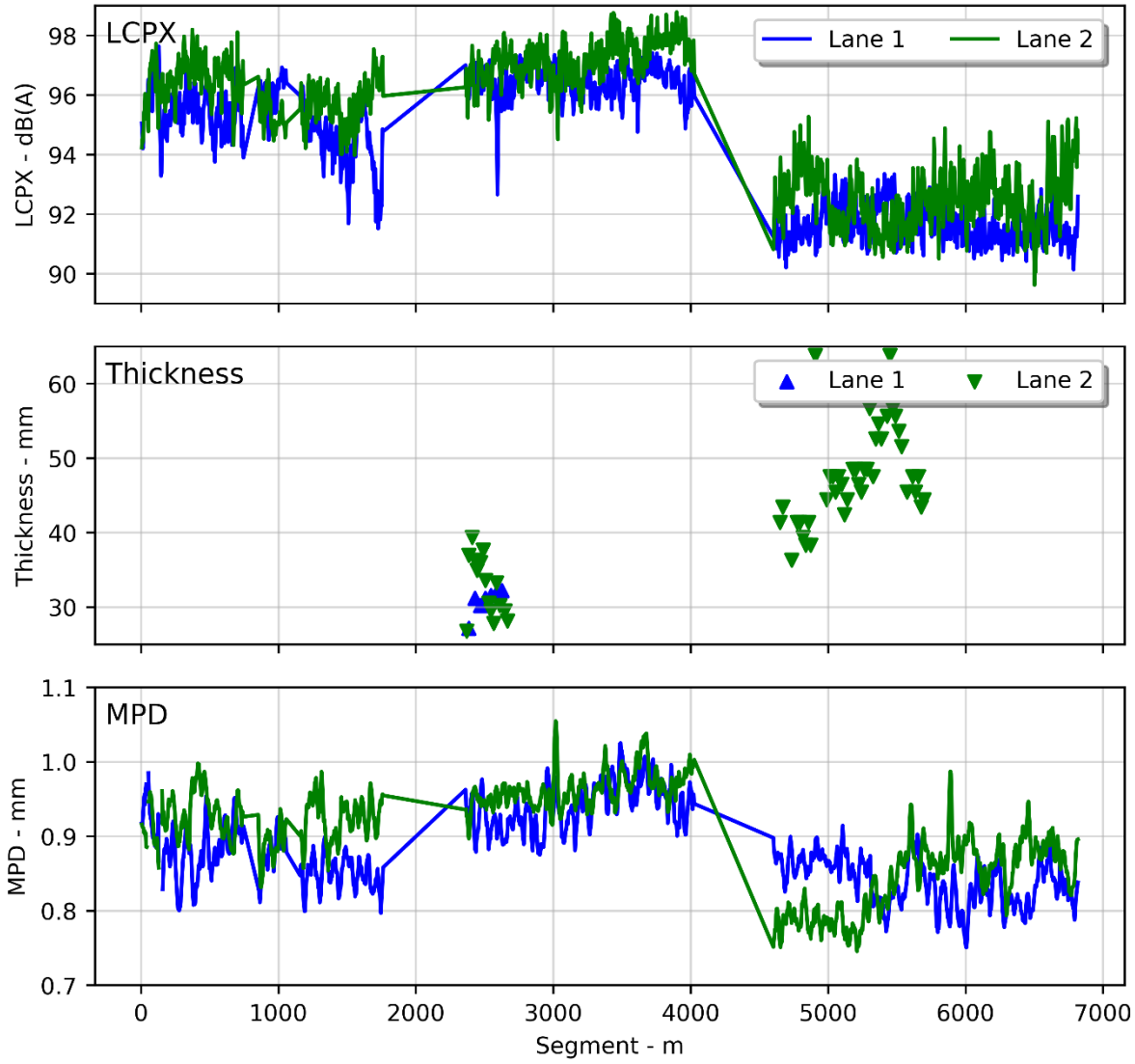

FIGURE 64. PA7-30 MM AND EPA7-50 MM ON CNC. LONGITUDINAL PLOTS OF L_{CPX}, THICKNESS, AND MPD.

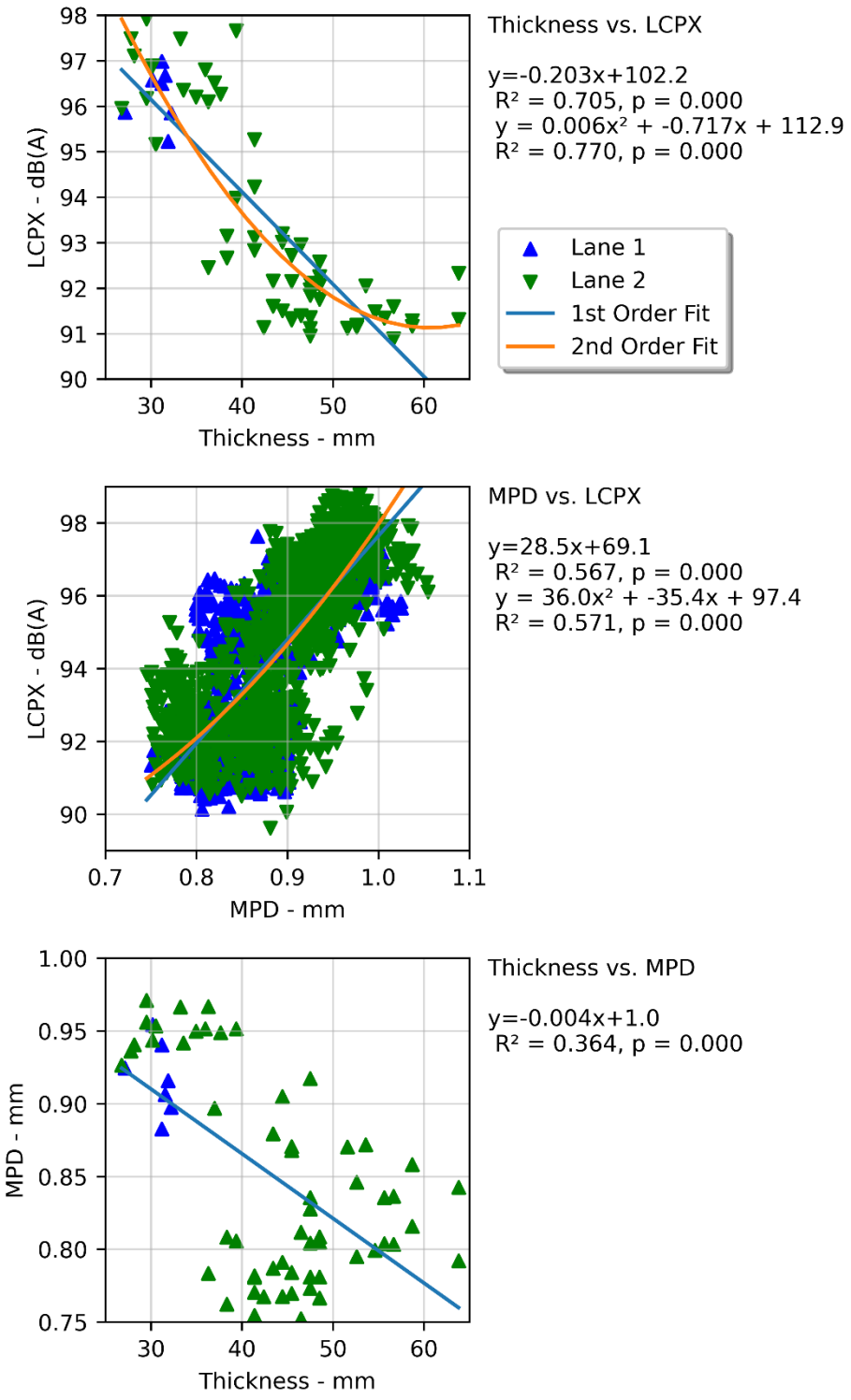

FIGURE 65. PA7-30 MM AND EPA7-50 MM ON CNC. L_{CPX} VS. THICKNESS, L_{CPX} VS. MPD, AND MPD VS. THICKNESS.

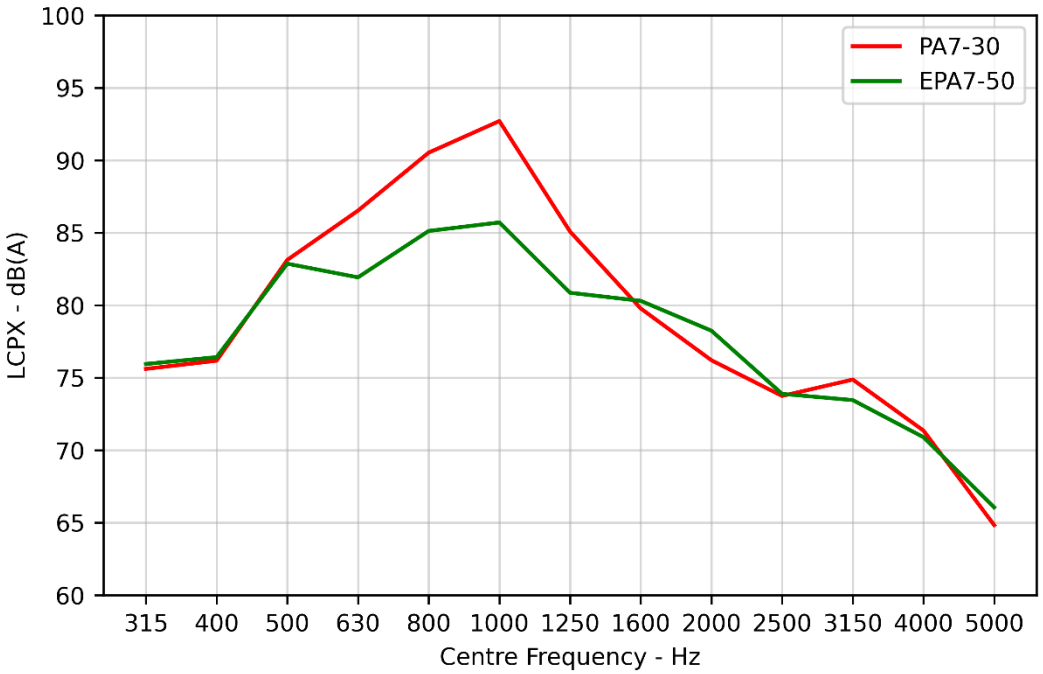

FIGURE 66. PA7-30 MM AND EPA7-50 MM ON CNC. ONE-THIRD OCTAVE BAND DISTRIBUTIONS.

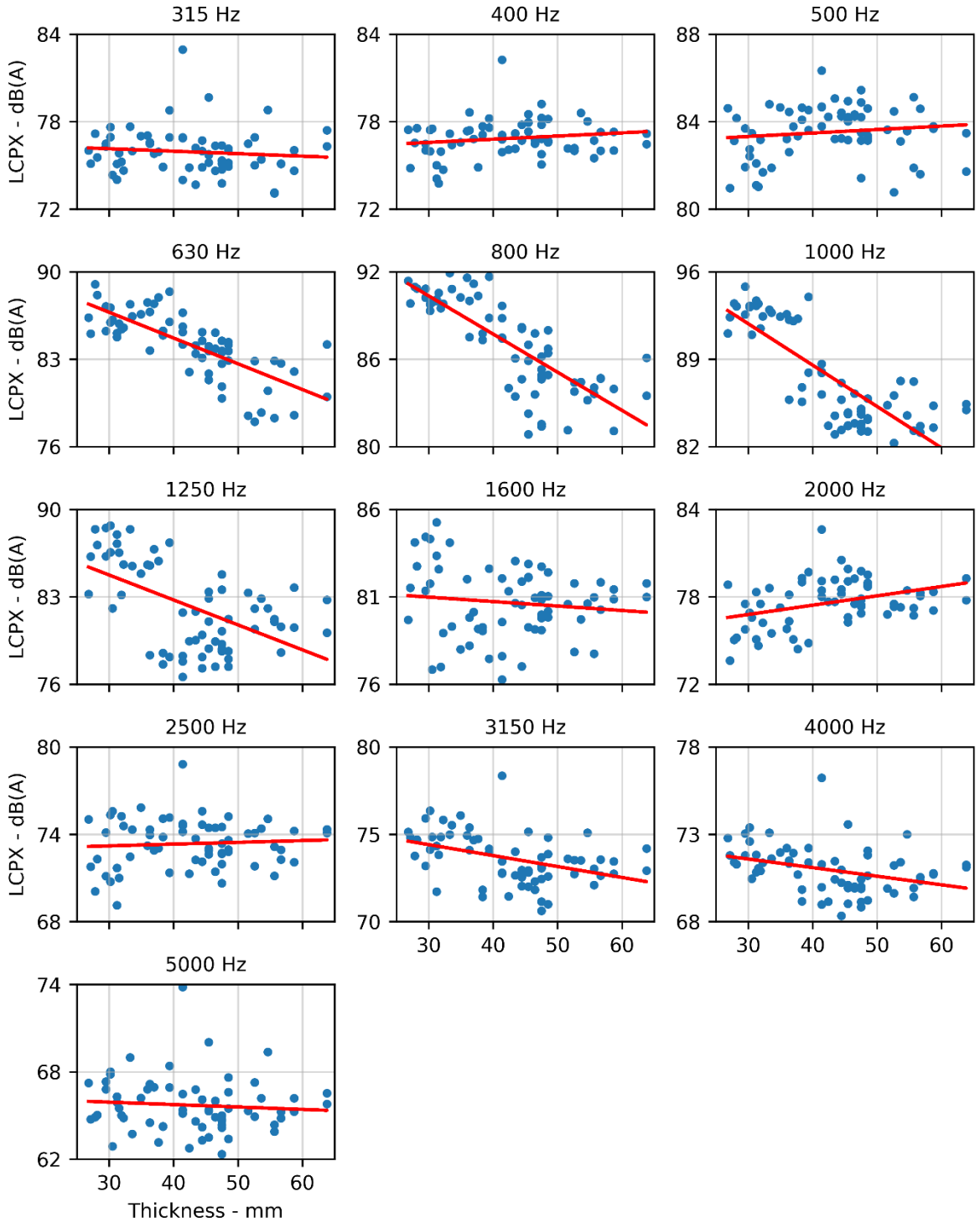

FIGURE 67. PA7-30 MM AND EPA7-50 MM ON CNC. ONE-THIRD OCTAVE BAND L_{CPX} VS. THICKNESS.

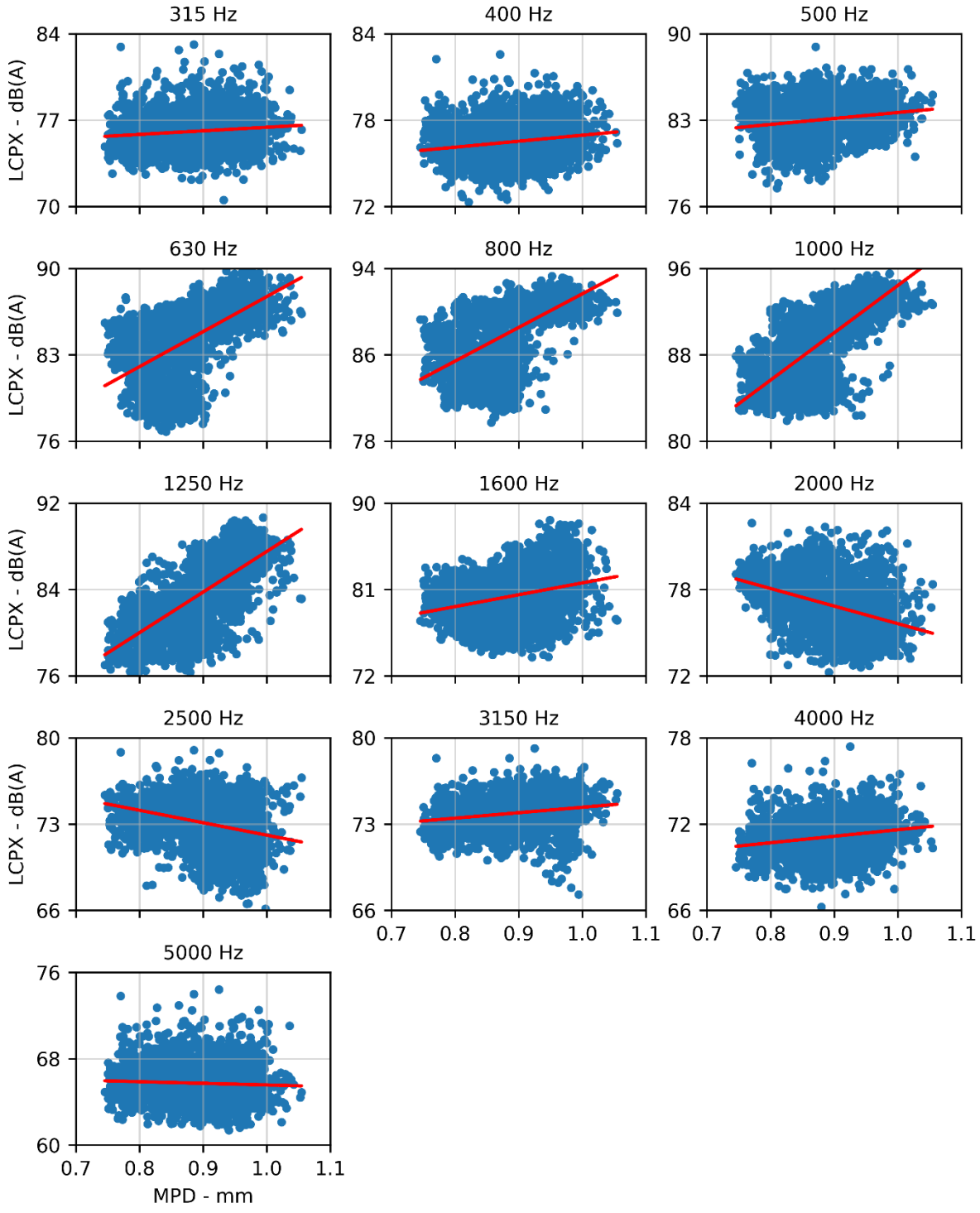

FIGURE 68. PA7-30 MM AND EPA7-50 MM ON CNC. ONE-THIRD OCTAVE BAND L_{CPX} VS. MPD.

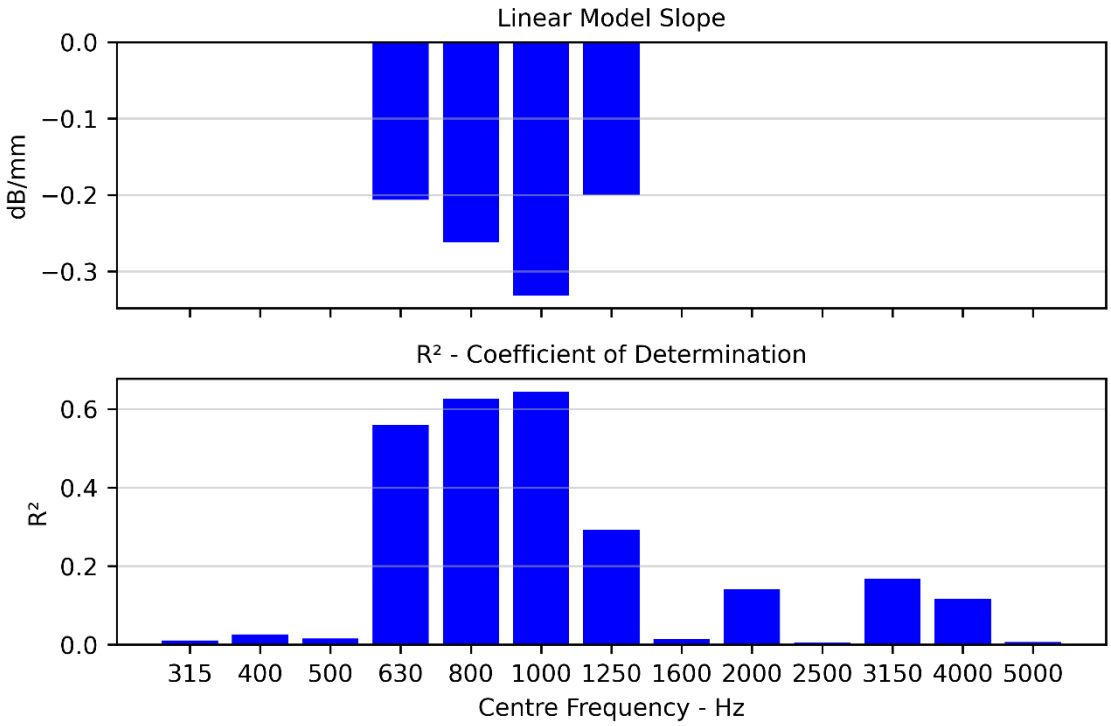

FIGURE 69. PA7-30 MM AND EPA7-50 MM ON CNC. ONE-THIRD OCTAVE BAND L_{CPX} AND THICKNESS CORRELATIONS. TOP CHART IS THE LINEAR FIT SLOPE AND BOTTOM CHART IS COEFFICIENT OF DETERMINATION (R^2).

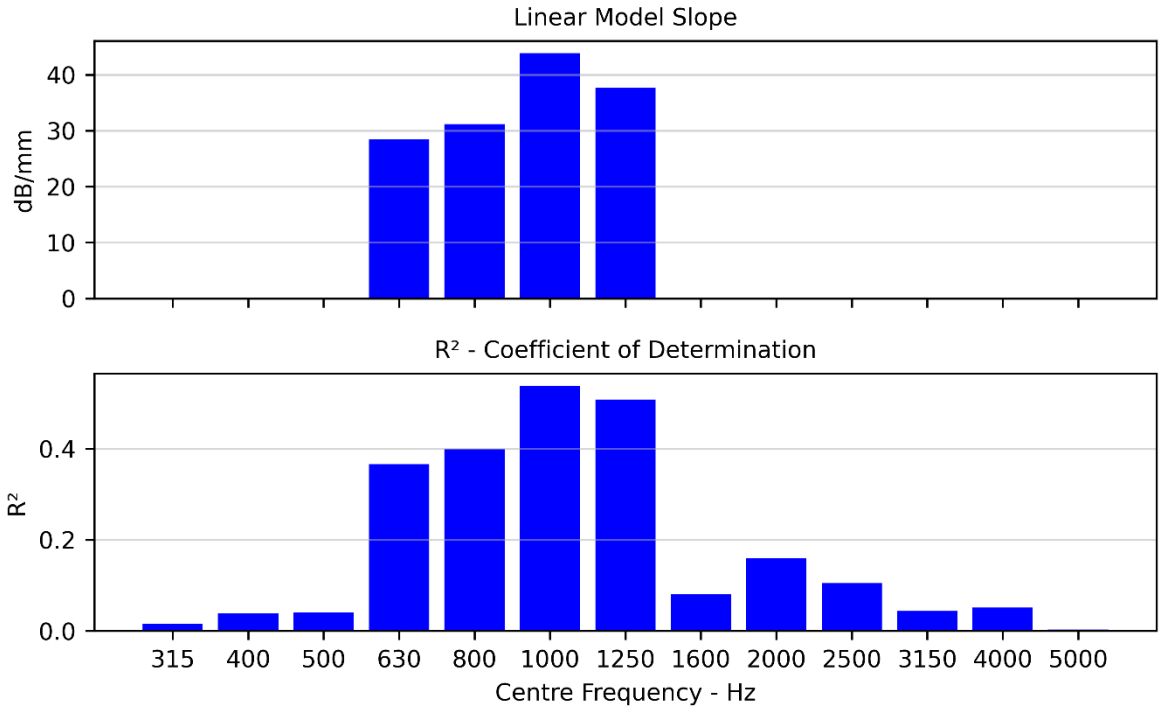

FIGURE 70. PA7-30 MM AND EPA7-50 MM ON CNC. ONE-THIRD OCTAVE BAND L_{CPX} AND MPD CORRELATIONS. TOP CHART IS THE LINEAR FIT SLOPE AND BOTTOM CHART IS COEFFICIENT OF DETERMINATION (R^2).

TABLE 24. PA7-30 MM AND EPA7-50 MM ON CNC. MULTI-VARIABLE LINEAR REGRESSION BETWEEN L_{CPX}, MPD, AND THICKNESS.

R^2	0.80	
Adj. R^2	0.79	
Thickness	-0.15 dB/mm	p = 0.00
MPD	12.4 dB/mm	p = 0.00

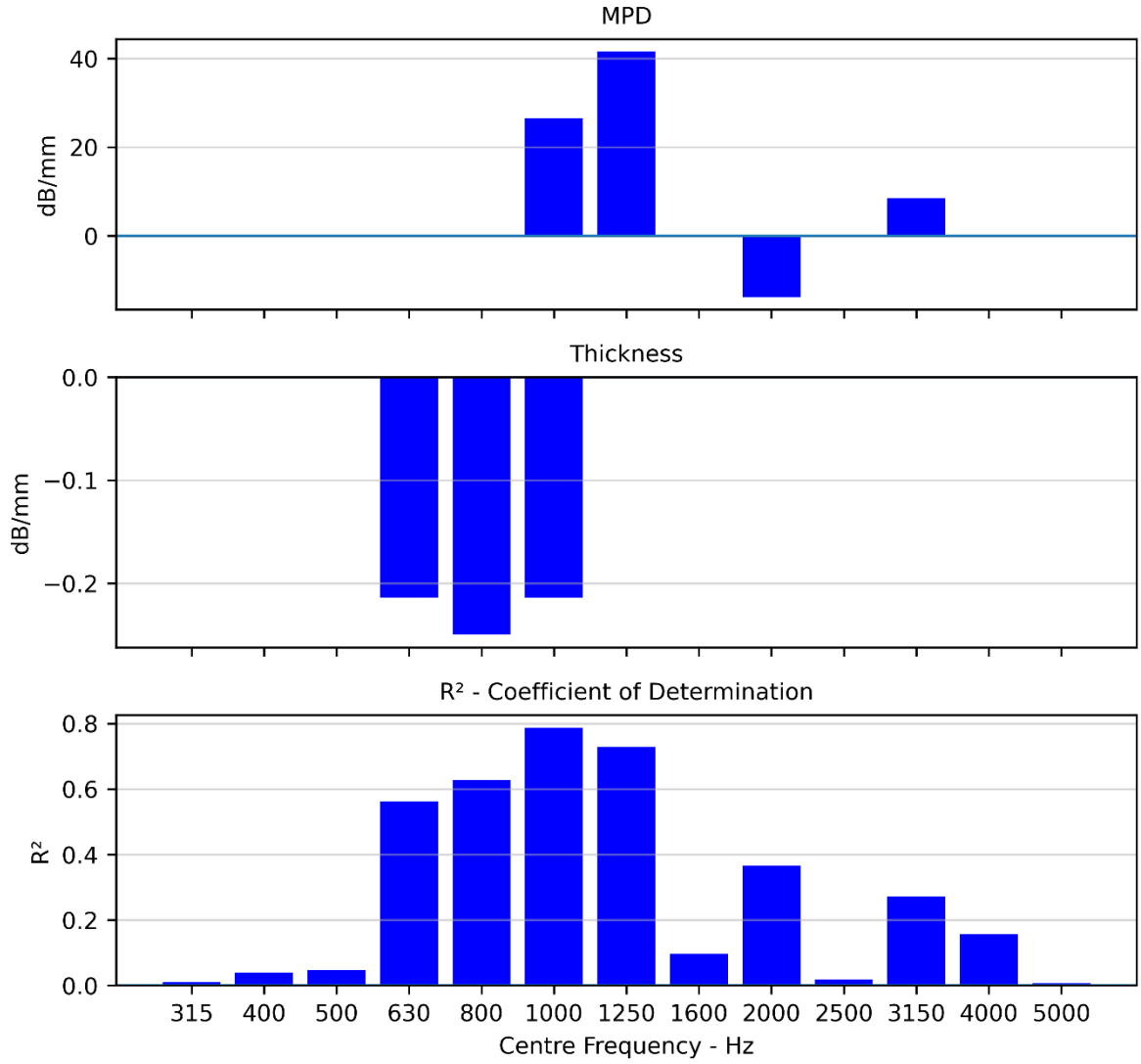

FIGURE 71. PA7-30 MM AND EPA7-50 MM ON CNC. ONE-THIRD OCTAVE BAND L_{CPX} VS. MPD AND THICKNESS CORRELATIONS. MAXIMUM P-VALUE OF 0.025.

7.2 Road Science Hawkeye vs. WDM HSD for CSM2

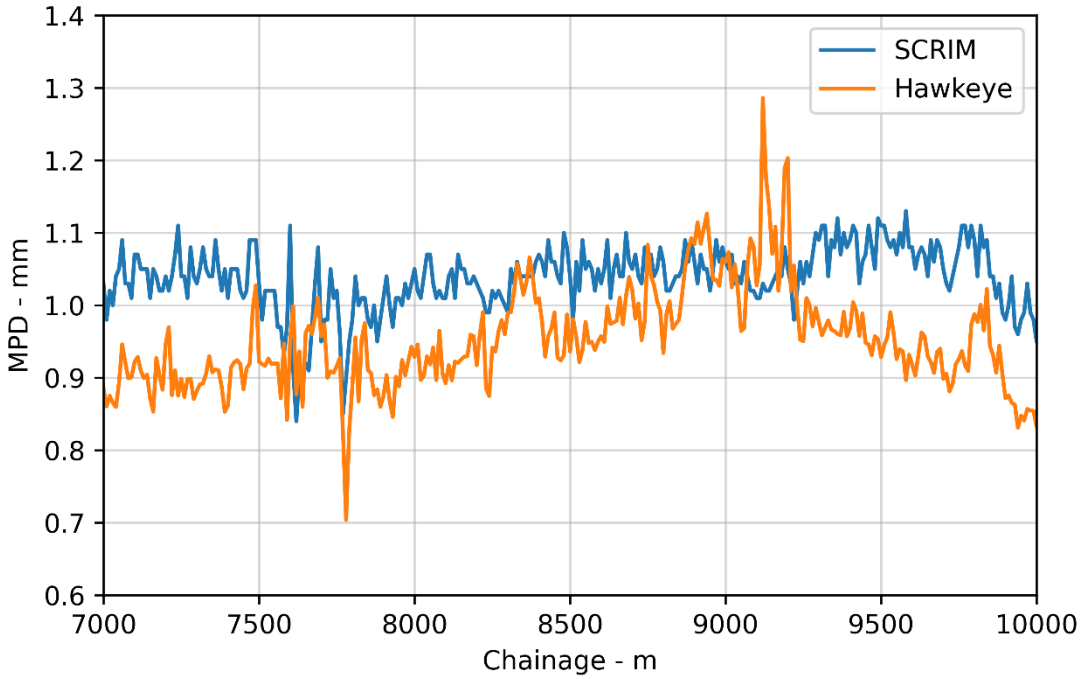

FIGURE 72. LONGITUDINAL COMPARISON BETWEEN MPD MEASURED BY ROAD SCIENCE HAWKEYE AND WDM HSD FOR CSM2 SOUTHBOUND LANE 2.

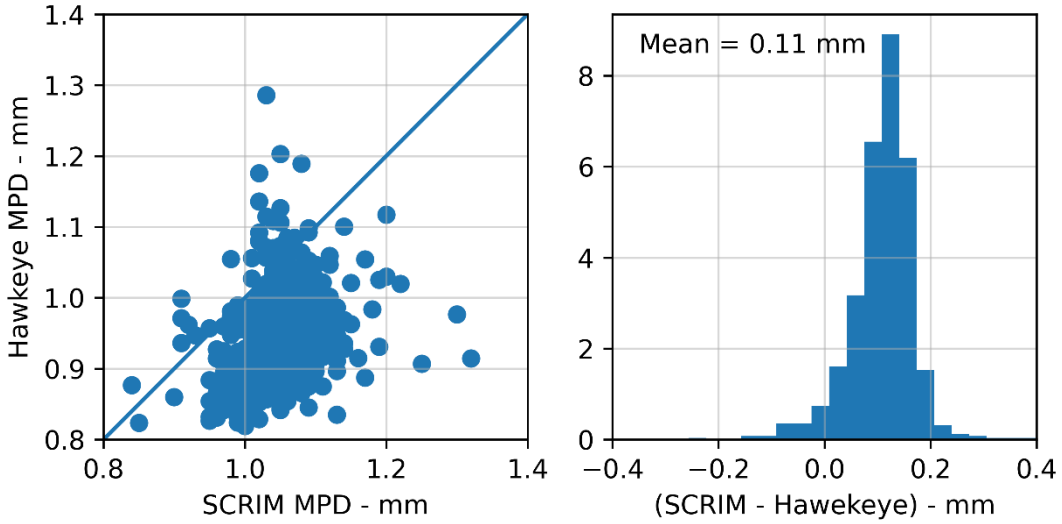

FIGURE 73. COMPARISON BETWEEN MPD MEASURED BY ROAD SCIENCE HAWKEYE AND WDM HSD FOR CSM2 SOUTHBOUND LANE 2.

7.3 Christchurch Southern Motorway – Stage 2 (CSM2)

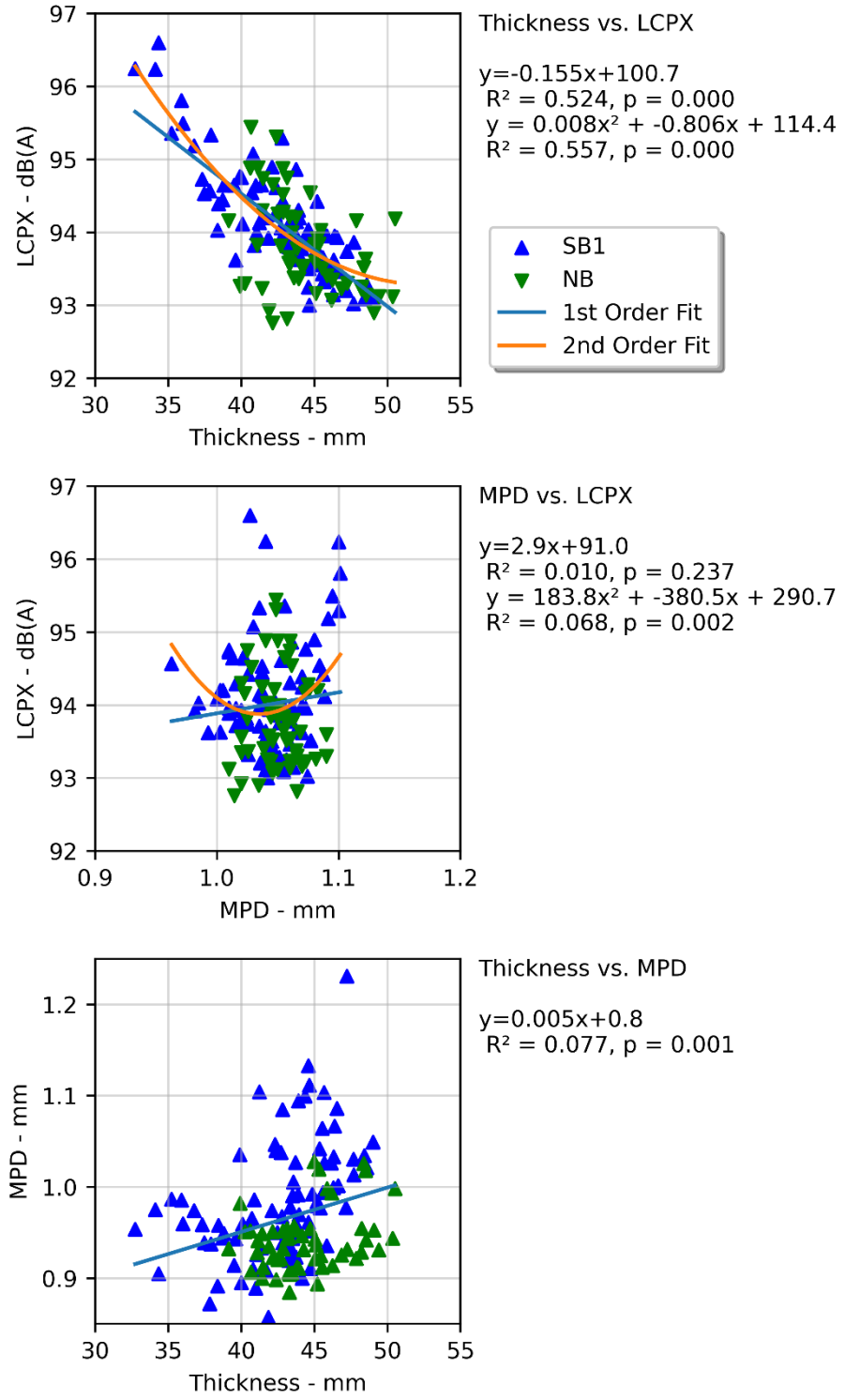

FIGURE 74. EPA7 ON CSM2. L_{CPX} VS. THICKNESS, L_{CPX} VS. MPD, AND MPD VS. THICKNESS.

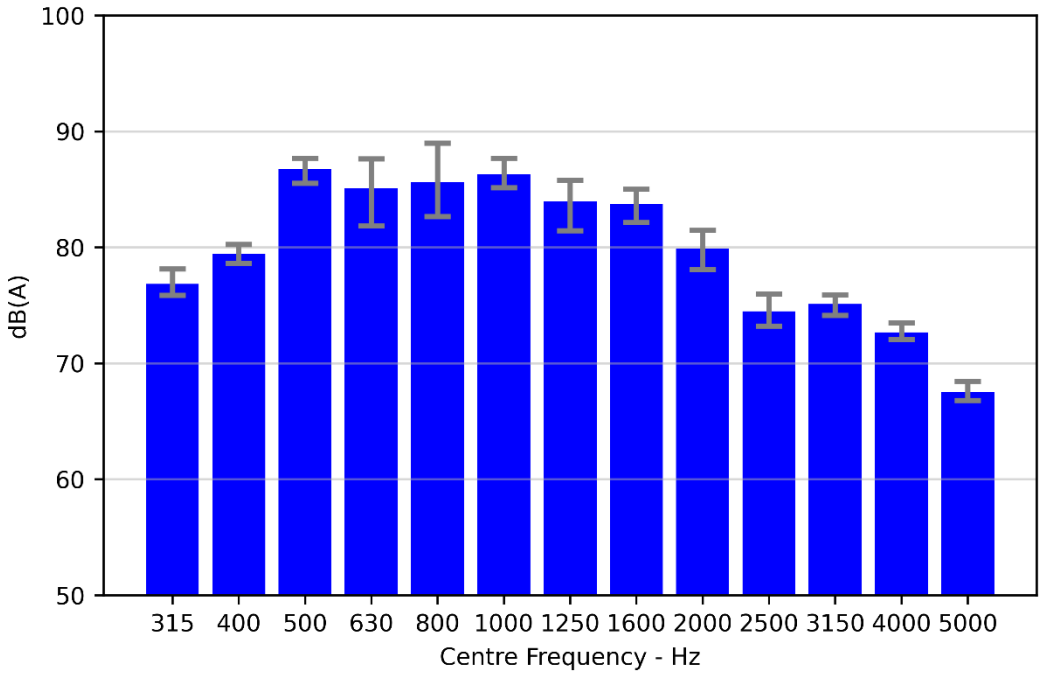

FIGURE 75. EPA7 ON CSM2. ONE-THIRD OCTAVE BAND DISTRIBUTION WITH 10-90TH PERCENTILE VARIATION.

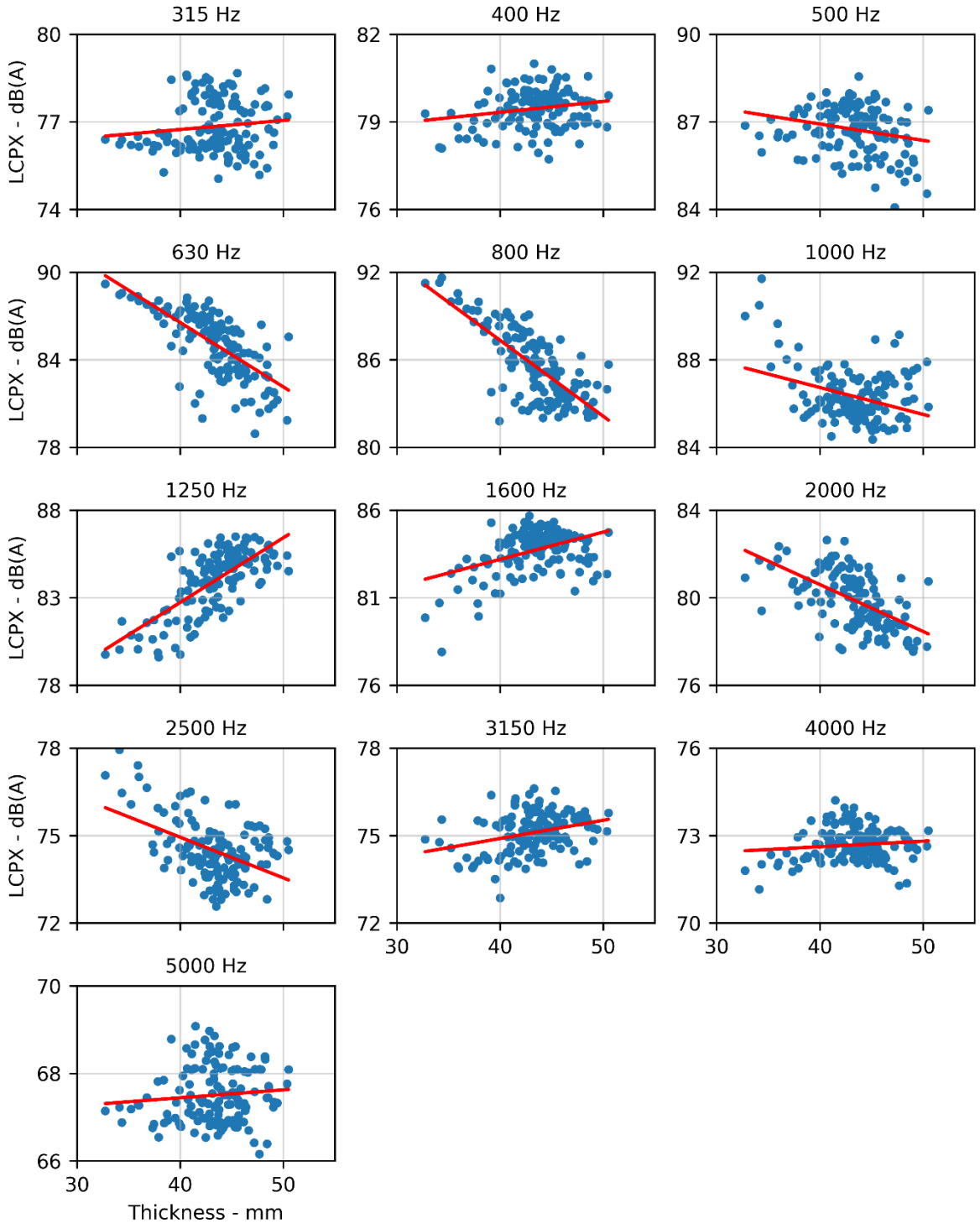

FIGURE 76. EPA7 ON CSM2. ONE-THIRD OCTAVE BAND L_{CPX} VS. THICKNESS.

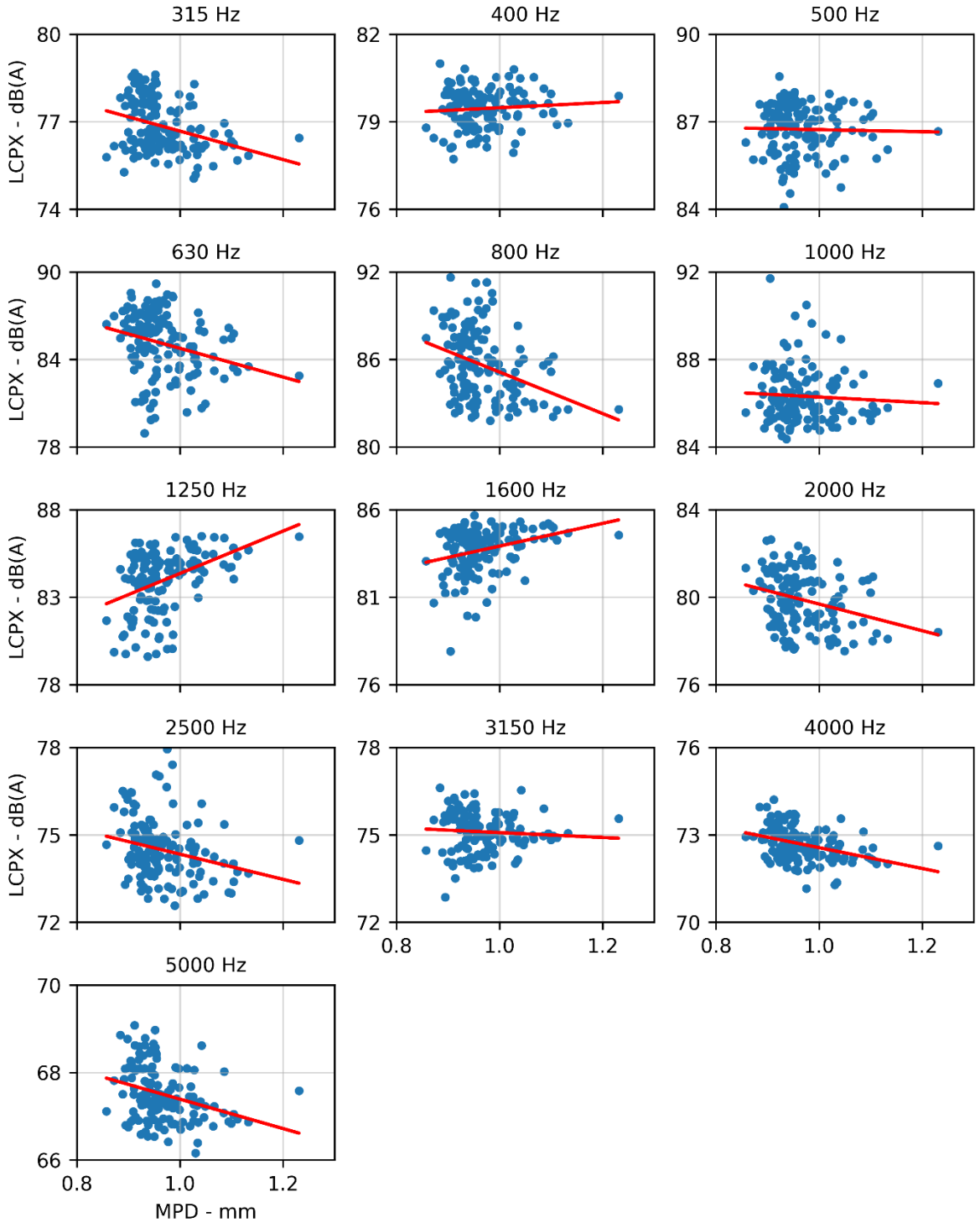

FIGURE 77. EPA7 ON CSM2. ONE-THIRD OCTAVE BAND L_{CPX} VS. MPD.

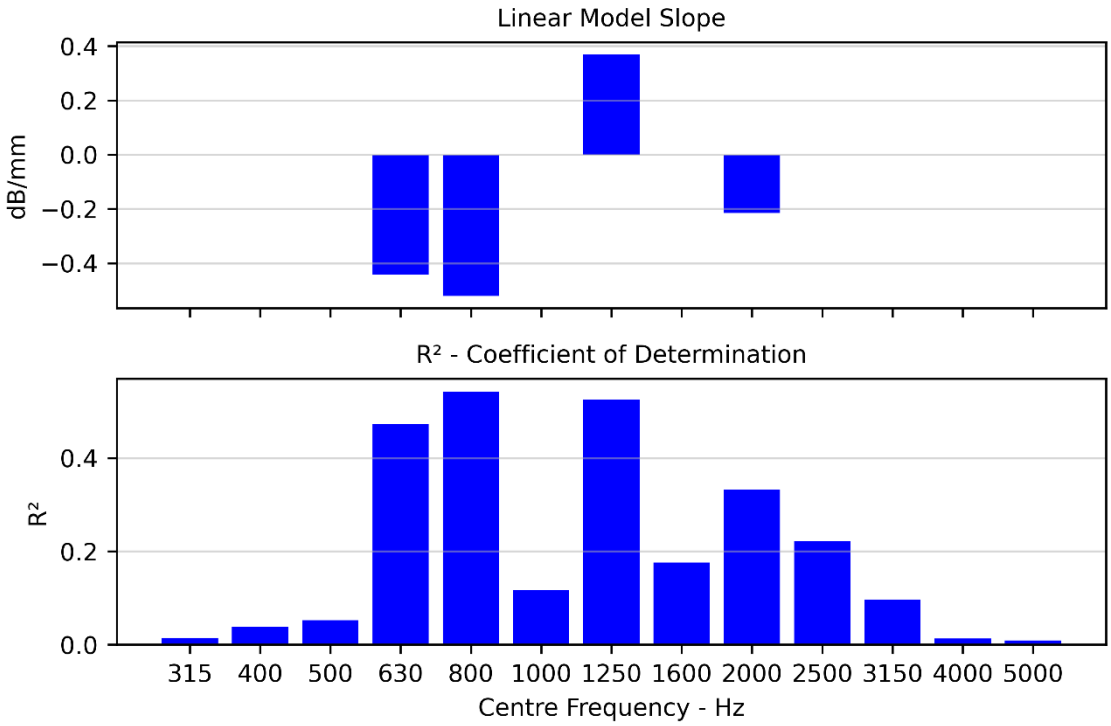

FIGURE 78. EPA7 ON CSM2. ONE-THIRD OCTAVE BAND L_{CPX} AND THICKNESS CORRELATIONS. TOP CHART IS THE LINEAR FIT SLOPE AND BOTTOM CHART IS COEFFICIENT OF DETERMINATION (R^2). MAXIMUM P-VALUE OF 0.025.

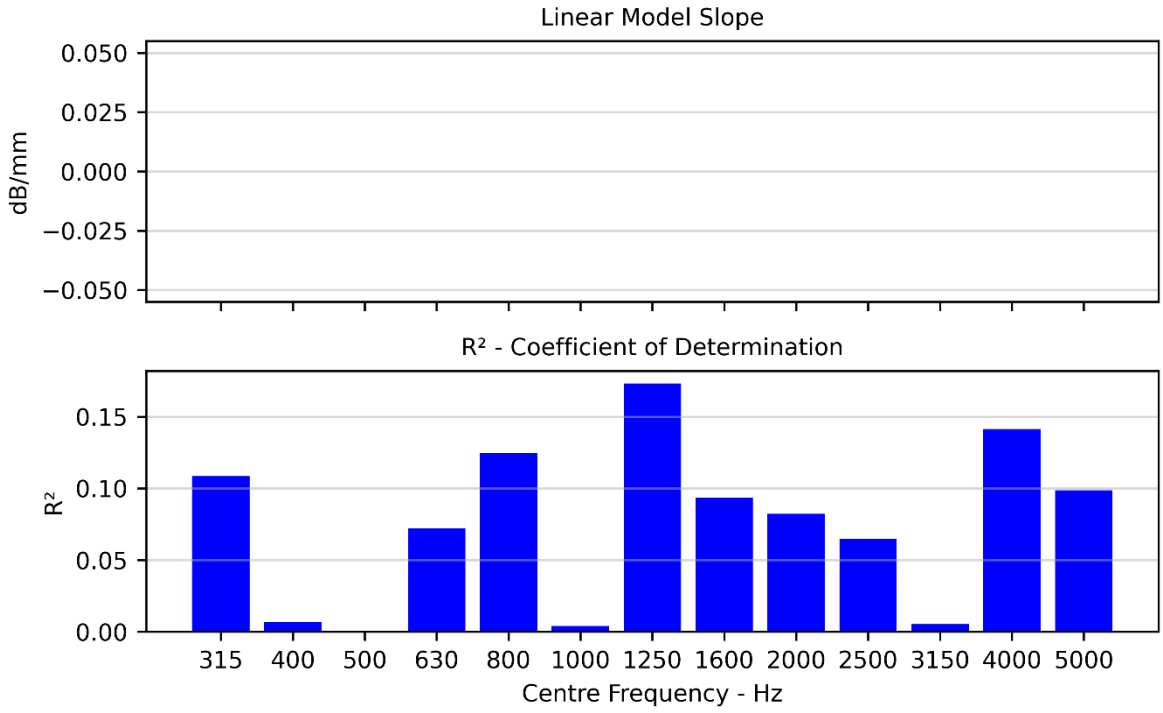

FIGURE 79. EPA7 ON CSM2. ONE-THIRD OCTAVE BAND L_{CPX} AND MPD CORRELATIONS. TOP CHART IS THE LINEAR FIT SLOPE AND BOTTOM CHART IS COEFFICIENT OF DETERMINATION (R^2). MAXIMUM P-VALUE OF 0.025.

TABLE 25. EPA7 ON CSM2 SOUTH-BOUND LEFT LANE. MULTI-VARIABLE LINEAR REGRESSION BETWEEN L_{CPX}, MPD, AND THICKNESS.

R^2	0.74	
Adj. R^2	0.73	
Thickness	-0.17 dB/mm	p = 0.000
MPD	4.5 dB/mm	p = 0.003

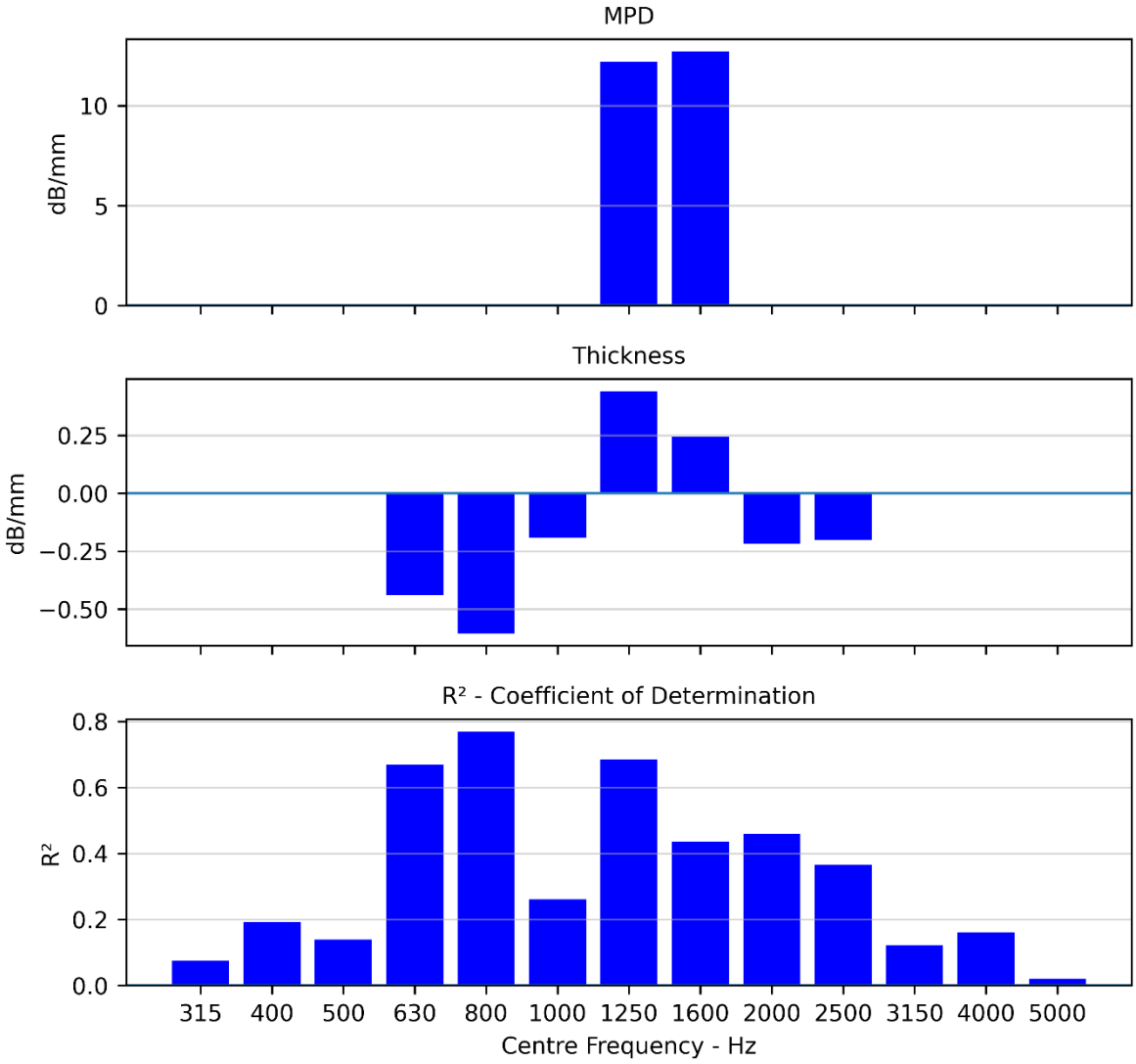

FIGURE 80. EPA7 ON CSM2 SOUTH-BOUND LEFT LANE. ONE-THIRD OCTAVE BAND L_{CPX} VS. MPD AND THICKNESS CORRELATIONS. MAXIMUM P-VALUE OF 0.025.

7.4 Sawyers to Groynes (S2G)

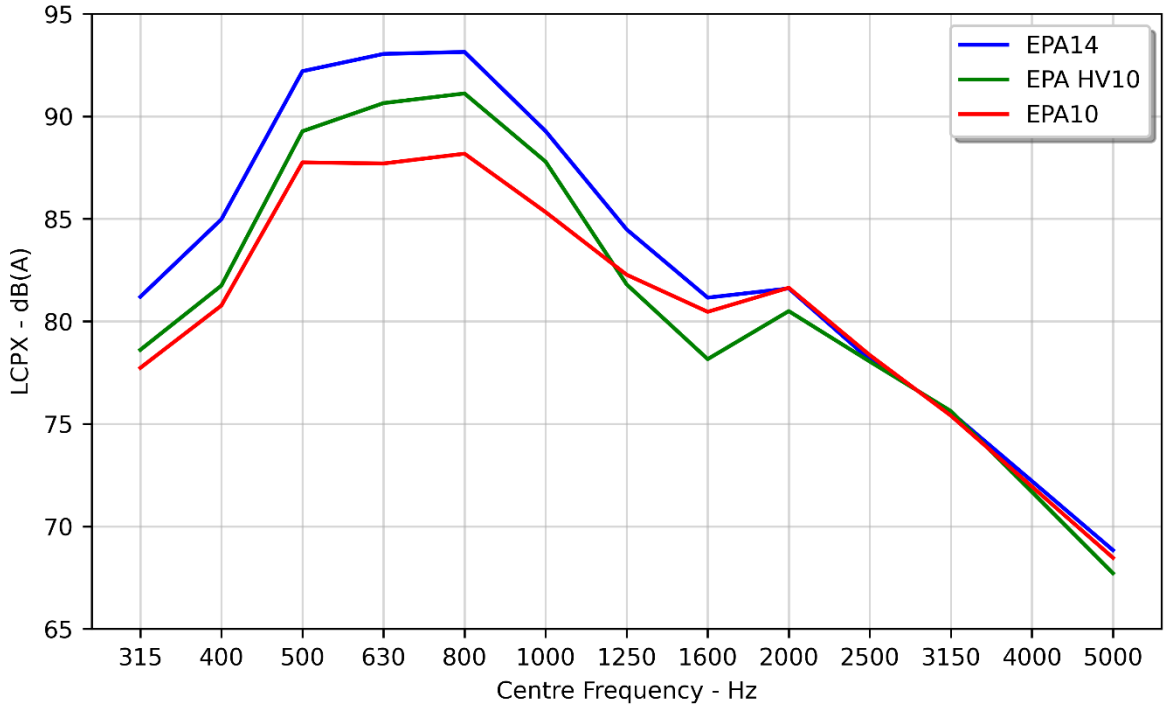

FIGURE 81. S2G TRIAL SITES. ONE-THIRD OCTAVE BAND DISTRIBUTIONS.

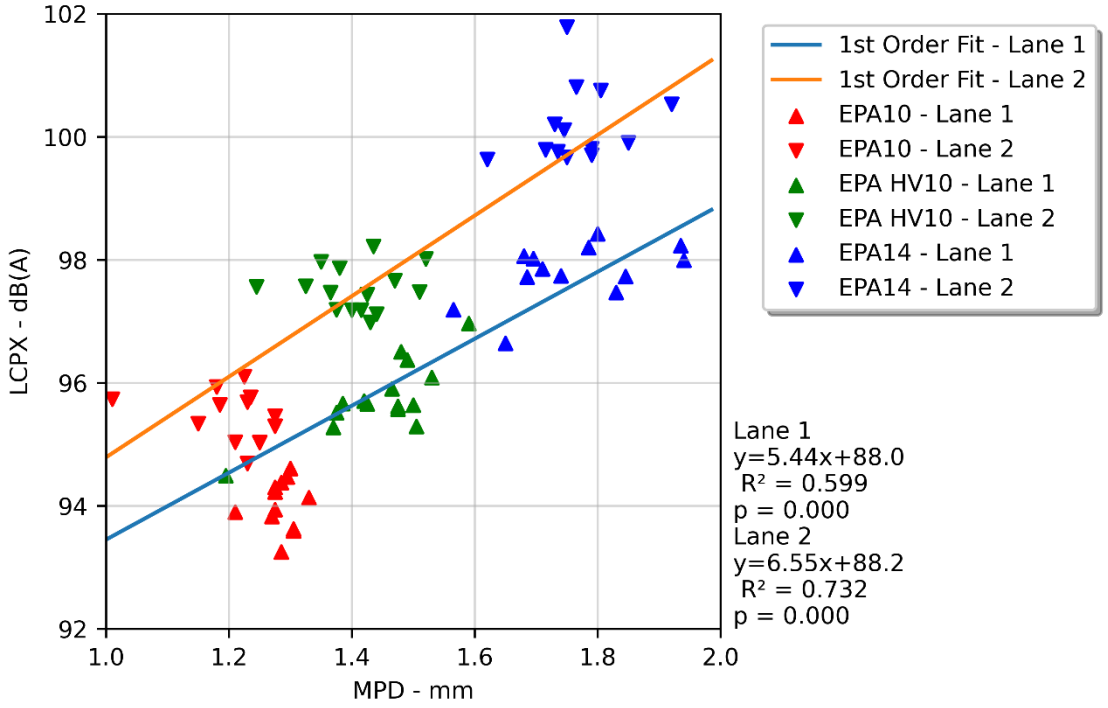

FIGURE 82. S2G TRIAL SITES. MPD VS. L_{CPX} BY TRIAL SITE AND LANE.

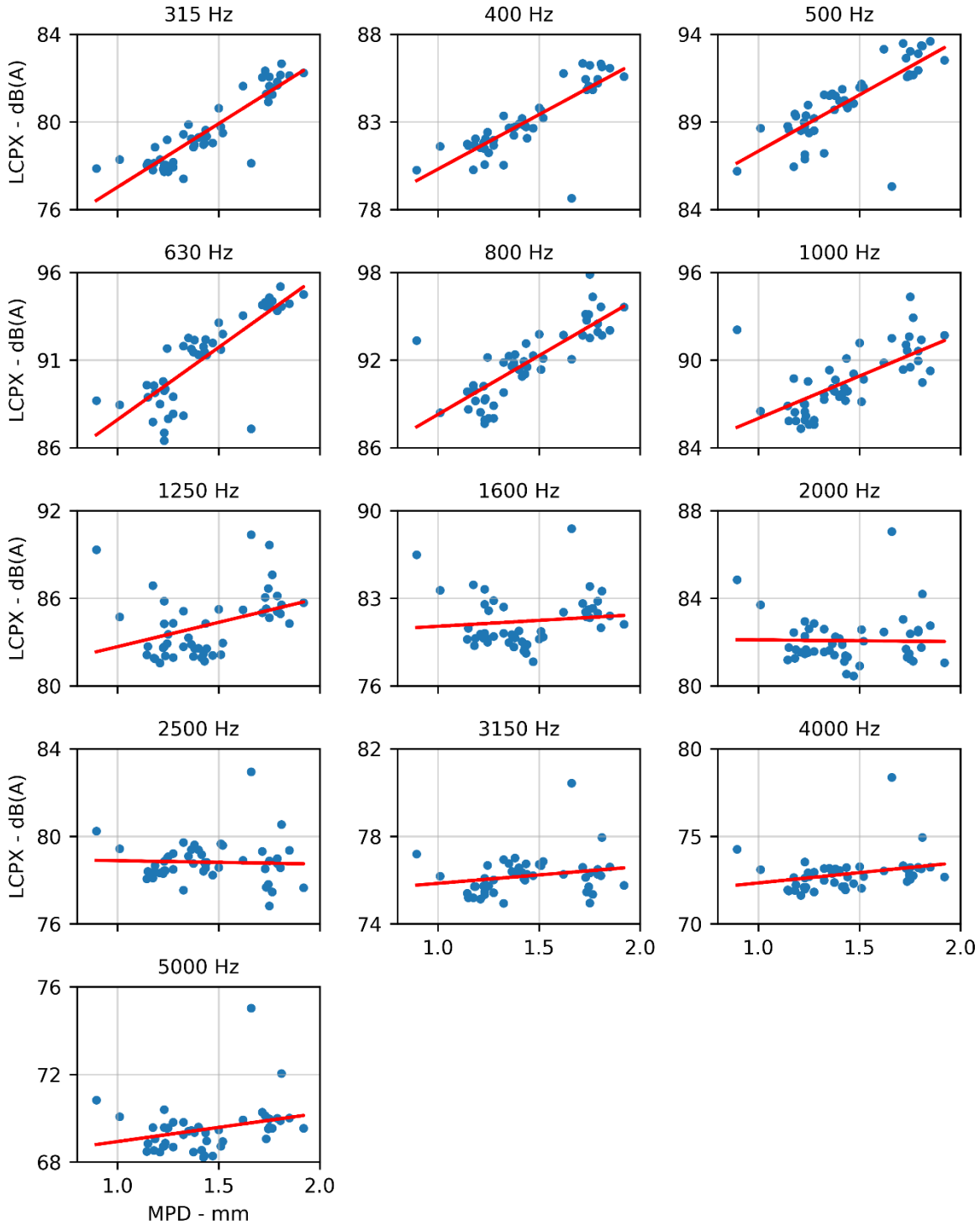

FIGURE 83. S2G TRIAL SITES. MPD VS. L_{CPX} BY ONE-THIRD OCTAVE BAND. ONLY SHOWING RESULTS FOR LANE 2.

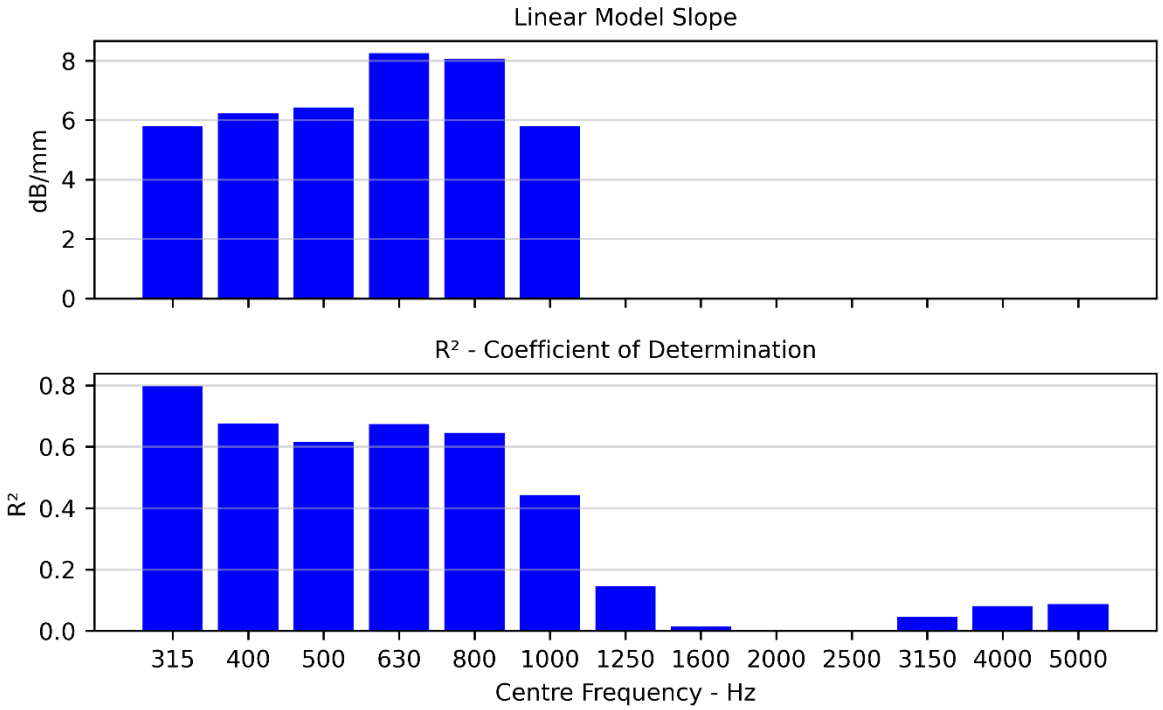

FIGURE 84. S2G TRIAL SITES. ONE-THIRD OCTAVE BAND L_{CPX} AND MPD CORRELATIONS. TOP CHART IS THE LINEAR FIT SLOPE AND BOTTOM CHART IS COEFFICIENT OF DETERMINATION (R^2). MAXIMUM P-VALUE OF 0.025. LANE 2 ONLY.

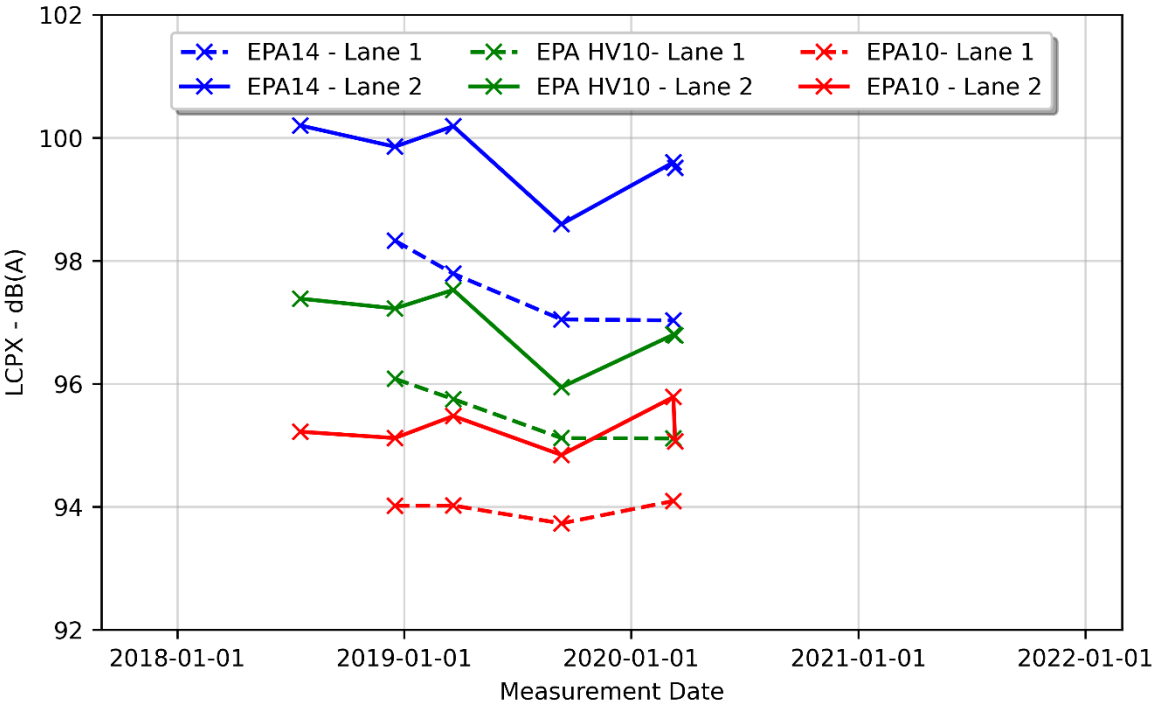

FIGURE 85. S2G TRIAL SITES. VARIATION IN L_{CPX} BY LANE AND SURFACE WITH TIME. ONLY USED ENCLOSURE CORRECTION SET "02".

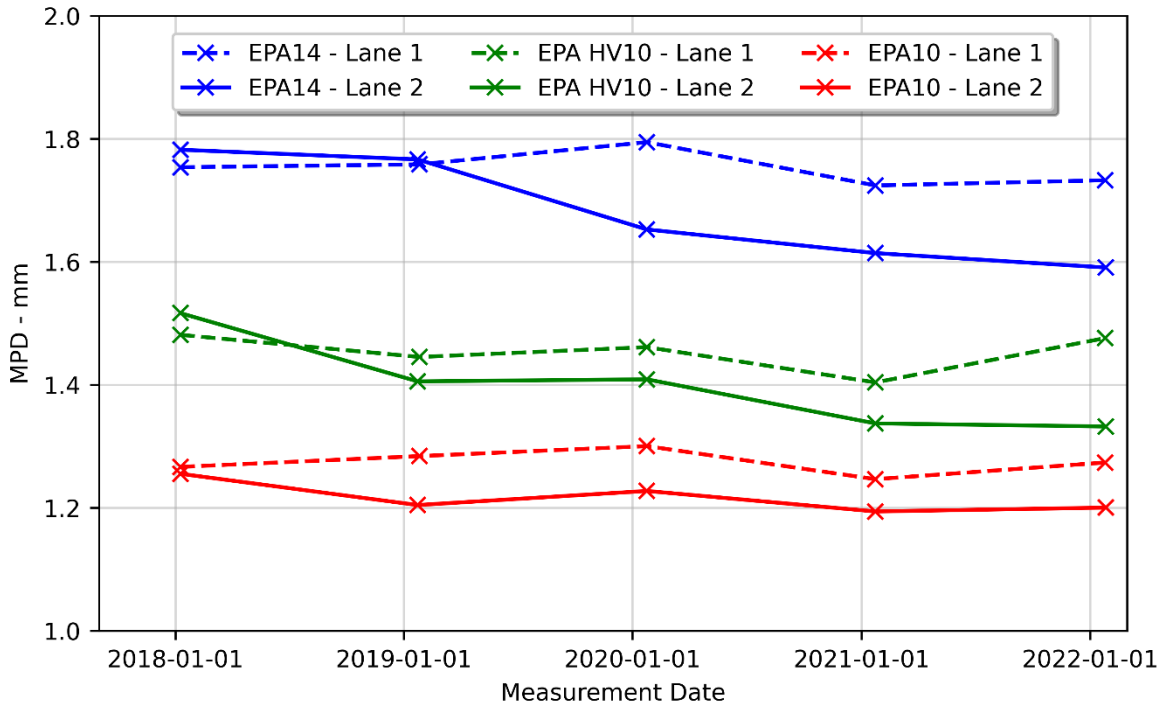

FIGURE 86. S2G TRIAL SITES. VARIATION IN MPD BY LANE AND SURFACE WITH TIME.

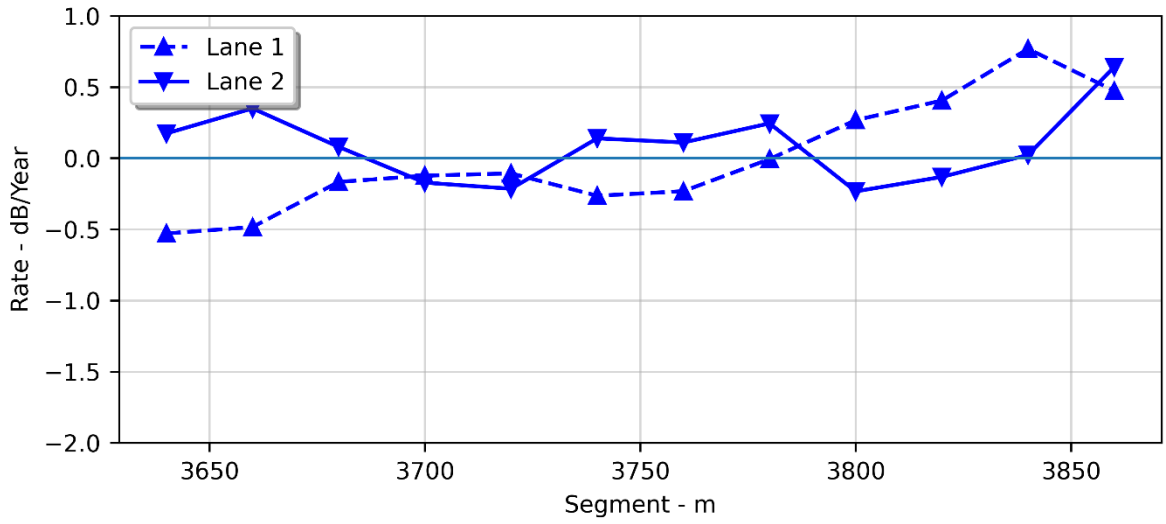

FIGURE 87. S2G EPA10. LONGITUDINAL VARIATION WITH TIME.

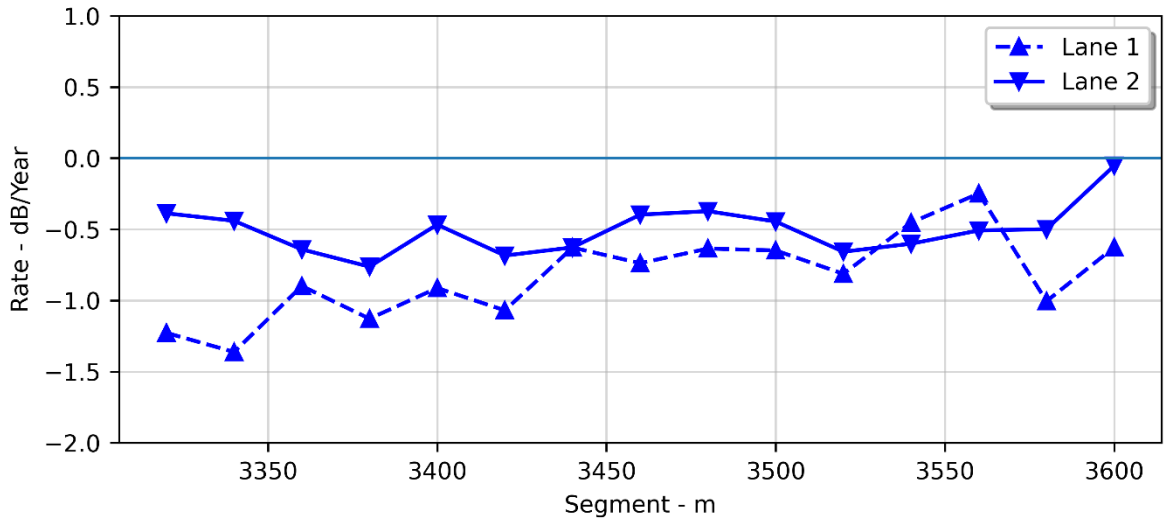

FIGURE 88. S2G EPA10 HV. LONGITUDINAL VARIATION WITH TIME.

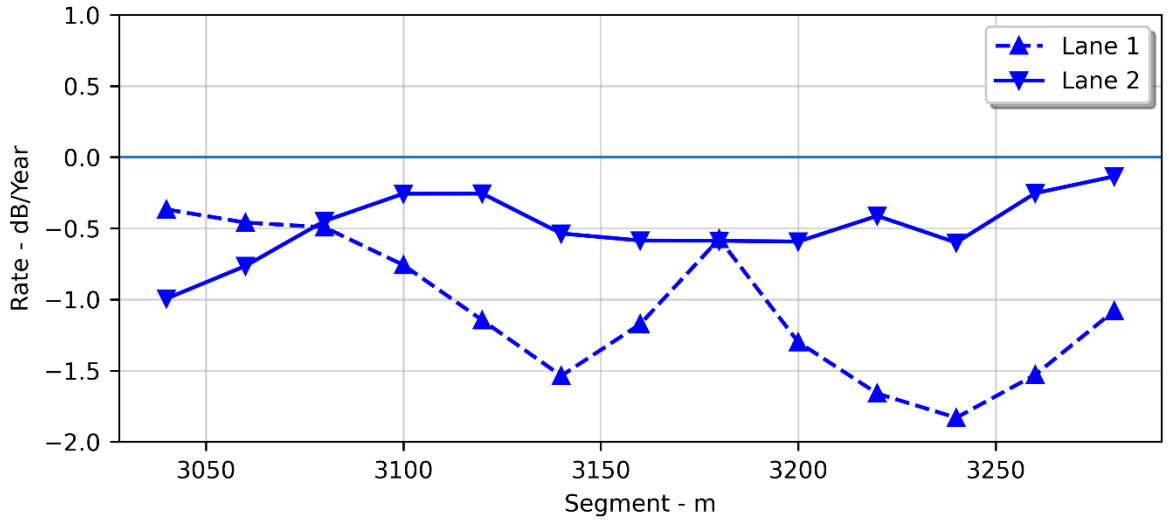

FIGURE 89. S2G EPA14. LONGITUDINAL VARIATION WITH TIME.

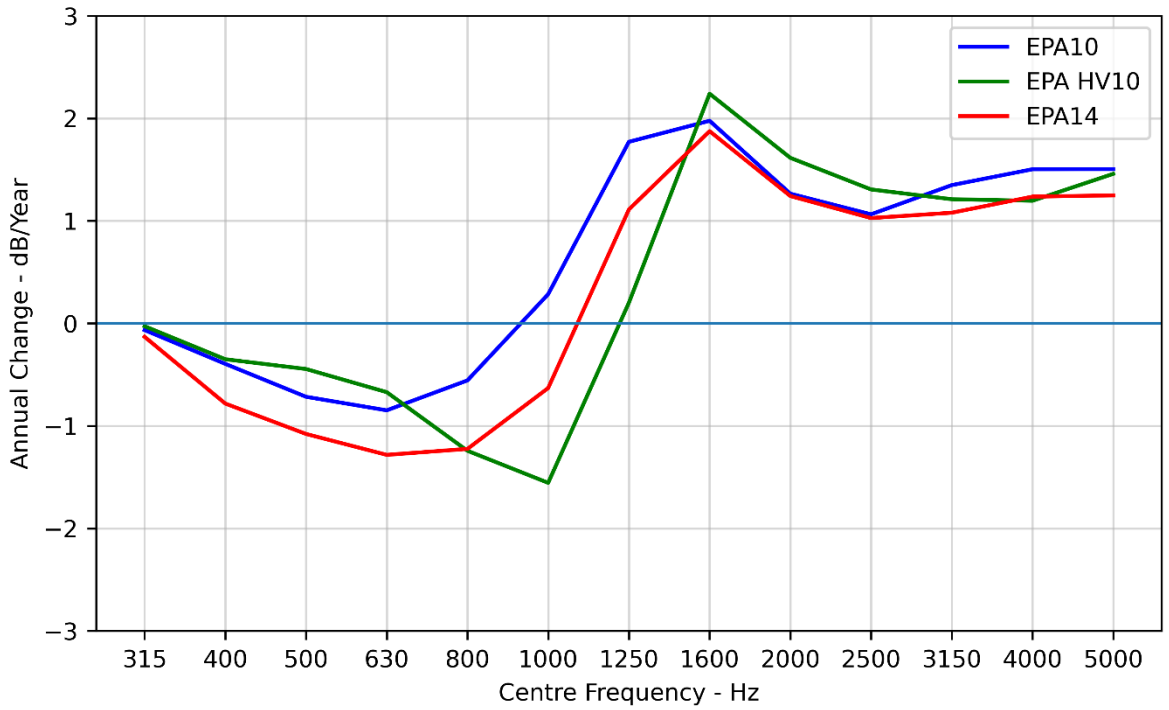

FIGURE 90. S2G TRIAL SITES. ONE-THIRD OCTAVE BAND VARIATION WITH TIME FROM JUL 2018 TO MAR 2020.

8 Appendix B – Project and Trial Section Locations

FIGURE 91. MAP OF CNC, CSM2, AND S2G PROJECTS.

9 Appendix C – Lane Numbering

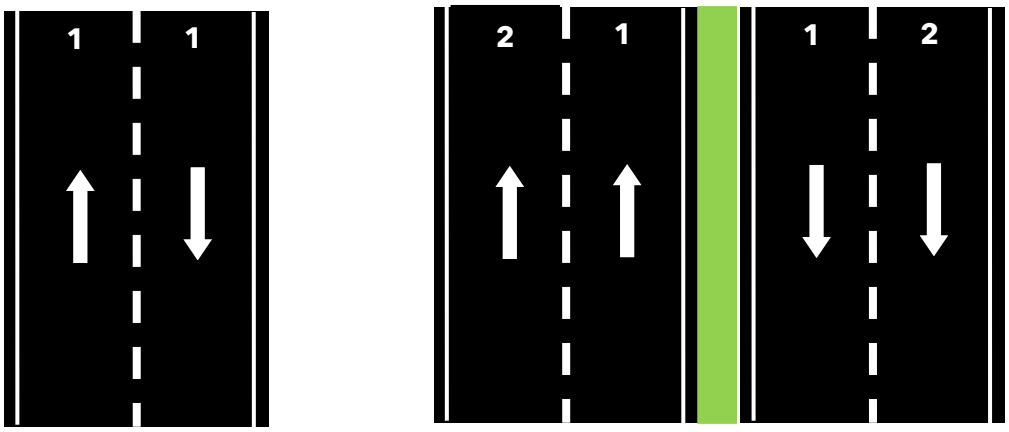

(A) SINGLE-CARRIAGEWAY (B) DUAL-CARRIAGEWAY

FIGURE 92. LANE NUMBERING CONVENTION.